A Study on the Wetting Behaviour of Ti-20Zr-20Cu-20Ni Brazing Filler on Ti-6Al-4V

Bolarinwa Komolafe

A Thesis

in

The Department

of

Mechanical and Industrial Engineering

Presented in Partial Fulfilment of the Requirements

for the Degree of Master of Applied Science (Mechanical Engineering) at

Concordia University

Montreal, Quebec, Canada

November 2014

CONCORDIA UNIVERSITY

School of Graduate Studies

This is to certify that the thesis prepared

By: Bolarinwa Komolafe

Entitled: A Study on the Wetting Behaviour of Ti-20Zr-20Cu-20Ni Brazing Filler on Ti-6Al-4V

and submitted in partial fulfillment of the requirements for the degree of

Master of Applied Science (Mechanical Engineering)

complies with the regulations of the University and meets the accepted standards with respect to originality and quality.

Signed by the final Examining Committee:

_____ Chair
Dr. C. Moreau

_____ Examiner
Dr M. Pugh

_____ Examiner
Dr. M. Nokken (External)

_____ Supervisor
Dr M. Medraj

Approved by _____

Chair of Department or Graduate Program Director

_____ 2014 _____

Dean of Faculty

Abstract

A Study on the Wetting Behaviour of Ti-20Zr-20Cu-20Ni Brazing Filler on Ti-6Al-4V

Bolarinwa Komolafe

The brazing of titanium alloys is nowadays a common and necessary industrial practice, because of the wide usage of these alloys in areas such as aerospace and chemical industries. However, to have a successfully brazed joint, it is important for the brazing filler to be able to wet the substrate. Unfortunately, there is a research gap with respect to the study on the wetting and spreading behaviour of brazing fillers on titanium alloys. In this work, wetting behaviour of Ti-20Zr-20Cu-20Ni brazing filler on Ti-6Al-4V was studied using sessile drop technique. Effects of the surface roughness of the substrate and heating scheme on wetting and spreading of the filler metal were evaluated. The degree of wetting was evaluated by measuring the apparent dynamic contact angle and calculating the spread ratio. The wetting mechanism was carefully studied too by the combination of quenching technique and microstructural analyses. Different wetting/spreading regimes were identified. The surface roughness of the substrate was found to have little or no effect on the final apparent contact angle in this work. The wetting behaviour of this system had a reactive nature. High heating rate (6.8^{o}C/s) limited metallurgical reaction between the substrate and the brazing filler, leading to wetting/spreading dominated by the primary stage. With the low heating rate scheme (1.7^{o}C/s), metallurgical reaction between the brazing filler and the substrate was more intense. High heating rate with soaking scheme is recommended for brazing because it entails good spreading and limited metallurgical reaction between the brazing filler and the substrate.

Acknowledgements

I will like to start by expressing my sincere and profound gratitude to my supervisor, Professor Mamoun Medraj, for his guidance, support, suggestions and positive and constructive criticism throughout my MASc program at Concordia University.

My sincere thanks also go to Dr. Dmytro Kevorkov for those great discussions. I also acknowledge the effort of Rafid Khoja-Mendwi for laying a solid foundation for this work. Dr. Yasser El-Shaer, though we had a short time together in TMG, your positive impact on me lives on; thank you a great deal. I will equally like to appreciate the technical assistance given to me by Henry Szczawinski, Robert Oliver and Michael Rembacz; you guys are great.

My gratitude also goes to Mazen Samara, what a gentle man and a great administrator. To my wonderful group members, thank you so much. To my great friend, Dina Ma, thank you so much.

History will not be kind to me if I fail to specially acknowledge the great assistance I received from Ahmad Mostafa towards the successful completion of my study. I have to admit that I have never met anyone like you. You are a man with a great soul, so selfless in service. I really cannot appreciate you enough, but please let me just say thank you.

I will also like to thank the financial partners of this project, CRIAQ and NSERC. My appreciation also go to our industrial partners, Pratt & Whitney Canada and SAFRAN (Turbomeca Canada). The contribution of ÉTS is also acknowledged.

Last but not least, my gratitude goes to my parents, siblings and other family members; thank you so much for your continual show of love. My lovely wife, Bolaji Komolafe, thank you a great deal.

Table of Contents

Table of Contents vi

List of Figures ix

List of Tables xiii

Chapter 1 Introduction 1

Chapter 2 Literature Review 6

2.1 Wetting and spreading 7

2.2 Critical issues with contact angle and its measurement 7

2.3 Contact angle hysteresis 8

2.4 Experimental methods for wettability study 9

2.5 Factors affecting wetting 12

2.5.1 Substrate surface roughness 12

2.5.2 Heterogeneity of the surface 15

2.5.3 Atmosphere 16

2.5.4 Temperature 17

2.5.5 Alloying elements 19

2.6 Marangoni convention 20

2.7 Non-reactive wetting 21

2.8 Reactive wetting 24

2.8.1 Purely dissolutive reactive wetting 25

2.8.2 Compound forming systems 30

2.8.3 Non-reactive stage in reactive wetting 31

2.9 Cold wetting 32

2.10 Modelling of kinetics of reactive systems 36

2.11 Wetting of titanium alloys by brazing filler metals 39

2.12 Objectives of this work 44

Chapter 3 Experimental Methodology 45

3.1 Wetting study apparatus 45

3.2 Heating scheme 47

3.3 Ti-6Al-4V sample preparation 50

3.4 Preparation of the brazing filler for the wetting test 52

3.5 Evaluation of the degree of wetting 55

Chapter 4 Results and Discussions 57

4.1 High heating rate 57

4.1.1 High heating rate (6.8^{o}C/s) with 120 grit SiC paper ground substrate 57

4.1.2 High heating rate (6.8^{o}C/s) with 1200 grit SiC paper ground substrate 61

4.1.3 Microstructural analysis 63

4.2 Low heating rate (1.7^{o}C/s) 71

4.2.1 Low heating rate (1.7^{o}C/s) with 120 grit SiC paper ground substrate 71

4.2.2 Low heating rate (1.7^{o}C/s) with 1200 grit SiC paper ground substrate 74

4.2.3 Microstructural analysis 76

4.3 High heating rate with intermediate soaking 79

4.3.1 High heating rate (5.6ºC/s) with soaking at 650ºC and 120 grit SiC paper ground substrate 80

4.3.2 High heating rate (5.6ºC/s) with soaking at 650ºC and 1200 grit SiC paper ground substrate 81

4.3.4 Microstructural analysis 84

4.4 Statistical analysis of the results 85

Chapter 5 Conclusions, Contributions and Suggestions for the Future Work 88

5.1 Conclusions 88

5.2 Contributions 89

5.3 Recommendations for future work 90

List of Figures

Figure 1-1. Variation of yield strength/density ratio of Ti-6Al-4V with service temperature, compared with other materials [10]. 3

Figure 1-2. Profiles of (a) wetting (b) non-wetting sessile drops resting on a horizontal surface [37]. 5

Figure 2-1. Shadow pictures of drop configuration in a transferred drop wetting experiment of Cu-Cr alloy on vitreous carbon (a) Initial configuration (b) drop configuration upon initial contact (c) hanging drop after separation from lower substrate [67]. 10

Figure 2-2. Schematic representation of dispense drop method [70]. 11

Figure 2-3. Schematic of the two-dimensional experimental set-up [69]..... 12

Figure 2-4. Spreading of (a) pure Cu (b) saturated Cu-Si on Si substrates after 50 ms [49]. 21

Figure 2-5. (a) Drop base radius and (b) visible contact angle as a function of time plotted on a logarithmic scale for Cu and Cu pre-saturated in Si on a (0 0 1) Si surface at 1100^{o}C [51]. 27

Figure 2-6. Normalised drop base diameter (a) and contact angle (b) as a function of logarithm of time for two saturated (S) and two non-saturated (NS) Ag-Cu drops spreading on monocrystalline Cu at $t < 4$ s [71]..... 28

Figure 2-7. Schematic representation of spreading stages in (a) Non equilibrium (b) Equilibrium Ag-Cu/Cu systems [71]. 30

Figure 2-8. Images of a pure Sn drop wetting pure Bi in a Hele-Shaw cell at different time intervals [49]. 32

Figure 2-9. Idealized diagram of a thin cross section of a liquid drop on a gradient surface [121]. 33

Figure 2-10. Photograph of a 2-µl drop of decane containing 1.5mM pentadecafluorooctanoic acid (PFOA) flowing up a glass microscope slide inclined at an angle of 43^{o} from the horizontal [117]. 34

Figure 2-11. Plot of the velocity of octane droplets of length L = 3.5 mm as a function of the concentration in silane. Inset: Receding contact angle of a pure octane measured on the hydrophobic trail left by the same droplets [118]. 36

Figure 2-12. The dynamic wetting angle of pure Ag on Ti-6Al-4V substrate [7]. 40

Figure 2-13. Dynamic wetting angle measurements of (a) Braze 580 (b) BAg-8 (c) Ticusil® on Ti-6Al-4V at different temperatures[126]. 41

Figure 2-14. The sessile drop test of BAg-8 on Ti-6Al-4V [128]. 43

Figure 3-1. Illustration of the furnace hot core design [130]. 47

Figure 3-2. A typical heating curve for a high heating rate scheme. 48

Figure 3-3. A typical heating curve for a high heating rate with intermediate soaking scheme. 49

Figure 3-4. A typical heating curve for low heating rate scheme. 50

Figure 3-5. Microstructure of the cross-section of the layered structure brazing filler. ... 52

Figure 3-6. EDS line scan across different layers of the filler material. 53

Figure 3-7. Wetting ball/substrate sample. 54

Figure 3-8. An image of a spreading droplet in the furnace. 55

Figure 4-1. Variations of contact angle and spread ratio with time under the condition of 6.8^{o}C/s heating rate with 120 grit SiC paper ground substrate. 59

Figure 4-2. Variations of contact angle and spread ratio with temperature under the condition of 6.8°C/s heating rate with 120 grit SiC paper ground substrate..... 60
Figure 4-3. Macrograph of sample (a) HHRR1 (b) HHRR2 after the wetting test. 60
Figure 4-4. Variations of contact angle and spread ratio with time under the condition of 6.8°C/s heating rate with 1200 grit SiC paper ground substrate. 62
Figure 4-5. Variations of the contact angle with temperature under the condition of 6.8°C/s heating rate with 120 and 1200 grit SiC paper ground substrates. 63
Figure 4-6. SEM back scattered electron image of (a) sample HHRR1 (b) intermediate layer (c) enlarged view of the interfacial layer. 64
Figure 4-7. SEM back scattered image of (a) sample HHRS3 (b) interface/contact line region, quenched after 5 s. Letters A and B in Figure 4-15b indicate the direction of the line scan, corresponding to that in Figure 4-16..... 67
Figure 4-8. Line scan across the quenched sample. Letters A and B in the figure indicate the direction of the line scan, corresponding to that in Figure 4-15b. 68
Figure 4-9. Spread ratio-time graph of fully annealed and furnace-cooled (HHRS1 and HHRS2), and quenched (HHRS4) samples. 69
Figure 4-10. SEM back scattered images of (a) sample B10 (b) contact line/interface region, quenched after 15 s. 71
Figure 4-11. Variation of contact angle with time under the condition of 1.7°C/s heating rate with 120 size SiC paper ground substrate. 73
Figure 4-12. Final macrographs of samples (a) SHRR1 and (b) SHRR2. 74
Figure 4-13. Variation of contact angle with time under the condition of 1.7°/s heating rate with 1200 grit SiC paper ground substrate. 75

Figure 4-14. SEM back scattered electron images of sample SHRR1 showing (a) left hand side (b) right hand side (c) top surface of the droplet at the contact line region. 78

Figure 4-15. SEM back scattered electron images of sample SHRR1 showing the formation of the interfacial layer ahead of the droplet at (a) left hand side (b) right hand side of the triple/contact line region. 79

Figure 4-16. Variation of contact angle with time under the condition of 5.6ºC/s heating rate with soaking at 650ºC. 81

Figure 4-17. Variation of spread ratio with time under the condition of 5.6ºC/s heating rate with soaking at 650ºC and 1200 grit SiC paper ground substrate. 83

Figure 4-18. The final macrograph of sample HHRSS1 after the wetting test. 84

Figure 4-19. SEM back scattered images of samples (a) HHRSS3 (b) HHRSS1. 85

Figure 4-20. Main effects of surface roughness and heating scheme on the apparent contact angle. 86

Figure 4-21. Interaction plot of the effects of surface roughness and heating scheme on the apparent contact angle. 87

List of Tables

Table 1-1. Compositions, mechanical properties and typical applications of some common titanium alloys [4]. 1

Table 2-1. Spreading regimes in non-equilibrium Ag-Cu/Cu system [71]. 29

Table 2-2. Summary of the work done on the wetting behaviour of brazing fillers on Ti-6Al-4V. 43

Table 3-1. Average surface roughness values of a sample with a relatively rough surface. 51

Table 3-2. Average surface roughness values of a sample with a relatively smooth surface. 51

Table 3-3. Experimental combination of the heating scheme and surface finish. 55

Table 4-1. EDS analysis of the intermediate layer in atomic %. 65

Table 4-2. Data from Ti-Cu and Ti-Ni binary phase diagrams [137]. 65

Table 4-3. EDS analysis of the shiny edge in atomic %. 79

Chapter 1 Introduction

Titanium alloys are widely used in many applications such as aerospace, biomedical, nuclear and chemical [1]. Classification of conventional titanium alloys depends on their composition and the constituent phase that predominates at room temperature. This could either be hexagonal α-phase or body-centered cubic β-phase [2]. They are classified as α-, near-α, α-β or β alloys [3]. Some common titanium alloys and their areas of applications are shown in Table 1-1 [4].

Table 1-1. Compositions, mechanical properties and typical applications of some common titanium alloys [4].

Alloy Type	Common Name (UNS Number)	Condition	Average Mechanical Properties			Typical Applications
			Tensile Strength [MPa (ksi)]	Yield Strength [MPa (ksi)]	Ductility [%EL in 50mm (2 in.)]	
Commercially pure	Unalloyed (R50250)	Annealed	240 (35)	170 (25)	24	Jet engine shrouds, cases and airframe skins, corrosion-resistant equipment for marine and chemical processing industries
A	Ti-5Al-2.5Sn (R54520)	Annealed	826 (120)	784 (114)	16	Gas turbine engine casings and rings; chemical processing equipment requiring strength to temperatures of 480°C (900°F)
Near α	Ti-8Al-1Mo-1V (R54810)	Annealed (duplex)	950 (138)	890 (129)	15	Forgings for jet engine components (compressor disks, plates and hubs)
α-β	Ti-6Al-4V (56400)	Annealed	947 (137)	877 (127)	14	High-strength prosthetic implants, chemical-processing equipment, airframe structural components
α-β	Ti-6Al-6V-2Sn (R56620)	Annealed	1050 (153)	985 (143)	14	Rocket engine case airframe applications.

Ti-6Al-4V(wt.%) is a typical example of α-β titanium alloys and it is reported to be the most widely used titanium alloy, accounting for around 60% of the total usage of Ti [5]. For this particular titanium alloy, aluminium (Al) and vanadium (V) are added as α and β stabilizers, respectively. This alloy can be strengthened by solution and aging treatments [6]. Ti-6Al-4V readily lends itself to wide usage in aerospace, chemical and medical industries, because of its good heat and corrosion resistance, high strength to weight ratio, weldability and good mechanical properties at elevated temperature, compared to commercially pure Ti [7-9]. The variation of strength-to-density ratio of Ti-6Al-4V with temperature (structural efficiency), compared with other materials, is shown in Figure 1-1 [10]

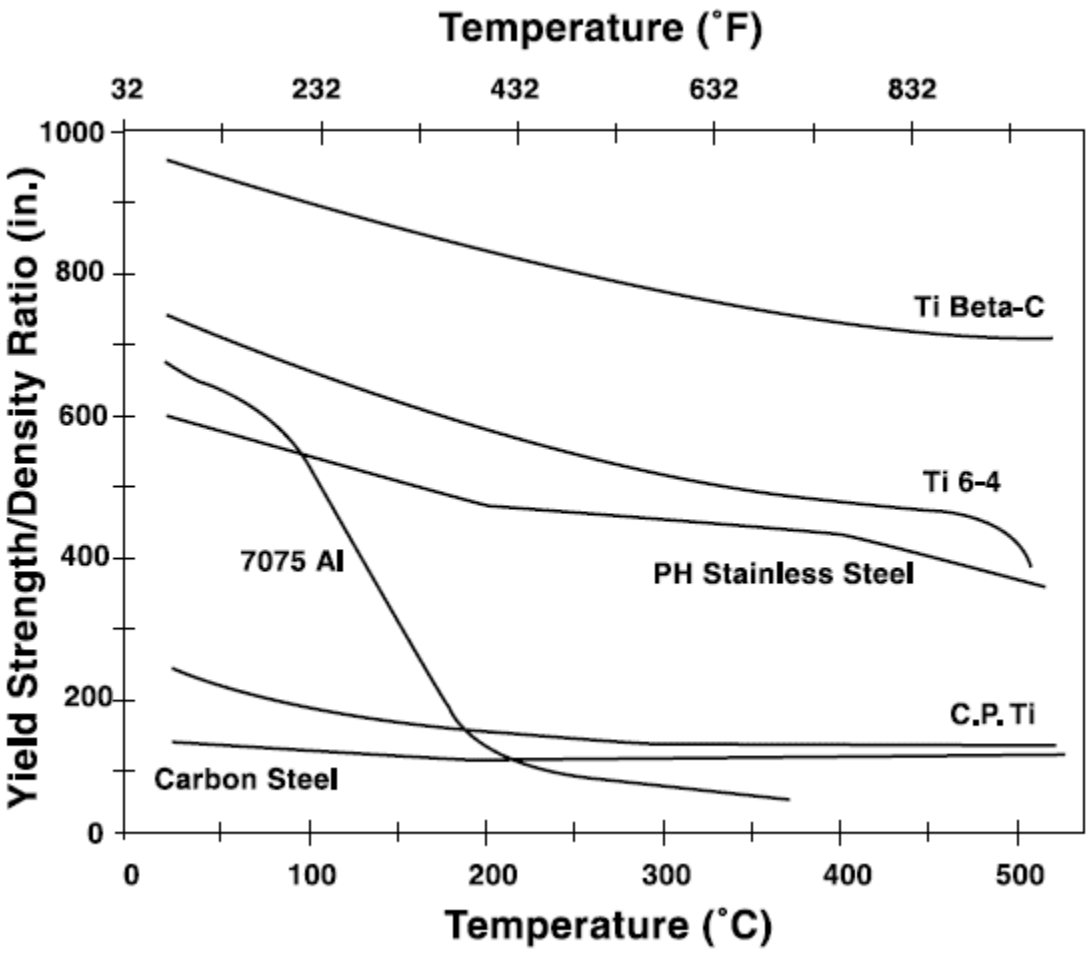

Figure 1-1. Variation of yield strength/density ratio of Ti-6Al-4V with service temperature, compared with other materials [10].

As a result of the use of titanium alloys to meet the ever increasing structural application demands, brazing of titanium and its alloys became much more prominent in the past decade [5]. Brazing, by definition, is generally regarded as a metal-joining process that is carried out at a temperature above 450^{o}C, high enough to melt the filler metal but not the base metals being joined [11]. It is based on the ability of the filler metal to be drawn into the joint between the base metals by capillary action and to form a metallurgical bond with the base metals [12].

Quite a number of pure metals and alloys are used as filler materials in brazing processes. The selection of a particular brazing filler metal for a particular operation depends on factors such as the parent materials, brazing temperature, joint configuration, operating temperature of the brazed assembly, melting characteristics of the brazing filler and economic considerations [13]. Ti alloys meant for elevated service temperature are usually brazed using Ti-based filler metals, with the addition of Cu, Ni and Zr as melting point depressants [5, 14]. Equally, the use of Ti-based fillers usually provide high joint strength with good corrosion resistance, compared with other types of brazing fillers [3]. However, regardless of the filler metal to be used for brazing, such filler metal must be able to wet the base metal and produce a joint with the required service capabilities and properties [15, 16].

Wettability study is an age-old field, with the pioneering theoretical work being credited to Young and Laplace [17]. It gives an indication of the extent of intimacy in contact between a liquid and a solid; making it, therefore, an important behaviour to evaluate the success of an industrial operation like brazing [18]. It is equally of great importance to other industrial practices such as soldering, coating and composite manufacturing [19-30]. The degree of wetting of a substrate by a liquid is usually quantified by the equilibrium or static contact angle, θ, which the liquid metal drop forms on such a substrate [21, 23, 31-36]. The system is usually described as wetting or non-wetting if the contact angle is lesser or greater than 90^{o} as shown in Figures 1-2a and 1-2b, respectively [37].

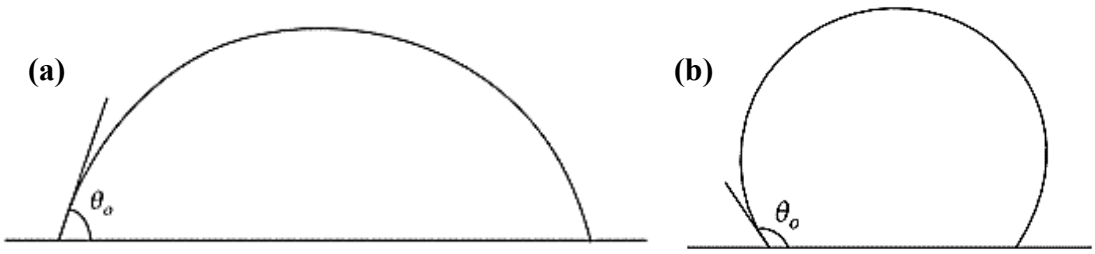

Figure 1-2. Profiles of (a) wetting (b) non-wetting sessile drops resting on a horizontal surface [37].

If the liquid droplet wets the substrate with a finite equilibrium contact angle, θ_e, it is referred to as partial wetting; but when θ_e is equal to zero, it is called complete wetting [38, 39].

Chapter 2 Literature Review

The earliest approach to wettability study was to use physical theory of surface tension to explain and characterize the phenomenon [17, 40, 41]. This idea is well reflected in Young's equation, which is expressed as [42]:

$$\gamma_{sv} - \gamma_{sl} = \gamma_{lv} \cos\theta \tag{2.1}$$

where θ represents the measured contact angle, and γ_{sv}, γ_{sl} and γ_{lv} represent the solid-vapour, solid-liquid and liquid-vapour interfacial tension, respectively.

Laplace, on the other hand, gave the mathematical description of the pressure difference between the two sides of a curved surface as [43]:

$$\Delta P = \gamma_{lv}(1/R_1 + 1/R_2) \tag{2.2}$$

where $R_1$and R_2 represent the two principal radii of curvature.

Dupre, defined the work of adhesion between a solid and a liquid, yielding the famous Young-Dupre equation [44]. The significance of the Young-Dupre equation lies in the fact that it relates the work of adhesion to the measurable quantities, surface tension of the liquid and the equilibrium contact angle, rather than to the inaccessible interfacial tensions involving the solid surface as [45, 46]:

$$W_{sl} = \gamma_{lv}(1 + \cos\theta) \tag{2.3}$$

where W_{sl} is the work of adhesion of the liquid to the smooth solid.

However, wetting is more complex than as described by eqn. 2.3 [47]. The derivations of Young's and Young-Dupre equations are made under the assumptions of spreading of non-reactive liquid on an ideal (chemically inert, smooth, homogenous and rigid) solid [44]. It also assumed that the contact angles are large enough to allow for accurate measurement and are unique in value [48]. However, these conditions are rarely met in practical situations [44].

2.1 Wetting and spreading

With respect to the literature, there seems to be no generally accepted distinction between wetting and spreading. According to Kumar and Prabhu [44], wetting is essentially a surface phenomenon in which a liquid covers the surface of a solid when it is placed over such a surface; while spreading is considered as a physical process by which the liquid wets the surface of the solid. Yin *et al*. [49] considered wetting to be a process confined to the contact line region only, and spreading as a macroscopic process, which involves the flow of a liquid mass over a solid surface, in response to an external effect such as capillary force. However, Sharps *et al*. [50] stated that for spreading to occur, the apparent contact angle must be zero; otherwise it is wetting or, at best, good wetting, depending on how close the angle is to zero. This view [50] represents the clearest distinction between wetting and spreading.

2.2 Critical issues with contact angle and its measurement

In non- reactive wetting systems, the final contact angle is truly the equilibrium contact angle because of the lack of reactivity in the system. However, in systems undergoing reactive wetting, chemical equilibrium is hardly achieved or takes a long period of time to achieve; making the use of equilibrium contact angle to assess the degree of wetting to lose

its meaning in some circumstances or cases. For a system in which the reaction leads to the formation of solid phases either at the contact line or throughout the brazing droplet, this might lead to isothermal solidification, thus leading to a premature arrest of the spreading [32]. Also, in cases involving the dissolution of the substrate, the contact angle that is observed at the macroscopic level is the apparent contact angle [51]. The true contact angle can only be observed through metallographic inspection. Therefore, the use of contact angle to quantify the degree of wetting in such systems has to be approached with caution.

2.3 Contact angle hysteresis

For many surfaces, different values of contact angle can be observed or measured depending on whether the measurement is performed with a drop of increasing size (the advancing contact angle, θ_a) or of diminishing size (the receding contact angle, θ_r) [45, 52]. This phenomenon of the existence of more than one contact angle for a particular drop is referred to as contact angle hysteresis [44]. θa corresponds to the highest static value that θ can attain [53]. The difference between the advancing and the receding contact angle gives the measure of the hysteresis [48, 54]. Hysteresis plays a special role in practical capillary problems, especially where supehydrophobicity of a surface is required [55-57]. This phenomenon is mostly attributed to surface roughness and chemical heterogeneity of a geometrical surface, among other factors [53, 54, 58, 59]. A very detailed theoretical analysis on contact angle hysteresis has been done by Joanny and de Gennes [60]. Also, Shanahan [52] linked the second order force ripple occasionally observed during dynamic experiments using the Wilhemy plate technique to the phenomenon of contact angle hysteresis, leading to the formation of protrusions on the wetting front. There are several

other relevant and important works that have been done on the study of contact angle hysteresis such as [61-66].

2.4 Experimental methods for wettability study

Various techniques abound in the literature to evaluate spreading and measure the equilibrium contact angle. Conventional sessile drop method is probably the most used technique in wettability studies [18, 23, 50]. This is due to its simplicity and ease of use. The conventional sessile drop approach/methodology for studying wettability involves placing a solid particle (pure metal, alloy, etc.) on the substrate and then heating up the assembly until the solid particle melts and flows on the substrate. However, there are some concerns with this approach.

In the course of this process, for the case of an alloy, its composition may change due to evaporation and/or diffusion. Also, it can be very difficult to identify when the solid particle is fully molten; which can affect the reference time for wetting/spreading in the study [67]. Equally, the wettability study is usually carried out at a temperature above the melting point of the solid particle (filler material). Therefore, this process cannot be described as strictly isothermal, because while the pure metal or alloy is melting, the temperature of the furnace is still increasing or yet to stabilize. This might explain some of the discrepancies in the spreading behaviour reported in the literature [44]. It must be stated, however, that this approach is still the best when it comes to simulating the real industrial brazing practice. Since wetting, in most cases, is spontaneous[49]; using this approach, therefore, offers a sound method of evaluating the solderability of surfaces, since commercial soldering processes also rely on spontaneous wetting [68, 69].

An improved form of the conventional sessile drop method for wettability study is the "drop-transfer technique" [28, 67]. In this approach, the brazing alloy is heated up until it is completely molten on a plate or material with which the alloy is known to have little or no reactivity, as shown in Figure 2-1a [67]. Once the furnace temperature is stabilized, the molten alloy is then "transferred" to the substrate. The sequence of operation is shown in Figure 2-1a-c [67]. However, the drawback attached to this approach is that the spreading drop might be driven at the beginning of wetting/spreading by the transfer inertia. Also, there might be an interaction between the wetting process and the drop transfer mechanism.

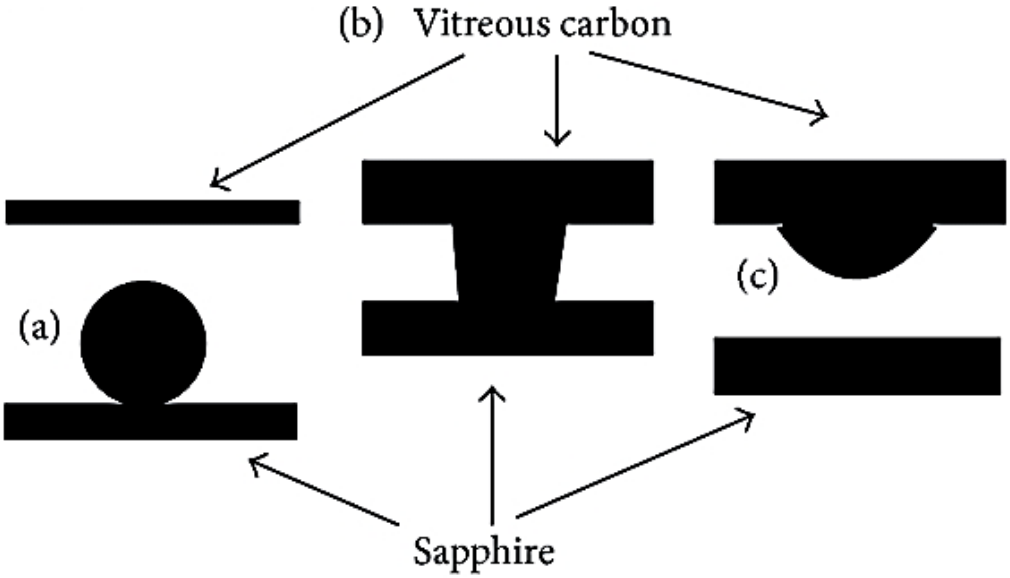

Figure 2-1. Shadow pictures of drop configuration in a transferred drop wetting experiment of Cu-Cr alloy on vitreous carbon (a) Initial configuration (b) drop configuration upon initial contact (c) hanging drop after separation from lower substrate [67].

Another method being employed in wettability study is the dispensed drop method [70, 71]. In this method, the droplet is extruded through a capillary introducer. The sequence of

operation is shown in Figure 2-2 [70]. However, this method is not free from the problem of perturbation, which occurs as the droplet initiates a contact with the substrate.

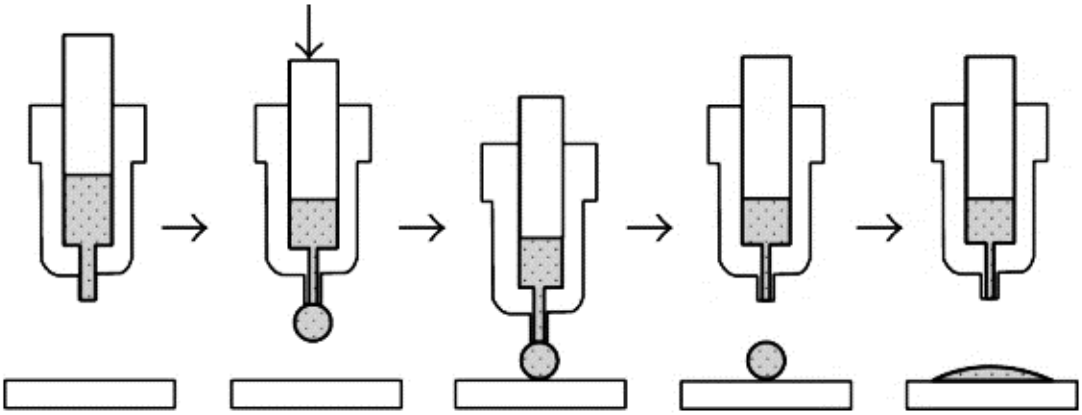

Figure 2-2. Schematic representation of dispense drop method [70].

One of the impediments to comprehensive understanding of reactive wetting, especially in high temperature experiments, is the difficulty of having in-situ and real-time monitoring of the interface between the solid and the spreading droplet, hence, quenching and subsequent microstructural analyses is usually the method used to study the interface [72]. However, a new drop experiment technique has been introduced that allows for real-time monitoring and observation of both the solid-liquid and liquid-vapour interface evolution. This was achieved by performing high temperature reactive wetting experiments in Hele-Shaw cells [28, 69]. This technique was based on drop transfer technique in a very small gap geometry. The metal substrate, in this method, is a thin foil, clamped between two glass windows. The wetting ball is compressed into a disk, with a thickness smaller than that of the substrate. The foil-wetting disk assembly is then placed on the hot stage. The transparent cell walls made a real-time observation of the interfaces possible, a schematic

of the experimental set-up is shown in Figure 2-3 [69]. The drop in this experiment was essentially 2-dimensional.

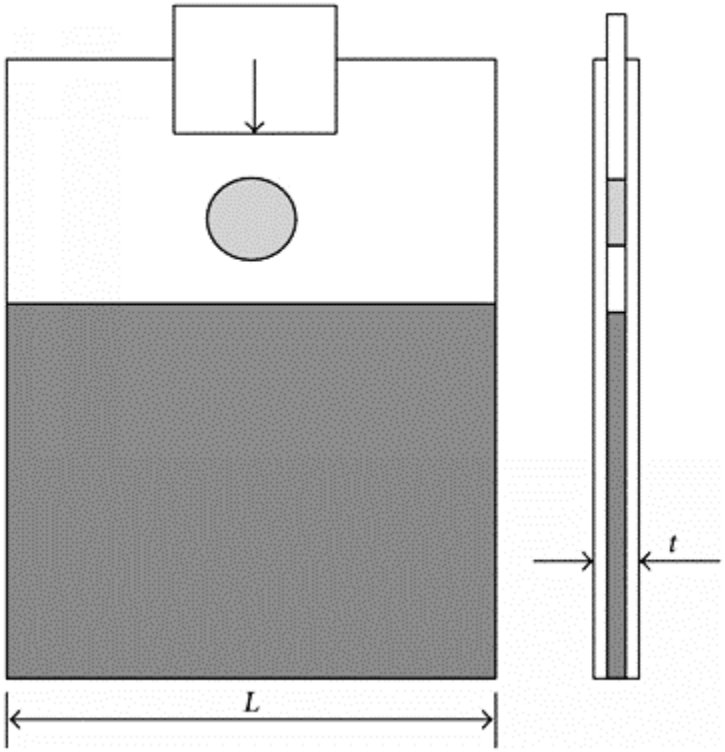

Figure 2-3. Schematic of the two-dimensional experimental set-up [69].

2.5 Factors affecting wetting

According to Shibata *et al*. [73]; issues such as metal purity, gas-phase oxygen content, surface roughness, and substrate purity must all be controlled in order to accurately carry out a wettability study.

2.5.1 Substrate surface roughness

The influence of roughness of the solid surface on the contact angle was first discussed by Wenzel [74, 75]. Wenzel [76], argued that for a drop of water resting on a horizontal solid

surface, the specific energy content of the solid interface will, in general, be different for the wetted area under the drop than for the dry area around it. He [76] stated that, for identically the same increase in the free liquid area at the upper surface of the drop, a greater amount of actual surface is wetted under it, when the surface of the solid is rough than when it is smooth. Consequently, for the process involving the rough surface, there is a greater net energy decrease to induce spreading, and the rough surface is wetted more rapidly. The same reasoning applies for a water-repellent surface, in which case, the dry interface has the lower specific energy [76]. The drop will then spontaneously assume a more spherical form. He proposed an equation that gives a relation between equilibrium contact angle and the apparent angle formed on a rough surface as [44, 75]:

$$\cos\theta_w = r\cos\theta \tag{2.4}$$

where θ is the equilibrium contact angle on a smooth surface, θ_w is the apparent contact angle on a rough surface (generally known as Wenzel angle) and *r* is the average roughness ratio, the factor by which roughness increases the solid-liquid interfacial area.

From this equation, it can easily be deduced that for any equilibrium contact angle less than 90^o, the apparent contact angle will decrease with increase in roughness, and vice versa.

2.5.1.1 Effect of surface roughness on hysteresis

Kandlikar and Steinke [77] observed the interfacial behaviour of deionized (DI) water on copper and stainless steel to investigate the effect of surface roughness and surface temperature on advancing and receding contact angles. The value of the static equilibrium contact angle was found to lie between the limits of the values of the corresponding advancing and receding contact angles for each condition of the copper substrate surface

roughness used in the study. The highest equilibrium contact angle was obtained with the smoothest surface in both stainless steel and copper. However, in the case of copper, as the surface roughness increased further, the contact angle was observed to go up again.

It is worth mentioning the fact that, in reactive wetting systems, the asperities and grooves associated with surface roughness may act as preferable sites for reaction and adsorption. Hence, the effect of surface roughness on wettability might be confounded with that of other factors [44].

Hysteresis of a Wenzel drop (a drop that wets the groove of a rough surface) on a rough hydrophobic surface made of polydimethylsiloxane (PDMS) was studied by He *et al.* [48]. The experiments were conducted to measure both the advancing and receding contact angles. The advancing contact angle for the Wenzel drop on the rough surface was found to lie between 142 and 143°. However, no conclusion could be drawn regarding the receding contact angle of a Wenzel drop because the apparent contact angle kept decreasing with decreasing droplet size down to the smallest drop volume that could be handled. They [48] predicted the advancing contact angle of the Wenzel drop using the Wenzel's formula in the form of:

$$\cos\theta_{adv}^{w} = r\cos\theta_{adv}^{f} \qquad (2.5)$$

where *f* is the area fraction of the peaks of the square pillars on the horizontal surface, subscript *'adv'* denotes advancing angle, *w* denotes a wetted contact area and *r* is the solid roughness, defined as the ratio of the actual solid-liquid contact area to the contact area projected on the horizontal plane.

Equation 2.5 gave the value of θ_{adv}^{w} as 149°.

2.5.2 Heterogeneity of the surface

The equilibrium contact angles are influenced by, among other factors, any surface impurities that may be present on the liquid-vapour interface or the solid surface [78]. Many materials of practical interest are multi-phase solids with heterogeneous surfaces [79]. Cassie extended Wenzel's treatment of rough surfaces to heterogeneous surfaces by deriving an important equation, analogous to Wenzel's, for such surfaces as [44, 79, 80]:

$$\cos\phi = \sigma_1 \cos\theta_1 + \sigma_2 \cos\theta_2 \quad (2.6)$$

where ϕ is the contact angle on the heterogeneous surface, σ_1 is fraction of the surface having the intrinsic contact angle θ_1, and σ_2 is the fraction of the surface having the intrinsic angle θ_2.

2.5.2.1 Effect of surface heterogeneity on contact angle hysteresis

He *et al.* [48] equally quantified the hysteresis of a Cassie drop (a drop that sits on the peak of the surface roughness) on a rough PDMS surface by measuring the advancing and receding contact angles. An advancing contact angle between 152 and 153° was observed experimentally for a Cassie drop on the rough substrate. The corresponding receding contact angle for the Cassie drop was found to be about 132°. They [48] predicted the advancing contact angle of the Cassie drop using Cassie formula of the form:

$$\cos\theta_{adv}^{c} = f\cos\theta_{adv}^{f} + f - 1 \quad (2.7)$$

where *c* represents composite contact, *f* is the area fraction of the peaks of the square pillars on the horizontal surface and subscript *'adv'* denotes advancing angle.

Using equation 2.7, a value of 153.5° was obtained for θ_{adv}^{c}.

They [48] also estimated the receding contact angle of the Cassie drop using an equation of the form:

$$\cos\theta_{rec}^{c} = f\cos\theta_{rec}^{f} + f - 1 \quad (2.8)$$

where *rec* represents receding angle.

An estimated value of 143º was obtained for θ_{rec}^{c} from equation 2.8. They [48] equally estimated the receding contact angle of the Cassie drop using a model proposed by Patankar [81]. A value of 127.6^0 was obtained for θ_{rec}^{c}, which was much more close to the experimental value. It must be noted that in the model proposed by Patankar [81], the droplet was assumed to leave a thin film of liquid behind on the peaks of the pillars of the surface roughness as against leaving behind a dry surface as assumed in equation 2.8.

2.5.3 Atmosphere

The surface tension of liquid metals is very sensitive to impurities and, in particular, to the oxygen concentration in the liquid phase [82]. If the liquid filler metal is to wet and flow over the base metal, any intervening oxide layers must be removed. Three methods are used in practice to reduce and control the formation of oxide layers in wettability studies: fluxing with molten salts, heating in a reducing atmosphere and heating in a vacuum [19, 83].

Takao *et al.* [84] investigated the effect of fluxes (ULF-300R and PO-Z-7) on the ability of Sn-3.5Ag to wet Cu substrate at 270ºC. UFL-300R is a more activated flux containing halogen while PO-Z-7 has no halogen. For UFL-300R, a final contact angle *(θ)* and interfacial liquid-flux tension *(γ_{lf})* of 38º and 0.406 N/m were obtained, respectively. While for PO-Z-7, the values of θ and $\gamma_{lf,}$ were reported to be 43º and 0.470 N/m, respectively.

The relative decrease of 5° in the contact angle was attributed to the relative 0.064 N/m decrease in γ_{lf} values of the two fluxes. López and Kennedy [18] investigated the effect of a K-Al-F-based flux on the spreading of Al on TiC, at temperatures up to 900°C, in Ar and in air. They reported that, while obtuse contact angles were observed without flux, the flux facilitated rapid spreading to a perfect wetting condition, in both Ar and air.

In all cases involving the use of reducing atmosphere, the active reducing constituent is hydrogen or carbon monoxide [19]. For a few metals, hydrogen is satisfactory as a reducing atmosphere [12]. However, practical limits are set to the use of hydrogen reduction. These are, firstly, in techniques for drying the gas, and secondly, in keeping it dry because it takes up moisture from the surfaces of the tubes through which it passes into the test chamber [83].

For high-temperature service alloys like Ti-6Al-4V, the use of flux for brazing might not be very satisfactory, because it can become pervious to oxygen at this high brazing temperature [85]. For these particular alloys, heating in a vacuum has been found satisfactory to obtain a clean surface [19]. Also, the cleanliness that will be obtained by heating in a vacuum atmosphere is expected to better than that of a hydrogen atmosphere [86]. Beaton set the maximum brazing pressure for Ti at 1000°C, in a vacuum, between 10^{-1} and 10^{-4} mmHg [85].

2.5.4 Temperature

The wetting behaviour of a liquid on a solid is sensitive to temperature changes, as temperature affects a number of properties of liquid such as viscosity and surface tension [87].

Samarasekara and Munir [88] investigated the contact angles formed by liquid tin, indium and gallium on zirconium and niobium over temperature range of 303-923 K. They observed three characteristic regions of the temperature dependence of contact angles. A steady-state region in which θ was relatively independent of temperature, was preceded and followed by regions in which θ decreased rapidly with increasing temperature.

An experimental investigation into contact angle temperature dependence of water droplets on practical aluminum surfaces was carried out by Bernardin *et al*. [78]. They observed two distinct temperature-dependent regimes. In the lower temperature regime, below 120^{o}C (surface temperature), a relatively constant contact angle of 90^{o} was observed. While in the high temperature regime, above 120^{o}C, the contact angle decreased in a fairly linear manner. It is worth noting that, they [78] used a pressure vessel to increase the water temperature up to 170^{o}C.

Feduska [89] studied the reactions between five high-temperature base metals and six high-temperature brazing alloys in three different atmospheres at nominal and superheat brazing temperature levels. He [89] observed that the wettability of the substrates by the brazing alloys decreased as the brazing temperature was increased above the nominal level. This trend was attributed to an increase in reactivity between the brazing alloy elements and the base metal at the higher brazing temperature.

Also, contact angle of pure aluminum on the surface of polycrystalline alumina substrate was studied in the temperature range of 750-1100^{o}C by Sangghaleh and Halali [90]. In this system, the contact angle was observed to reduce with increasing temperature. In

temperatures in excess of 1050°C, the behaviour of the system changed from non-wetting to wetting.

With reference to the works of López and Kennedy [18], the spreading process was seen to exhibit a temperature dependency. The spreading time was considered to follow an Arrhenius behaviour [4] of the form:

$$\frac{1}{t_0} = Kexp(-\frac{E_a}{RT}) \quad (2.9)$$

where t_0 corresponds to the spreading time, E_a is the apparent activation energy of the process, R is the universal gas constant, T is the absolute temperature, with K being a pre-exponential constant.

2.5.5 Alloying elements

Yang *et al*. [91] investigated, in detail, the effects of Ni and Cr contents and wetting temperatures on the wettability and the wetting mechanisms of copper on tungsten substrate. The results showed that the wetting angles of Cu on the W substrate decreased with an increase in the content of Ni or Cr, and also decreased with increase in the wetting temperatures.

Equally, wettability at a liquid Al alloy/SiC interface was evaluated by the sessile drop method at 750°C by Candan [92]. The wetting angle, θ, of the sessile drop on SiC substrate was equally reported to decrease with the addition of Pb, Mg and Ca to pure Al. The reduction in θ, obtained with the Al-Pb alloy drop, was proportional to the reduction in surface tension, γ_{lv}, of Al. For Al-Mg and Al-Ca alloys, the reduction in θ was greater than

the reduction in γ_{lv} of Al. The reduction in contact angle was attributed to reactions that took place at the Al-alloy/SiC interface.

Yu *et al.* [93] studied the interfacial microstructure and wetting property of Sn-Zn-Cu solders with Cu substrate. They reported that wettability improved remarkably with increasing Cu content in the solder. This was attributed to the reduction in the surface tension of the liquid solder.

2.6 Marangoni convention

In reactive wetting systems where there is alloying between the chemical species of the liquid and the solid substrate, there is a likely tendency for solute-capillary effect, if the difference in surface tension between the two chemical species is large [49, 71]. In the early stages of reactive regime in wetting, where there is dissolution of the substrate into the liquid droplet, the concentration of the solute is usually larger at the contact line/solid-liquid interface than at the top of the droplet [94]. This concentration gradient is likely to set up a solute-capillary flow. The presence of this effect was demonstrated in the spreading of pure Cu and saturated Cu-Si drops on pure Si substrate, after 50 ms from the initiation of wetting, as shown in Figure 2-4 [49]. This observation was related to the fact that the surface tension of pure Cu (1280 $mN.m^{-1}$) is higher than that of saturated Cu-Si solution (840 $mN.m^{-1}$) at 1100°C. The effect of early dissolution of Si into the drop at the contact line reduces the surface tension at the contact line relative to that at the top of the drop. Therefore, spreading was retarded at this stage. On the other hand, spreading will be accelerated if the surface tension of the solute is higher than that of the liquid [71].

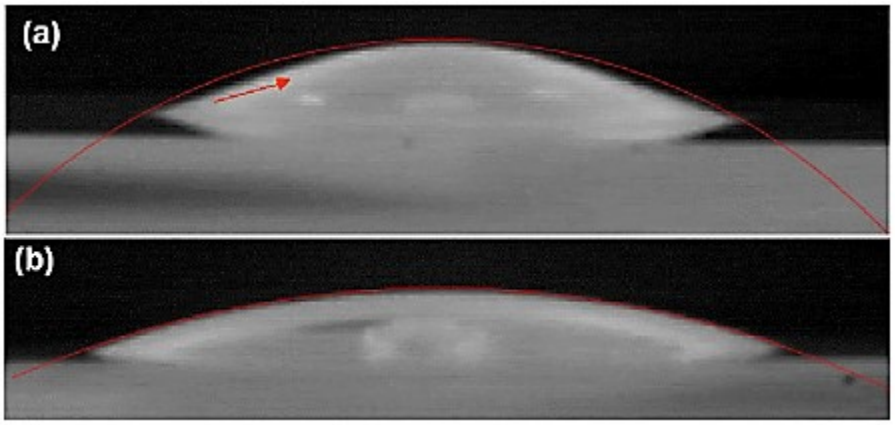

Figure 2-4. Spreading of (a) pure Cu (b) saturated Cu-Si on Si substrates after 50 ms [49].

2.7 Non-reactive wetting

When a liquid spreads on a dense and non-porous solid substrate without any reaction, it is referred to as a non-reactive or an inert wetting [95]. For this kind of system, the interface remains flat and unchanged materially [50]. The system is in chemical equilibrium and the degree of wetting is determined by the Young's equation for a flat and non-deformable solid [42]. Also, the spreading time for a metallic millimeter sized droplet in a non-reactive system in which the equilibrium contact angle value is higher than 20^{o} is reported to be less than 10^{-1} s [71, 96]. For the case of complete wetting of a solid surface by a liquid, wetting dynamics are reportedly dominated by a precursor film which spreads ahead of the main body of fluid [17, 38]. A precursor film can either be a bulk liquid phase identical to the drop phase or an adsorption layer [59].

Contact line motion is normally correlated with the dynamic contact angle to describe the kinetics of a wetting system using both theoretical (hydrodynamic, molecular kinetics and combined hydrodynamic-molecular kinetics) and empirical approach [22].

For droplet spreading, where the effect of gravitation is minimal, the macroscopic shape of the droplet is found to be close to a spherical cap [17, 97]. In the case of complete wetting, the shape of the drop is circular, and at late times of spreading the flow dynamics can be described by Tanner's law [98, 99]:

$$\frac{r}{R} \sim \left(\frac{\gamma t}{\eta R}\right)^{1/10} \tag{2.10}$$

where r is the instantaneous radius of the wetted area, R is the initial radius of the drop at the start of spreading, t is time, η is viscosity of the liquid and γ represents the liquid surface tension.

Tanner's law does not apply to early stages of spreading where the shape of the drop is completely different (high curvature at the contact line) from that at late time [30]. At short time of spreading, Biance *et al.* [97] reported the presence of an inertial regime in the spreading drop of water on glass plate. The duration of this regime was found to be in the order of 1 ms for a millimetric water drop and the wetting rate followed a square root growth of the form:

$$r^2(t) \sim \sqrt{\frac{\gamma R}{\rho}}\, t \tag{2.11}$$

where ρ represents the density of the liquid.

The characteristic time or duration of this inertial regime was found to be mainly dependent on the drop size.

In partial wetting experiment of different water-glycerol mixtures on solid surfaces with various degree of wettability, early-time inertially dominated wetting was also reported [39]. The spreading dynamics was fit with a power law in the form of:

$$r/R = C(t/\tau)^{\propto}, where\ \tau \equiv \sqrt{\rho R^3/\gamma} \tag{2.12}$$

where C is a prefactor and $\propto$ is an exponent.

They [39] found that for low equilibrium angles (θ_e < 10°), $\propto \approx 0.5$, and the spreading dynamics is similar to that of complete wetting. However, both $\propto$ and C were found to decrease with increase in contact angle.

In the short time dynamics of viscous drop spreading investigated by Eddi *et al.* [30], however, spreading did not follow a pure power-law growth. The spreading velocity was, instead, found to decrease logarithmically in time and the dynamics was reported to be identical to that of coalescing viscous drop. The initial stage of wetting was also found to be independent of the substrate wettability. The effective exponent for coalescence was derived as:

$$\propto = \frac{\ln\frac{r}{R}}{\ln\frac{r}{R} - 1} \tag{2.13}$$

Lavi and Marmur [22] investigated the partial spreading of organic liquids on coated silicon wafer. They suggested an exponential power law for the kinetics in systems with partial wetting as:

$$\frac{A}{A_f} = 1 - \exp(-\frac{K}{A_f}\tau^n) \tag{2.14}$$

Where A is the normalized and dimensionless drop base area, A_f is the final, equilibrium value of the normalized wetted (solid-liquid) area, τ is the dimensionless time, and K and n are empirical constants.

Another empirical model for describing the mobility relations of partially wetting systems is [72]:

$$\frac{\cos\theta_0 - \cos\theta_D}{\cos\theta_0 - 1} = \tanh(4.96Ca^{0.702}) \quad (2.15)$$

where Ca is the capillary number (ratio of viscous force to surface tension force), while θ_0 and θ_D represent the static and dynamic contact angles, respectively. There are other relevant works that have been done on non-reactive wetting [62, 100-110].

2.8 Reactive wetting

This type of wetting is characterized with dissolution of the substrate and/or formation of intermediate compounds at the liquid alloy-substrate interface [49]. The wetting kinetics, in this case, is controlled not by viscous dissipation but by the rate of interfacial reaction and the spreading time is reported to be in the range of 10^1-10^4 s [67, 70, 96, 111-113]. Reactive wetting is very important in metal-metal joining processes, such as brazing and soldering.

The main difference between wetting in purely dissolutive systems and wetting in compound forming systems is the formation of intermetallic compounds in the latter, which tend to arrest the spreading at the triple line (solid-liquid-vapour interface) [69]. Interfacial reactions have often been suggested to lead to the reduction of the corresponding interfacial

energy, and attempts have been made to relate the degree of wetting with the free energy of interfacial reactions by replacing the γ_{sl} term in Eq. 2.1 by [114]:

$$\gamma_{sl}(t) = \gamma_{sl} + \Delta G_r(t) \tag{2.16}$$

where $\Delta G_r(t)$ corresponds to the change in Gibbs energy released per unit area by the reaction in the "immediate vicinity of the solid/liquid interface" [114].

2.8.1 Purely dissolutive reactive wetting

This kind of wetting is synonymous with high degree of dissolution of the substrate in the molten alloy, leading to a non-planar solid-liquid interface [72]. It occurs not only in metal/metal systems, but also in metal/ceramic systems [115]. In this kind of wetting, the contact angle that is observed at the macroscopic level is called apparent contact angle [44, 49].

Protsenko *et al.* [51] studied the wetting of single crystal silicon wafers (0 0 1) by pure copper and silicon-saturated CuSi alloy, using the dispensed drop technique at 1100ºC under high vacuum. This was done to investigate both dissolutive (non-equilibrium) and non-reactive (equilibrium) wetting for the same system. The spreading time for the non-reactive CuSi/Si was observed to take place in a few milliseconds with an average final visible contact angle of 19 ± 3º. In the Cu/Si system, wetting occurred in two different stages. In the first stage (non-reactive), a visible contact angle close to 40º (angle formed by pure Cu on nearly unreacted Si) was observed after a few milliseconds. The second stage (dissolutive) led to the formation of a visible contact angle of 5º on a non-planar interface within 1-2 s. This second reactive or dissolutive stage was subsequently broken down into two steps. The first step involved the decrease of the contact angle from 40º to

19°, which is formed on Si by Si-saturated copper. This angle decrease took place rapidly in about 40 ± 10 ms. At this point, the solid Si was reportedly in equilibrium with the liquid at the solid-liquid interface but not in equilibrium with the bulk liquid. The implication of this is that dissolution rate at the solid-liquid interface was higher than the transport rate of the Si atoms from the interface to the bulk liquid. The second reactive step led to the decrease of the visible contact angle from 19° to 5°, coupled with the formation of a crater at the interface. The variation of the drop base diameter and visible contact angle with time, on a logarithmic scale, is shown in Figure 2-5 [51]. It is important to know that Protsenko *et al.* [94] obtained similar result on (1 1 1) Si wafers.

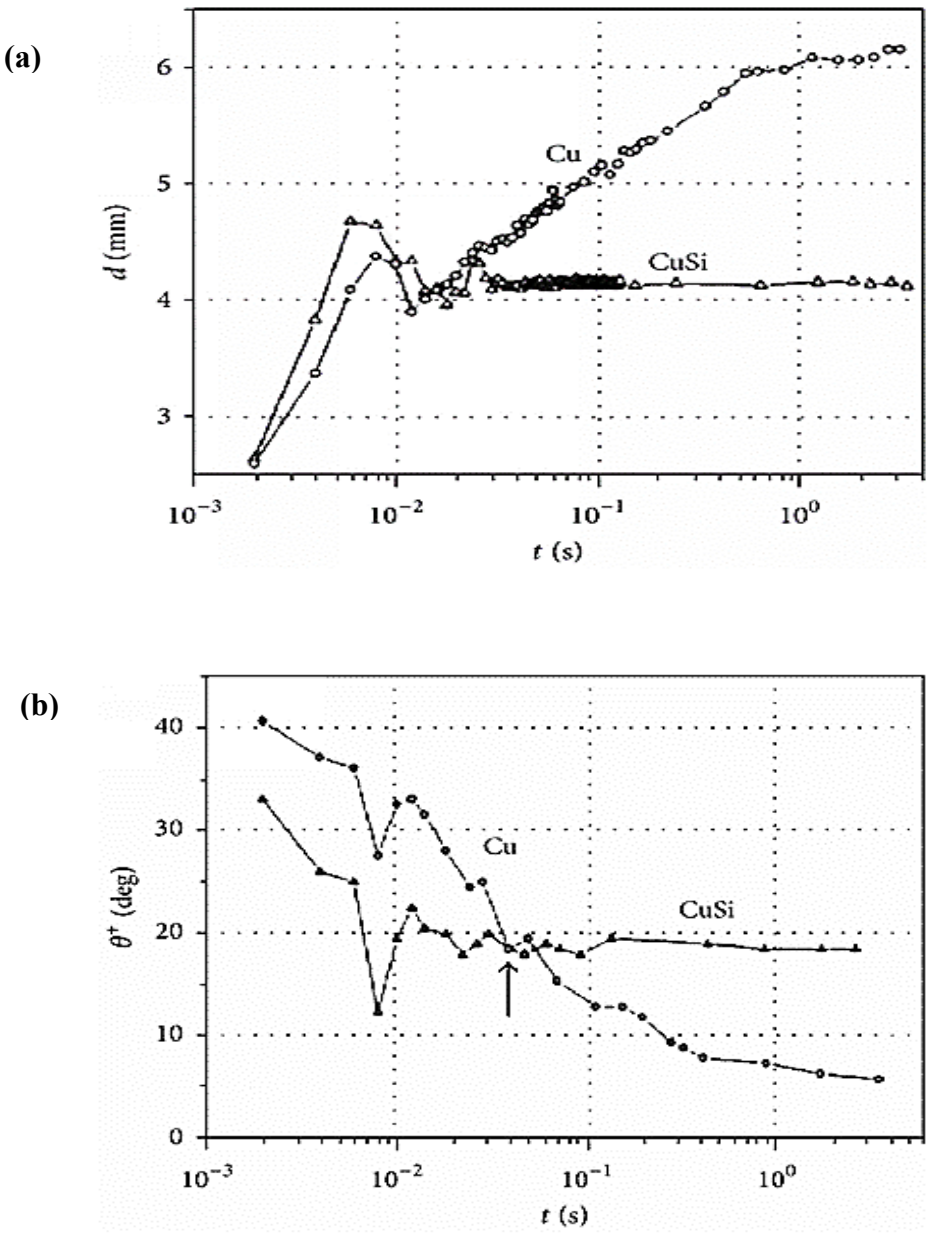

Figure 2-5. (a) Drop base radius and (b) visible contact angle as a function of time plotted on a logarithmic scale for Cu and Cu pre-saturated in Si on a (0 0 1) Si surface at 1100ºC [51].

Recently, an interesting study was made into the wetting of Ag-Cu alloys on Cu substrates at 900ºC, using dispensed drop technique [71]. Equilibrium and non-equilibrium systems were considered by using Cu-saturated and non-Cu-saturated liquid. The plotted variation

of the drop base diameter, d, and contact angle, θ, with time on a logarithmic scale is shown in Figure 2-6 [71].

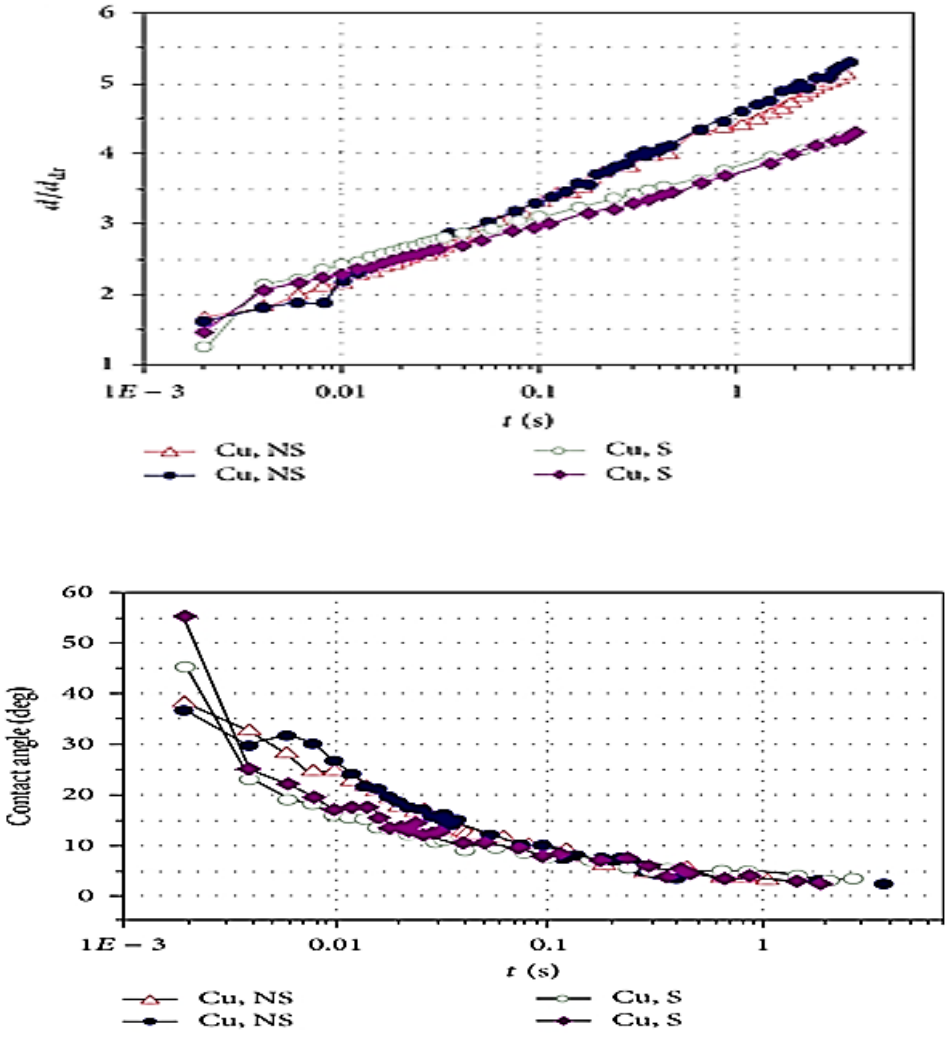

Figure 2-6. Normalised drop base diameter (a) and contact angle (b) as a function of logarithm of time for two saturated (S) and two non-saturated (NS) Ag-Cu drops spreading on monocrystalline Cu at t < 4 s [71].

For both the equilibrium and non-equilibrium systems, the spreading curves were nearly overlapping up to 20 – 30 ms. Based on this observation, the early stage of wetting was described as non-reactive, suggesting the absence of dissolution and its effects in the non-

equilibrium system at this stage. However, after 30 ms, the spreading of the non-Cu-saturated drop became faster than the Cu-saturated drop. This observed faster spreading in the non-equilibrium system was attributed to the dissolution of Cu into the Ag-Cu alloy. In both cases, the spreading time exceeded 100 s. This observed long spreading time in the equilibrium Ag-Cu/Cu system is unusual, considering the lack of any significant reaction between the solid and liquid phases. The long spreading time observed in the equilibrium system was attributed to the very low equilibrium contact angle, about 1°, of the system.

Three distinct spreading stages were observed in the non-Cu-saturated system, as shown in Table 2-1 [71]. The highlight of this is the presence of non-reactive spreading both before and after the dissolutive stage. Schematic representation of the spreading stages for both non-equilibrium and equilibrium Ag-Cu/Cu systems are shown in Figure 2-7 [71].

Table 2-1. Spreading regimes in non-equilibrium Ag-Cu/Cu system [71].

Time interval (s)	**Drop base diameter (d/d_{dr}) evolution**	**Spreading regime**	**Average spreading rate (m/s)**
0-0.03	0-2.6	Non-reactive	10^{-1}
0.03-1	2.6-4.6	Dissolutive	10^{-3}
1-100	4.6-7.3	Diffusion into the solid	10^{-5}

T = 900 °C

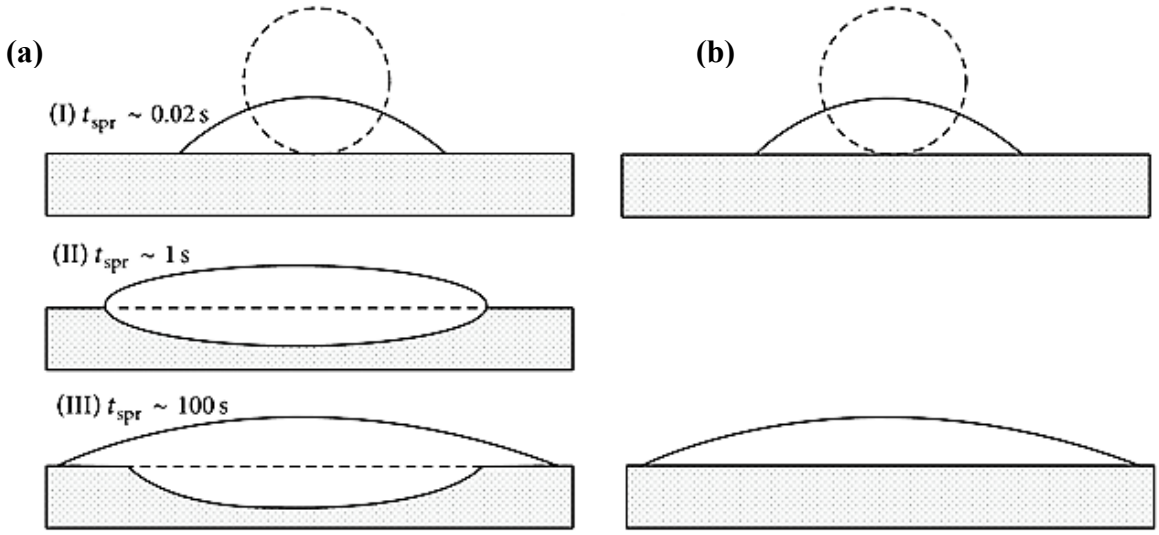

Figure 2-7. Schematic representation of spreading stages in (a) Non equilibrium (b) Equilibrium Ag-Cu/Cu systems [71].

2.8.2 Compound forming systems

One way of improving the wetting of a substrate by a metal is to alloy such a metal with chemical species that react with the substrate to form a reaction product that is more wettable than the original substrate [67, 70, 91, 113]. One of the earliest efforts towards understanding this type of reactive wetting was made by Aksay *et al.* [42], using a thermodynamic approach. They [42] concluded that under chemical non-equilibrium, mass transfer across the interface leads to a transient decrease in the corresponding interfacial energy.

Landry and Eustathopoulos [111] made a significant contribution towards understanding this reactive wetting by relating the experimentally obtained wetting radius, *R(t)*, curves for Al/C_v with the mechanism of growth of the interfacial reaction product (Al_4C_3) at 1100 K. The main feature of the *R(t)* curve was the presence of a nearly linear spreading

region/regime during which the liquid/solid interface was completely covered by a layer of Al_4C_3. The wetting kinetics was suggested to be controlled by the kinetics of lateral growth of Al_4C_3 at the triple line.

Also, in the experimental study of wetting of Cu-Si alloys on carbon substrate [114], linear spreading was observed. A 3-step change in contact angle and base radius was noticed. Spreading was described as rapid in the first stage, before slowing down significantly in the second stage (linear spreading regime). The drop radius and contact angle remained steady in the third stage. The presence of a continuous layer of silicon carbide was noticed at the solid/liquid interface.

The concept of diffusion-limited reactive wetting was introduced in 1999 by Voitovitch *et al*. [67], in the study of the spreading kinetics of Cu-Cr alloys on carbon. A dense reaction layer, Cr_7C_3, was formed at the solid/liquid interface, with the thickness depending on Cr concentration and the time of holding. The observed triple line velocity was not constant with time, it was found to be a function of the contact angle. A final contact angle of 40^o was observed, which was reported to be nearly equal to the contact angle of Cu-Cr alloy on a substrate of chromium carbide. The diffusion of chromium to the triple line was concluded to be the rate limiting factor in the spreading kinetics of Cu-Cr/C system.

2.8.3 Non-reactive stage in reactive wetting

Different stages have been observed in different reactive systems [23, 51, 70, 71, 96, 114, 116]. However, there has been a common observation, among researchers, of the existence of a non-reactive stage at the onset of this wetting. This particular stage is said to be characterised with fast spreading with no reaction with the substrate, thereby leaving the

solid/liquid interface in its original flat state. However, until recently, there was no physical proof of this due to lack of in-situ and real time observation of the solid/liquid interface.

Yin *et al.* [49] performed experimental investigation into dissolutive wetting of Bi-Sn system in Hele-Shaw cells. The obtained results, as shown in Figure 2-8 [49], tend to support the presence of this non-reactive stage at the onset of reactive wetting. At the early stage of wetting (less than 100 ms), no change in the solid/liquid interface was observed.

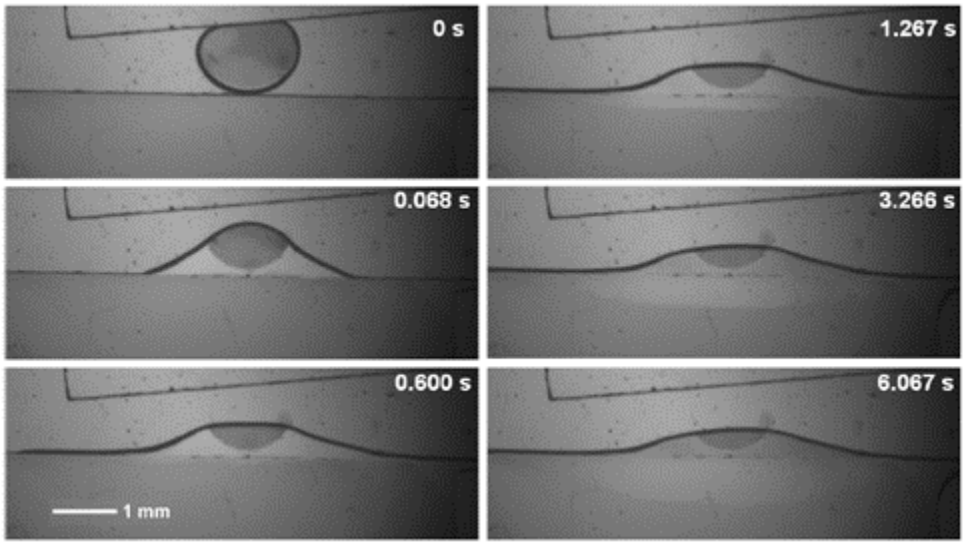

Figure 2-8. Images of a pure Sn drop wetting pure Bi in a Hele-Shaw cell at different time intervals [49].

2.9 Cold wetting

Application of hysteresis phenomenon and reactive wetting to liquid droplets spreading on solid surfaces is well documented in the literature [117-121]. A surface having primarily polar groups will have a strong affinity for water and a low contact angle will be formed on it by water. Such a surface is referred to as being hydrophilic [45]. On the other hand, if the surface is made up of non-polar groups, a large contact angle will be formed on it by

water and such a surface is termed hydrophobic [45]. The idea of free and rapid motion of liquid droplets on solid surface is essentially based on the ability of a liquid to modify a hydrophilic surface by some reactive mechanism and render it hydrophobic. The droplet would then be out of equilibrium between the hydrophilic surface it meets at the front and the hydrophobic trail it leaves behind; thereby, leading to a free running droplet [118].

Chaudhury and Whitesides [121] equated the unbalanced force experienced by a drop placed on a surface with gradient in surface tension, as shown in Figure 2-9 [121], to the unbalanced Young's force (dF_Y), as given in Equation 2.17 [121].

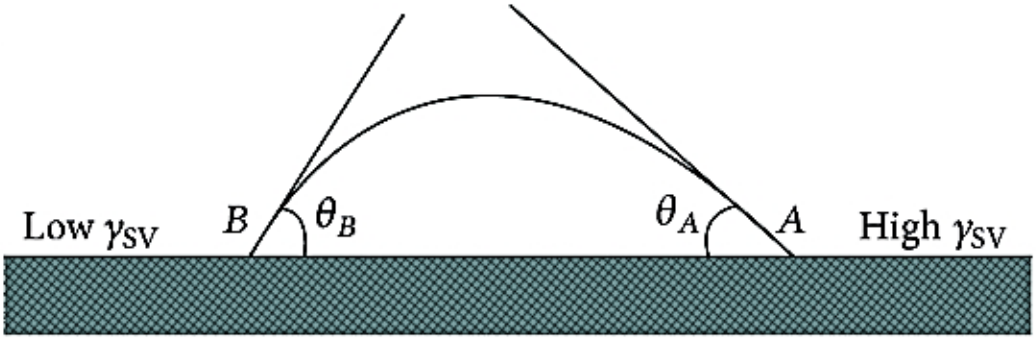

Figure 2-9. Idealized diagram of a thin cross section of a liquid drop on a gradient surface [121].

$$dF_Y = [(\gamma_{SV} - \gamma_{SL})_A - (\gamma_{SV} - \gamma_{SL})_B]dx \quad (2.17)$$

where *dx* is the thickness of the section of the drop.

In terms of contact angles at point A and B, the unbalanced Young's force was represented as:

$$dF_Y = \gamma_{LV}(\cos\theta_A - \cos\theta_B)dx \quad (2.18)$$

They [121] stated that the presence of gradient in surface tension only on a solid surface, is not sufficient to ensure motion of liquid drops; the surface must also have low hysteresis in contact angles and be free of defects that can pin the edge of the drop. By producing gradients in chemical compositions and surface tension on solid surfaces through silanization reaction, they [121] were able to cause 1-2 µl drops of water to move up a 15° slope along the direction of increasing surface free energy with average velocities of 1 to 2 mm/s.

Bain *et al.* [117] put to test the concept of reactive flow of liquid droplet on solid surface by experimenting with a drop of decane containing a fluorinated fatty acid, $CF_3(CF_2)_6CO_2H$ (PFOA) on an ordinary glass microscope slide inclined at an angle of 43° to the horizontal. The drop was observed to flow up the slide as shown in Figure 2-10 [117].

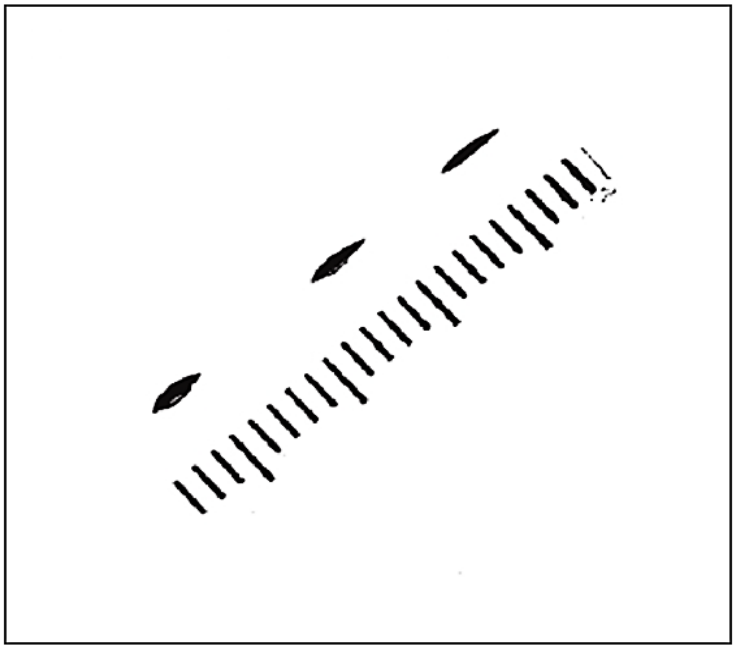

Figure 2-10. Photograph of a 2-µl drop of decane containing 1.5mM pentadecafluorooctanoic acid (PFOA) flowing up a glass microscope slide inclined at an angle of 43° from the horizontal [117].

The chemistry occurring at the surface of the glass was identified to be the key behind this behaviour. The PFOA was reported to adsorb from decane to form an oriented monolayer attached to the glass through the carboxylic acid group. The outer surface of the monolayer allegedly consists of oil-repelling CF_2 and CF_3 groups. While decane beads up on a fluorinated surface because of its lower surface energy, it spreads on a clean surface of glass.

The idea of reactive wetting in free-running droplet was also established by Dos Santos and Ondarçuhu [118]. They experimented with the flow of droplets of *n*-alkanes (*n*-octane and *n*-dodecane) containing 1H,1H,2H,2H-perfluorodecyltrichlorosilane on a glass surface. They reported that the silane molecules can form dense grafted monolayers on silicon or glass, thereby rendering the surface hydrophobic. Two types of droplets were used for the experiment, based on the capillary length ($\kappa^{-1} = (\gamma/\rho g)^{1/2}$, γ is the surface tension of the liquid; ρ is its density). After dropping the droplet on the glass surface, motion was initiated by pushing it with a pipette. The droplet was observed to move on the substrate. and the self-supporting movement ended only when the droplet had no more hydrophilic surface available. The movement was equally observed on an inclined substrate with the droplet running uphill. For droplets with length smaller than the capillary length, they were observed to move with constant velocity V and constant length L. When the silane concentration of the small droplets was changed, the velocity initially increased with increase in concentration before reaching a saturation level at high concentrations, as shown in Figure 2-11 [118].

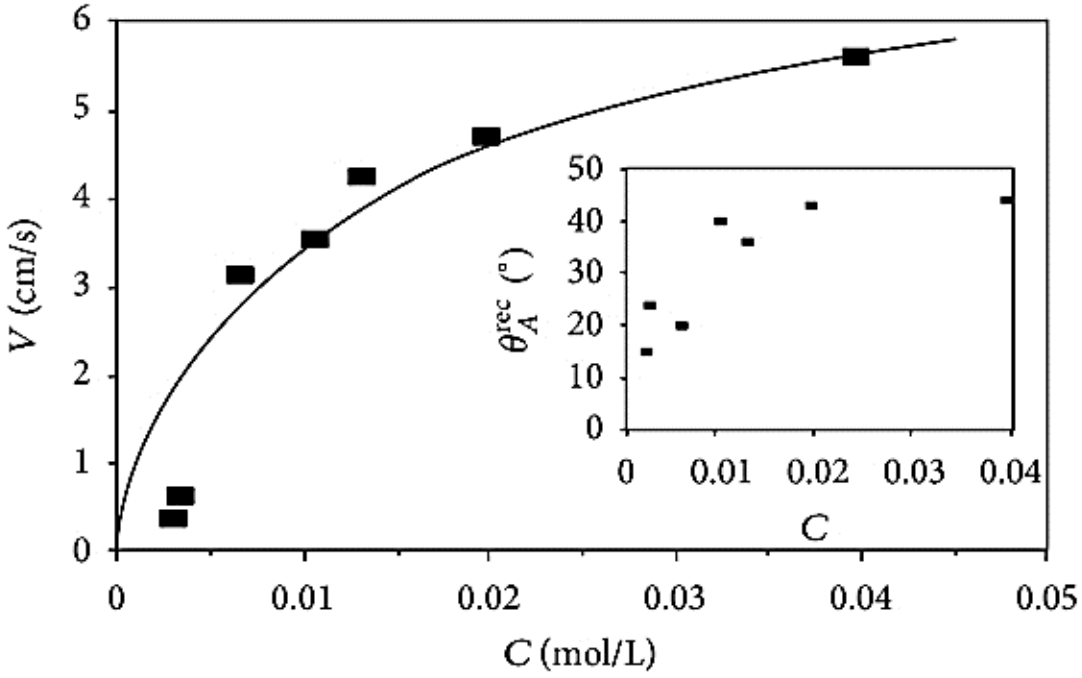

Figure 2-11. Plot of the velocity of octane droplets of length L = 3.5 mm as a function of the concentration in silane. Inset: Receding contact angle of a pure octane measured on the hydrophobic trail left by the same droplets [118].

There are other important contributions to the field of liquid cold wetting [122, 123].

2.10 Modelling of kinetics of reactive systems

Due to the lack of thorough understanding and complexity of reactive wetting systems, there is still no single model that is generally applicable to all reactive systems.

In the Cu/Si system studied by Protsenko *et al.* [51], the wetting rate was modelled by an equation of the form:

$$U = \frac{4}{3\theta_Y^2} \cdot \frac{D}{\delta}(\theta^+ - \theta_F^+) \quad (2.19)$$

where θ_Y, θ^+, θ_F^+ and $\frac{D}{\delta}$ represent Young's contact angle, instantaneous visible contact angle, final visible contact angle and mass transport parameter, respectively.

When the transport of Si in the liquid was assumed to be purely diffusion based, the experimental data fit the equation well but with a much higher than usual value for the diffusion coefficient, indicating that the diffusion coefficient lost its physical meaning and became an adjustable parameter.

Also, Kozlova *et al.*[71] reported that the spreading kinetics of saturated Ag-Cu alloy on Cu followed the relation:

$$R^n \sim At \tag{2.20}$$

where R represents the droplet base radius, t is the time, n and A are empirical constants.

The diffusion-limited spreading kinetics of Cu-Cr/C_v was equally described with an equation of the form [67]:

$$\frac{dR}{dt} = \frac{2DF_{(t)}}{en_v}(C_0 - C_e)\theta \tag{2.21}$$

where D is the diffusion coefficient in the liquid phase, n_v is the number of moles of reactive solute per unit volume of the reaction product, e is the reaction thickness at the triple line, $F_{(t)}$ is the dynamic spreading force, C_o is the bulk drop concentration, and C_e is the concentration of the reactive solute at the triple line.

However, the experimental results obtained for this system, Cu-Cr/C_v, disagreed with this model. The intercept of the line described by Eq. 2.21 should be at $\theta = 0$. But for this system, it was at finite angle of 40°. Eq. 2.21 was based on the assumption that all solute flux is consumed by the reaction at the triple line, therefore neglecting any thickening of

the reaction layer behind the triple line. This was cited as the reason for the disagreement between the model and the experimental results for this system [96]. On the other hand, experimental results obtained for CuSn-Ti/C_V system was successfully modelled by the equation [96].

For reaction-limited spreading, Dezellus *et al.* [70] suggested that instantaneous contact angle, *θ(t),* could be defined by the relation:

$$\cos\theta_F - \cos\theta = (\cos\theta_F - \cos\theta_0).\exp(-kt) \tag{2.22}$$

with k being the kinetic constant.

For liquid droplet spreading in cold wetting systems, Raphaël [124] showed that for an ideal surface, the droplet will reach a constant velocity given by:

$$V = \frac{\gamma}{6l\eta}\tan\theta^*(\cos\theta_{Pe} - \cos\theta_{Ae}) \tag{2.23}$$

where γ is the surface tension of the liquid, η is its viscosity, l is a logarithmic factor ($l = \ln {x_{max}}/{x_{min,}}$ the ratio of macroscopic and molecular lengths), θ_{Pe} is the equilibrium angle on the hydrophilic surface (P), θ_{Ae} is the equilibrium angle on the hydrophilic surface (A) and θ^* is the dynamic contact angle of the droplet given as:

$$2\cos\theta^* = \cos\theta_{Ae} + \cos\theta_{Pe} \tag{2.24}$$

Dos Santos and Ondarçuhu [118] applied Eqn. (2.23) and (2.24) to real surface by replacing θ_{Pe} and θ_{Ae} by θ_P^{adv}(advancing contact angle on P) and θ_A^{rec}(receding contact angle on A), respectively and they succeeded in fitting the obtained experimental results.

For a droplet with size lesser than the capillary length; Brochard and de Gennes [125] presented a model predicting the steady state velocity V as a function of the drop size L, while incorporating the reaction kinetics as:

$$L = V\tau \ln\left(\frac{V_1}{V_1 - V}\right) \tag{2.25}$$

$$V_1 = \frac{\gamma_1 \theta^*}{6l} \tag{2.26}$$

where τ is the reaction time and γ_1 is a constant.

2.11 Wetting of titanium alloys by brazing filler metals

The dynamic wetting behaviour of pure silver on Ti-6Al-4V was studied by Chan and Shiue [7]. Using a near spherical ball of 0.12 g in weight, the dynamic wetting experiment was performed in a vacuum furnace at a temperature range of 1000 – 1050ºC for 1800 s. Based on the result of the dynamic angle measurement at test temperature of 1000ºC, as shown in Figure 2-12 [7], the pure molten silver could not wet Ti-6Al-4V until after 1200 s. However, at 1050ºC, complete spreading of molten silver on the substrate was obtained in about 600 s.

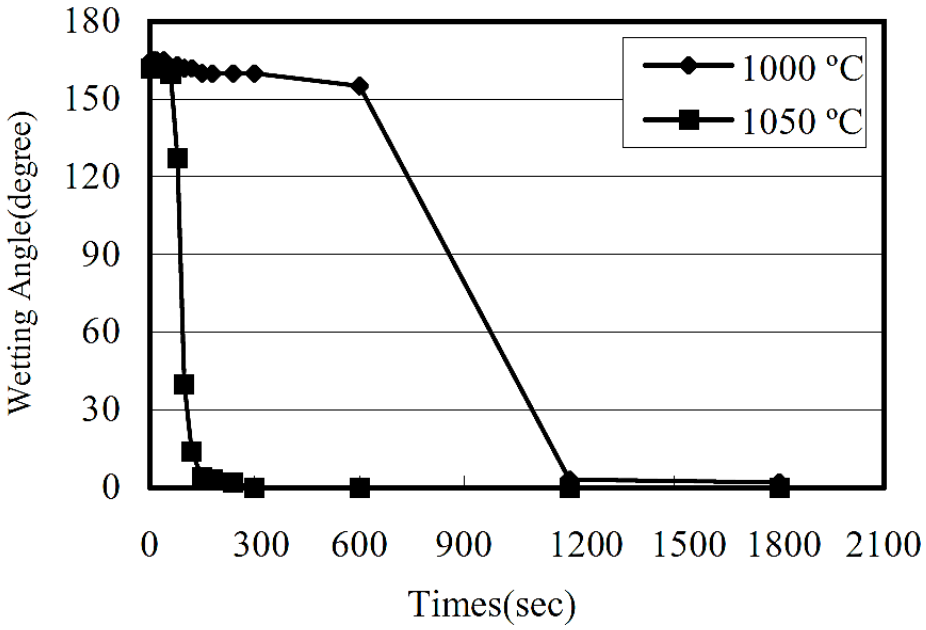

Figure 2-12. The dynamic wetting angle of pure Ag on Ti-6Al-4V substrate [7].

Dynamic wetting angles of Braze 580 (Ag-33Cu-7Sn-3Mn, wt%), BAg-8 (Ag-28.1Cu, wt%) and Ticusil® (Ag-26.7Cu-4.5Ti, wt%) on Ti-6Al-4V substrates were measured by Liu *et al.* [126]. Each test was conducted for 1800 s in a vacuum atmosphere using 0.15 g of the brazing alloy. Good wetting of Ti-6Al-4V by Braze 580, BAg-8 and Ticusil® brazing alloys could not be obtained until about 860°C, 840°C and 880°C, respectively. Graphical representation of the results is shown in Figure 2-13 [126].

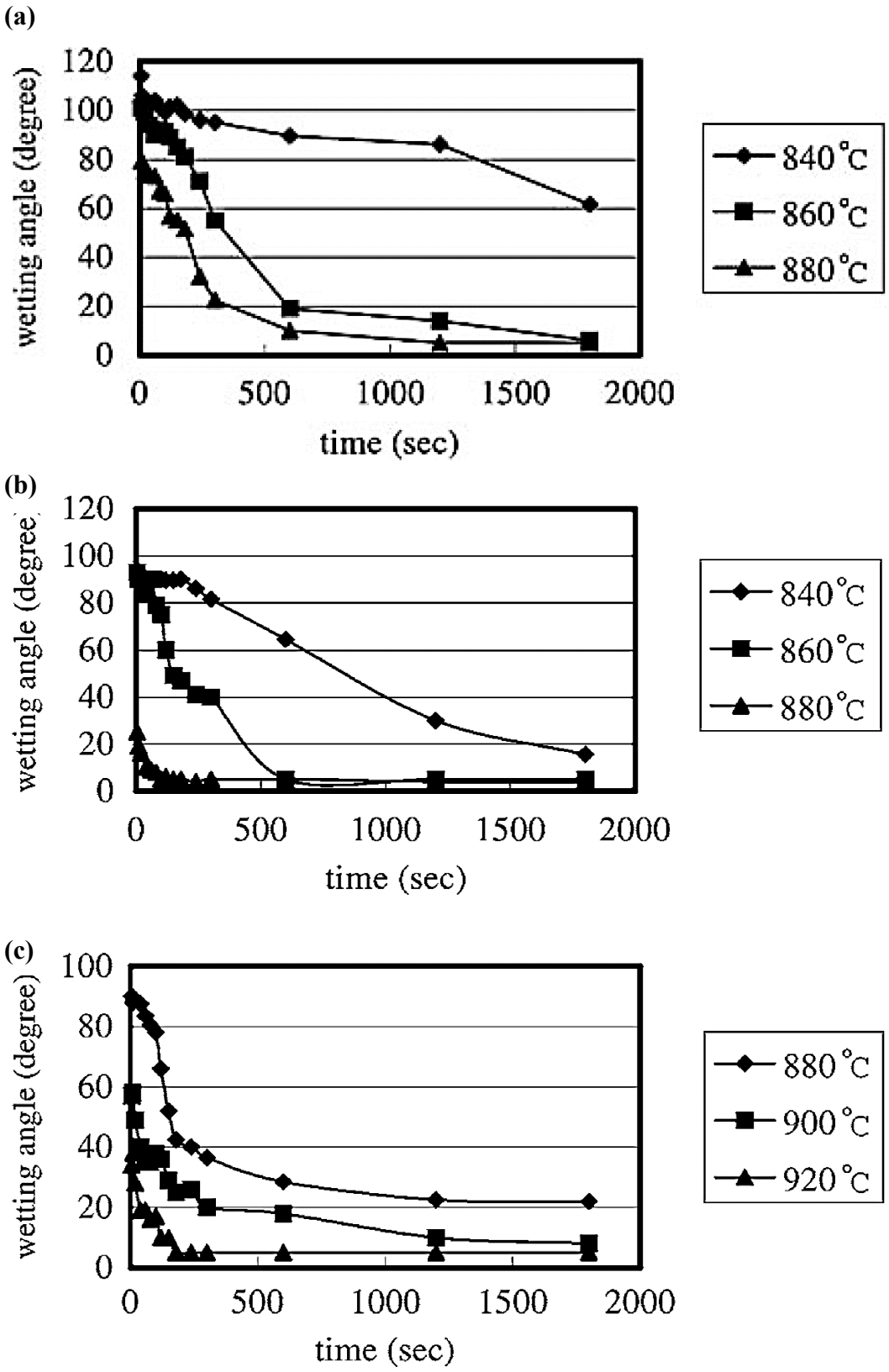

Figure 2-13. Dynamic wetting angle measurements of (a) Braze 580 (b) BAg-8 (c) Ticusil® on Ti-6Al-4V at different temperatures[126].

Equally, Chang and Shiue [6] made an effort to measure the dynamic wetting angles of Ti-15Cu-15Ni brazing filler on Ti-6Al-4V. Using a near spherical ball of 0.12 g, the experiment was done in a conventional vacuum furnace for 2400 s in the temperature range of 970-1030^{o}C. However, the wetting mechanism was never discussed, nor was the wetting/spreading contact angle-time graph presented. It was only reported that the brazing filler could wet Ti-6Al-4V substrate at 970^{o}C. The ability of the brazing filler to wet the substrate was attributed to the dissolution of the substrate into the filler.

Also, the tendency of Ti-20Zr-20Cu-20Ni, Ag-5Pd, BNi_2 and BNi_7 brazing fillers to wet titanium alloy (Ti-Al-V) was studied by Chung *et al.* [127]. For each brazing filler, the wetting test was carried out at 50^{o}C above the liquidus of each filler metal. Only the final (static) contact angle of the filler metal on the substrate was determined by observing the filler-substrate cross-section using scanning electron microscope (SEM). Final contact angles of 24^{o}, 24^{o}, and 22^{o} were reported for Ti-20Zr-20Cu-20Ni, BNi_2 and BNi_7, respectively. However, the contact angle-time graphs for the wetting/spreading were not presented. Also, no information was given on the mechanism of wetting. The wetting behaviour of Ag-5Pd on the substrate could not be determined due to the reported erosion of the substrate.

Chan *et al.* [128] equally studied the wetting behaviour of BAg-8 (Ag-28Cu) on Ti-6Al-4V, using sessile drop test in a traditional vacuum furnace. The test lasted for 0-1800 s and the temperature range used was between 800 and 900^{o}C. The approximate weight of the spherical ball used was 0.12 g. While the brazing filler could not wet the substrate at 800^{o}C, almost complete wetting was achieved at 850^{o}C, after 1200 s, as shown in Figure 2.14 [128].

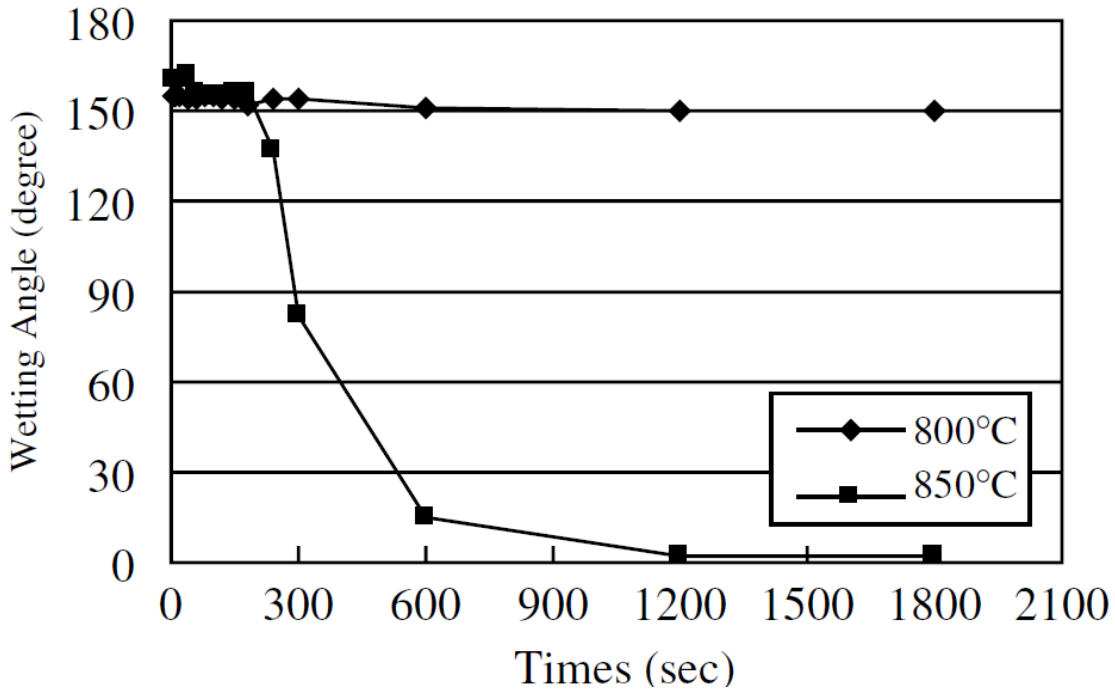

Figure 2-14. The sessile drop test of BAg-8 on Ti-6Al-4V [128].

Summary of the work done on wettability study of Ti-6Al-4V is given in Table 2-2.

Table 2-2. Summary of the work done on the wetting behaviour of brazing fillers on Ti-6Al-4V.

Substrate	Brazing Filler	Parameters	Response	Reference
Ti-6Al-4V	Ti-15-Cu-15Ni	Temperature Time	Dynamic contact angle	[6]
Ti-6Al-4V	Pure silver	Temperature Time	Dynamic wetting angle	[7]
Ti-6Al-4V	Braze 580 BAg-8 Ticusil®	Temperature Time	Dynamic wetting angle	[126]
Ti-6Al-4V	Ti-20Zr-20Cu-20Ni Ag-5Pd BNi_2 BNi_7	Temperature	Static contact angle	[127]
Ti-6Al-4V	BAg-8	Temperature Time	Dynamic contact angle	[128]

2.12 Objectives of this work

Despite the importance of wettability study to brazing, the wetting behaviour of Ti-based brazing fillers on titanium alloys has been grossly understudied. Little is known about the wetting mechanism of this system. Therefore, the objective of this work is to study the wetting behaviour of Ti-20Zr-20-Cu-20Ni (wt.%) on Ti-6Al-4V. This particular brazing filler has been chosen for this study because of its relatively low solidus and liquidus temperature of 848 and 856^{o}C, respectively. It is preferred to braze α-β titanium alloys below the beta transus temperature which varies from 900 to 1040^{o}C, to maintain their fine, equiaxed duplex structure which gives optimum mechanical properties [5]. Therefore, with the use of Ti-20Zr-20Cu-20Ni as the brazing filler, Ti-6Al-4V can be brazed below its beta transus, thereby avoiding the formation of coarse grains and Widmanstätten structure in the brazed joint [129].

In this work, the influence of substrate roughness and heating rate on wetting are evaluated.

Chapter 3 Experimental Methodology

3.1 Wetting study apparatus

In this work, the study is carried out by using the sessile drop method under a vacuum atmosphere. The equipment or apparatus used for the wettability study can be described as a collection of subsystems or units, integrated to produce the desired performance. The classification of the subsystems of the apparatus, based on their function, is detailed below.

- Furnace subsystem: This subsystem is responsible for heating up the sample to the required test temperature. It is made up of the heating core and the controller, designed by Thoughtventions Unlimited LLC. The heating core is comprised of alumina tube furnace, surrounded by heating element and heat insulator. The controller ensures a precise temperature control. The heating core has aluminum end blocks through which cooling water runs. An illustration of the furnace hot core design is shown in Figure 3-1 [130].
- Vacuum subsystem: It is responsible for evacuating the heating chamber and creating a high vacuum, needed for wetting of titanium alloy, because of the high susceptibility of titanium alloys to oxidation. This unit has 2 pumps; a mechanical pump and an oil diffusion pump. The mechanical pump creates both the rough vacuum and the backing vacuum required to operate the diffusion pump. This unit can create a vacuum level that is as high as 10^{-6} Torr under an experimental condition.
- Water cooling subsystem: This unit provides cooling for the furnace walls and the diffusion pump, as their operations require water cooling. This unit is also used for

quenching of test samples for subsequent metallographic analyses by virtue of the circulating cooling water.

- Control subsystem: Due to the fact that the apparatus has so many valves, this unit controls the sequence of opening, the logic and operations of these valves.
- Sample delivery subsystem: This unit is responsible for transferring the sample from the cold zone to the furnace core hot zone without breaking the vacuum. It has a K-type thermocouple and a temperature data logger attached to it for temperature acquisition. The thermocouple has a maximum temperature range of -200 to 1250^{o}C [131].
- Imaging subsystem: This is a very critical and important unit. It is responsible for the illumination of the sample and image acquisition in the course of the experiment. It is made up of a high speed camera, a lens assembly and a light source for illumination. The camera can capture up to 264 frames per second.

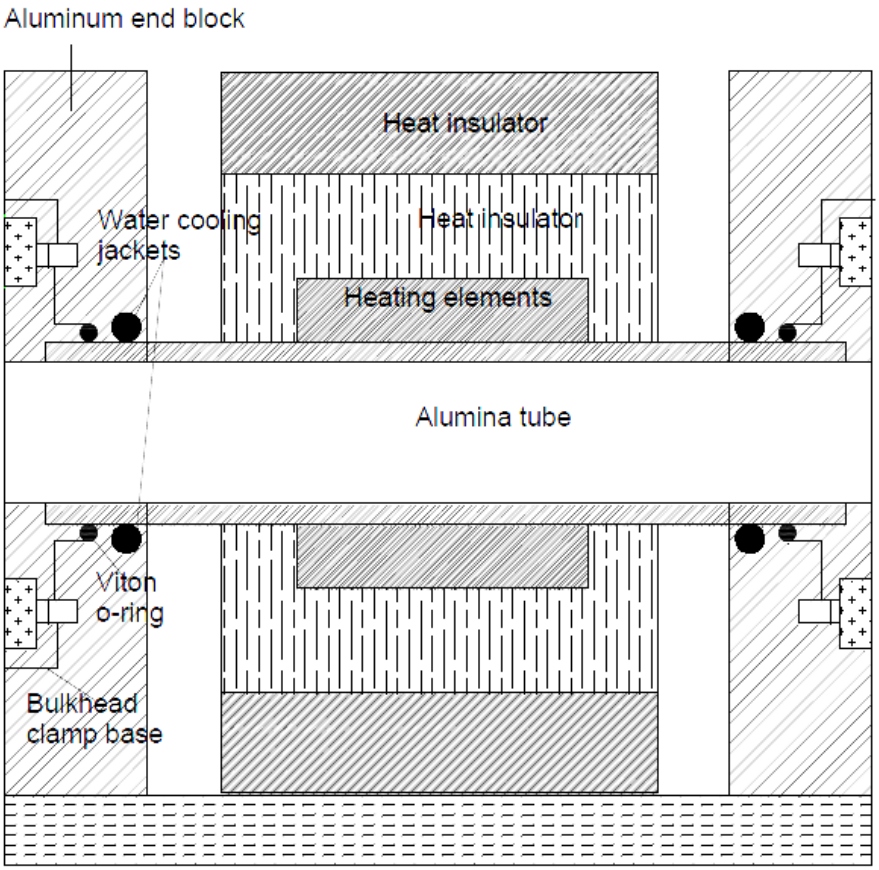

Figure 3-1. Illustration of the furnace hot core design [130].

3.2 Heating scheme

One of the objectives of this work is to evaluate the effect of heating rate and scheme on wettability. Therefore, in this work, 3 different heating rates and schemes have been used.

- High heating rate scheme (6.8°C/s): This type of heating scheme is achieved by keeping the sample (the substrate and the ~1 mm wetting filler ball) at the water-cooled end (cold zone) while heating up the furnace hot core (hot zone) to the required test temperature (900°C). The sample is kept at the cold zone for about 40 minutes to allow the hot zone to reach uniform and steady-state temperature. After this time period, the sample is then pushed straight, using the sample delivery unit,

to the furnace hot core centre, to carry out the wetting test. With this scheme, the average heating rate to the point of melting of the wetting filler ball (848ºC) is 6.8ºC/s. This high heating rate minimises metallurgical interaction between the substrate and the wetting ball before the melting of the ball. A typical heating curve of this heating scheme is shown in Figure 3-2. Another advantage of this heating scheme is that it helps to preheat the furnace, thereby eliminating adsorbed gases on the walls of the furnace.

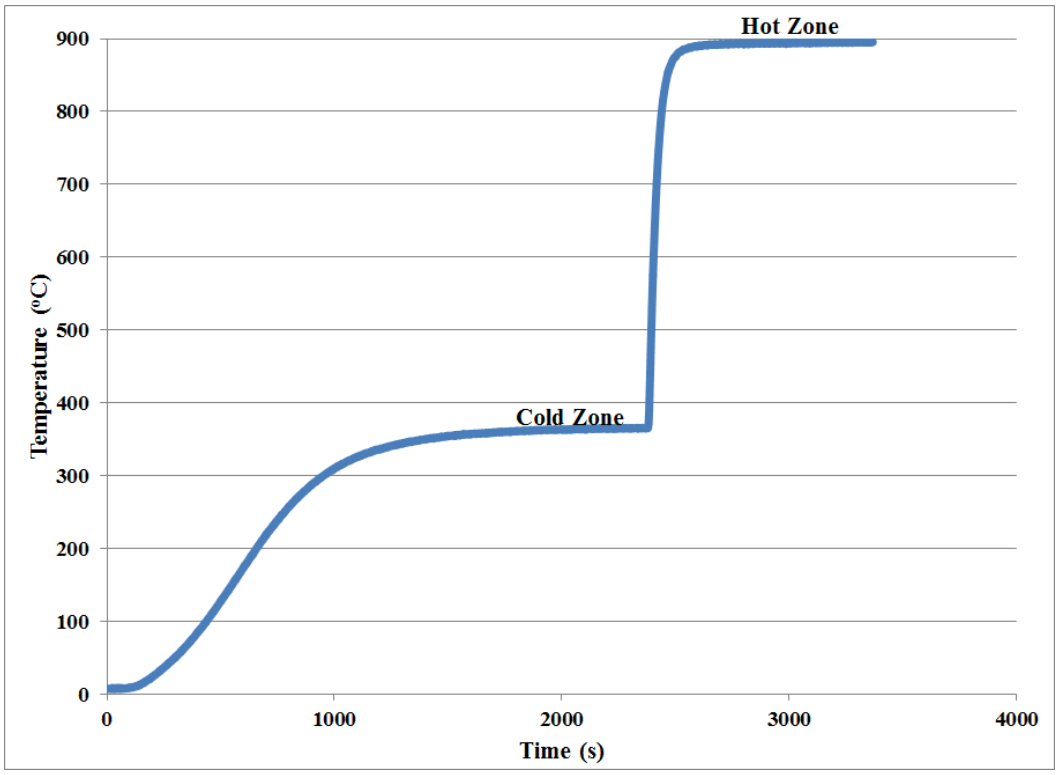

Figure 3-2. A typical heating curve for a high heating rate scheme.

- High heating rate (5.6ºC/s) with intermediate soaking scheme: With this scheme, after keeping the sample at the water-cooled end for about 30 minutes, the sample is pushed half-way through to the furnace hot zone. The sample is kept at this stage

for between 5 – 10 minutes to allow the sample (both the ball and the substrate) to achieve equilibrium in temperature. The soaking temperature is around 650°C. After this soaking stage, the sample is then pushed all the way to the centre of the furnace hot zone, to carry out the wetting test. With this scheme, the average heating rate to the point of melting of the wetting filler ball is 5.6°C/s. A typical heating curve of this heating scheme is shown in Figure 3-3.

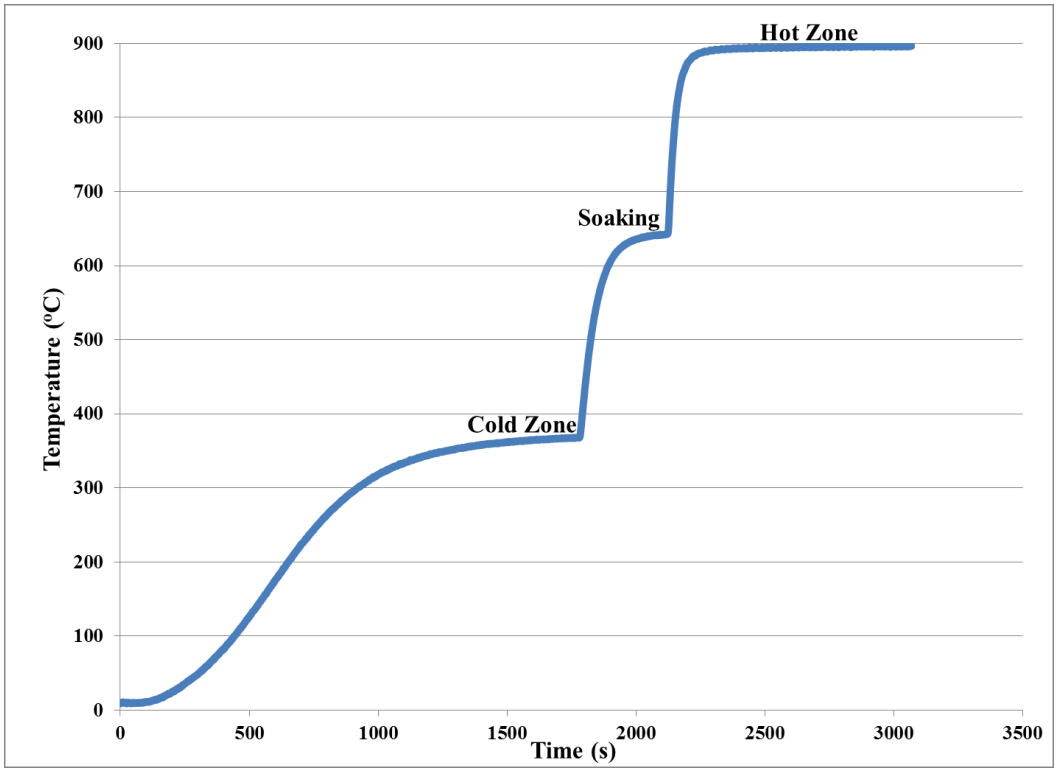

Figure 3-3. A typical heating curve for a high heating rate with intermediate soaking scheme.

- Low heating rate scheme (1.7°C/s): In this scheme, the sample is placed right at the centre of the furnace hot core before heating up the furnace. Therefore, the sample is heated up to the test temperature from the room temperature. For this scheme,

the average heating rate to the point of melting is 1.7°C/s. A typical curve of this heating scheme is shown in Figure 3-4.

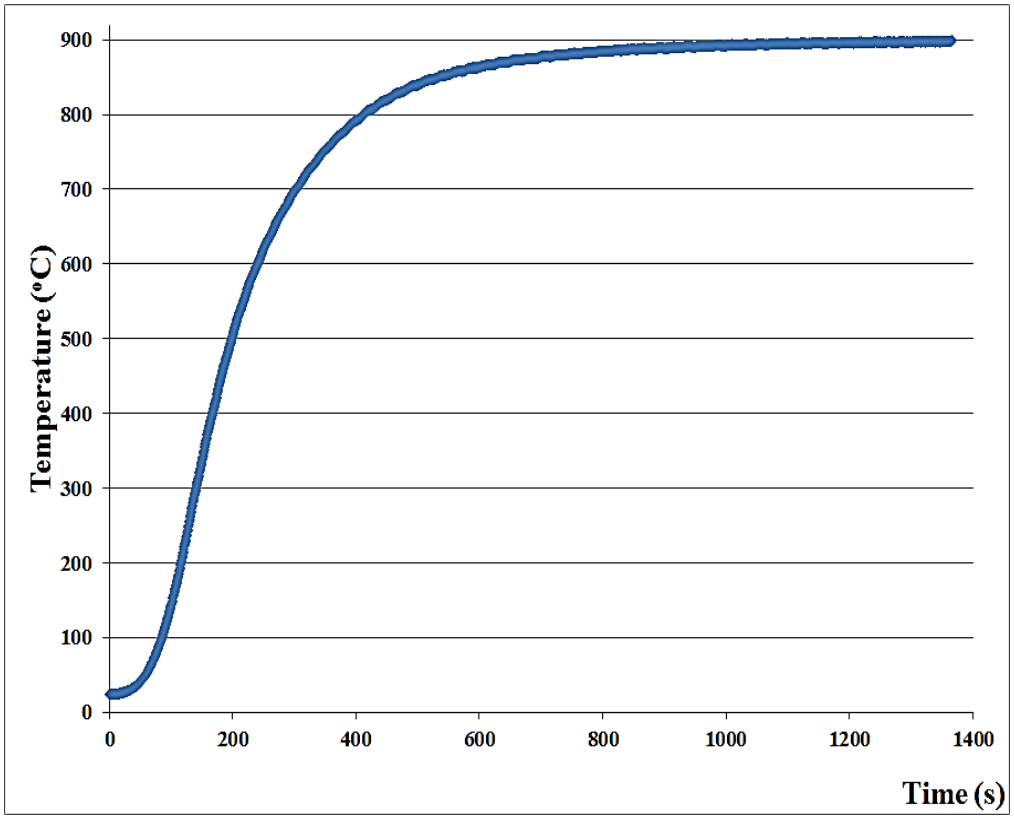

Figure 3-4. A typical heating curve for low heating rate scheme.

3.3 Ti-6Al-4V sample preparation

Ti-6Al-4V foils, supplied by Turbomeca Canada, with initial dimension of 2 × 1 × 0.002 inch were cut into smaller pieces of 0.47 inch × 0.47 × 0.002 inch. Since, one of the objectives of this work is to evaluate the influence of surface roughness on the wetting behaviour of Ti-20Zr-20Cu-20Ni on Ti-6Al-4V, some of the samples were ground using a SiC paper of 120 grit to initiate a relatively "rough" surface. The remaining samples were ground using SiC of 1200 grit to initiate a relatively "smooth" surface. The grinding was done in such a way to ensure a relatively equal average roughness value in both

perpendicular directions on the plane surface of the substrate. Typical examples of the average roughness values, R_a, obtained for samples ground with 120 grit and 1200 grit SiC papers are shown in Tables 3-1 and 3-2, respectively. The two directions of measurement of the surface roughness were perpendicular to each other. The roughness values were measured using Mitutoyo Surftest SJ-210 surface roughness gauge.

Table 3-1. Average surface roughness values of a sample with a relatively rough surface.

Point	Direction 1 R_a (μm)	Direction 2 R_a (μm)
1	0.44	0.42
2	0.40	0.41
3	0.37	0.32

Table 3-2. Average surface roughness values of a sample with a relatively smooth surface.

Point	Direction 1 R_a (μm)	Direction 2 R_a (μm)
1	0.08	0.08
2	0.08	0.11
3	0.09	0.9

3.4 Preparation of the brazing filler for the wetting test

Brazing filler (Ti-20Zr-20Cu-20Ni) in form of foil was supplied by LucasMilhaulpt®. A brazing filler of this form is usually produced by cold roll-bonding process, which combines Ti, Cu, Ni and Zr strips into a layered composite structure [5]. In this work, the microstructure of this filler was examined and analysed using a scanning electron microscope (SEM) Hitachi S-3400N, equipped with energy/wavelength dispersive X-ray spectroscopy (EDS/WDS) capabilities. The layered structure of the filler could be seen clearly in Figure 3-5. The result of an EDS line scan across the filler material, in terms of number of counts, is shown in Figure 3-6. An EDS spot analysis was also performed at each layer, to determine its chemical composition. Layers 1 and 7 are an alloy, containing 50Cu-50Ni at.%, layers 2 and 6 are essentially Zr strips, layers 3 and 5 are pure Cu strips, while layer 4 is pure Ti. The layered structure of the filler makes it even more paramount to remelt the filler in order to homogenize it.

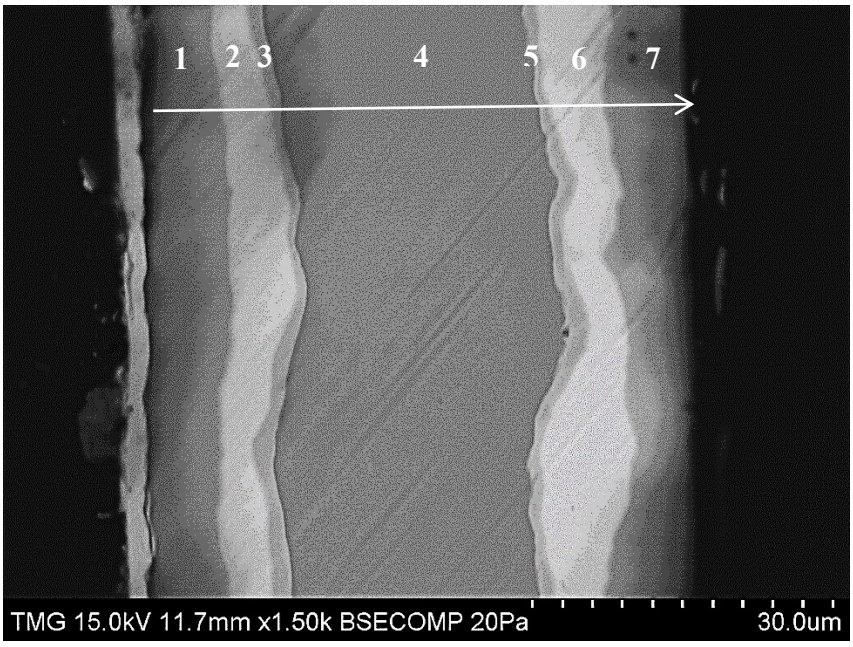

Figure 3-5. Microstructure of the cross-section of the layered structure brazing filler.

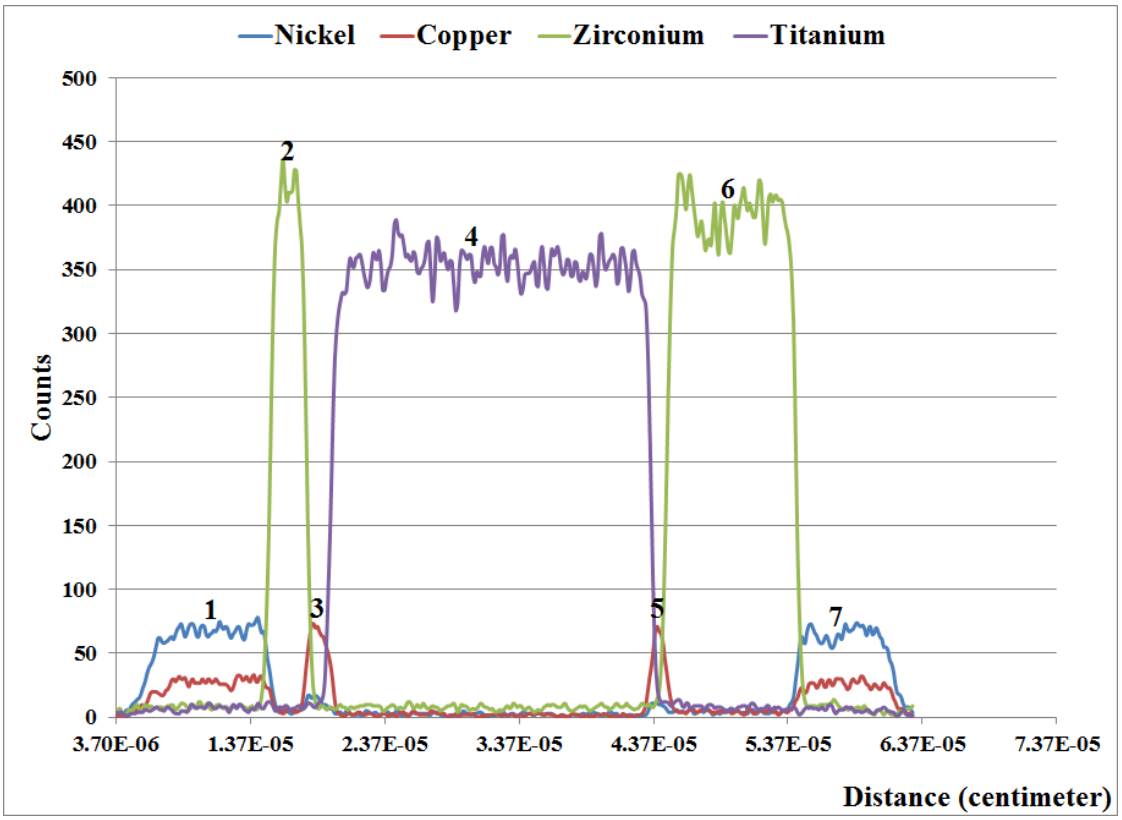

Figure 3-6. EDS line scan across different layers of the filler material.

It is very important to minimize the effect of gravity on wetting/spreading process. For this purpose, the radius, R, of the droplet must be such that R << L_c [132], where the capillary length, L_c, is given as:

$$L_c = \sqrt{\left(\frac{\alpha}{\rho_o g_o}\right)} \tag{3.1}$$

α is the surface tension, ρ_o is density and g_o is acceleration due to gravity.

For millimeter-sized drops, effect of gravity can be ignored [133]. Therefore, in this work, a wetting ball of an average diameter of 1 mm was used for the experiments. To produce the wetting ball, the foil was cut into small pieces of 0.157 × 0.157 × 0.002 inch. Each piece of foil was then remelted, into a sphere shape, under an argon atmosphere, in an arc

melting furnace, using a current of 60 A only, to prevent the foil piece from being charred. A typical example of a successfully remelted brazing foil placed on a Ti-6Al-4V substrate is shown in Figure 3-7. A scale of mm units was used to describe the aspect ratio for this micrograph (Fig. 3-7), and the same procedure was followed for other macrographs in this work. The average mass of the wetting ball used in this work is 0.0048 g. Each wetting ball, including the Ti-6Al-4V substrate, is ultrasonically cleaned with acetone for 15 minutes and dried before each test. The chemical composition of the filler material after remelting was determined, using EDS spot analysis, to be Ti-20Zr-20Cu-20Ni wt.%.

Figure 3-7. Wetting ball/substrate sample.

An image of a spreading droplet in the furnace is shown in Figure 3-8. The spherical shape of the surface of the droplet indicates not only that effect of gravity is negligible but also that the effect of oxidation on the droplet is minimal.

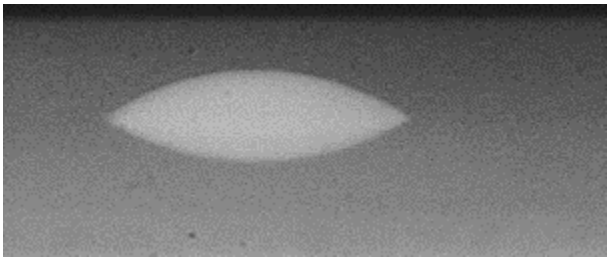

Figure 3-8. An image of a spreading droplet in the furnace.

The various combinations of the heating scheme and the substrate surface roughness used in this work are shown in Table 3-3.

Table 3-3. Experimental combination of the heating scheme and surface finish.

Heating Scheme	SiC Paper Used for Substrate Grinding
High heating rate (HR)	120 (Rough)
High heating rate	1200 (Smooth)
High heating rate with intermediate soaking	120 (Rough)
High heating rate with intermediate soaking	1200 (Smooth)
Low heating rate	120 (Rough)
Low heating rate	1200 (Smooth)

3.5 Evaluation of the degree of wetting

The degree of wetting of the substrate by the brazing filler was quantified by measuring two different responses.

- The apparent dynamic contact angle: This remains one of the most used responses to monitor and describe the evolution of the wetting process and to give an idea of

the degree of wetting of the substrate by the liquid. It is also very useful because it is insensitive to small variation in mass of the brazing filler samples. A sequence of the side view images of the wetting process, acquired by the high speed camera attached to wetting study apparatus, were processed using AutoCAD 2012 to determine the apparent dynamic contact angle. Basic procedure of image processing was used to determine the free surface of the droplet and its reflection on the surface of the substrate. The triple point was subsequently established and a tangent was drawn at this point, relative to the free surface of the droplet. The angle between this tangential line and the line of symmetry of the droplet was taken as the dynamic apparent contact angle.

- The spread ratio: This is also frequently used to evaluate and quantify the degree of wetting [71, 94]. It is the ratio of the instantaneous base diameter of the spreading droplet (D) to the initial diameter of the brazing ball (D_o) used for the experimental test. The diameter of the droplet was extracted with the aid of a modified version of an algorithm in Matlab [134]. Mathematically,

$$Spread\ ratio = \frac{D}{D_o} \tag{3.2}$$

For each experimental combination of heating scheme and substrate surface roughness, the experiment was repeated twice to ensure repeatability of the results. The target test temperature for all experiments was 900^{o}C and each experimental run, from the point of melting of the brazing filler, lasted for 15 minutes.

Chapter 4 Results and Discussions

The wetting results obtained under each heating scheme are presented in sequential order. Microstructural analysis of fully annealed samples and those quenched at strategic points and time in the course of the experiments has been employed in this work, to shed more light on the wetting mechanism in this system. This approach is a very common one [49]. It was done with the aid of the scanning electron microscope. The samples were prepared for the analysis by cutting perpendicularly to the interface, using a low speed diamond saw and then polished up to 1 μm diamond paste. The discussion is also done and presented with respect to each heating scheme.

4.1 High heating rate

4.1.1 High heating rate (6.8^{o}C/s) with 120 grit SiC paper ground substrate

Two replica wetting samples, HHRR1 and HHRR21, were used for the experiments, under high heating rate (6.8^{o}C/s) condition with 120 grit SiC paper ground substrate. The variations of the contact angle and spread ratio with time and temperature are shown in Figures 4-1 and 4-2, respectively. The origin of the time scale of Fig. 4.1 indicates the time that melting started relative to the temperature-time graph of the heating scheme (Figure 3-2). Similar time scale is used for other graphs.

The results are repeatable, as seen from the graphs. With respect to the spread ratio-time graph (Fig. 4-1), at the very early stage, till about 6 s, the wetting remained confounded with melting. But after this early stage, which corresponds to approximately full melting of the brazing ball, a very high wetting/spreading rate is observed. The spread ratio increases in a monotonous manner. After this fast spreading stage, little or no increase

could be observed in the spreading ratio, with the spread ratio-time graph effectively reaching a plateau. This type of fast spreading/wetting has also been observed in other reactive wetting systems in the literature and this stage of wetting/spreading is referred to as the primary spreading stage [68, 72]. The rapid advancement of the triple point of the molten drop at this stage is attributed to the uncompensated Young's force, and reaction is not expected to exert a first-order or dominant effect in the triple point region, thus, making this regime of spreading to be termed non-reactive [49, 51, 69, 71, 94]. The industrial implication of this very high wetting/spreading rate is that successful brazing can be done within a short period of time. This is very significant because, in some cases, very long brazing time has been found to have detrimental effects on the strength of the brazed joint [135, 136].

This trend could also be observed in the contact angle-time graph (Fig. 4-1), with the contact angle decreasing in a monotonous manner until a plateau is reached. Variations of the spread ratio and contact angle with temperature (Fig. 4-2) indicate that noticeable wetting/spreading ceases before the temperature reaches 900^{o}C. This is very significant for industrial application, because it shows that brazing, using this filler metal, can be done well below the beta transus temperature which varies from 900 to 1040^{o}C [5]. The average final apparent contact angle of sample HHRR1 was 34^{o}, while that of sample HHRR2 was 37.8^{o}. The final macrographs of samples HHRR1 and HHRR2, after wetting test, are shown in Figure 4-3. The clean and shiny surfaces of the substrates indicates that the samples were free from oxidation. Also, the edges of the brazing filler droplets were fairly smooth, which can suggest that the reaction between the brazing filler and substrate was not intense.

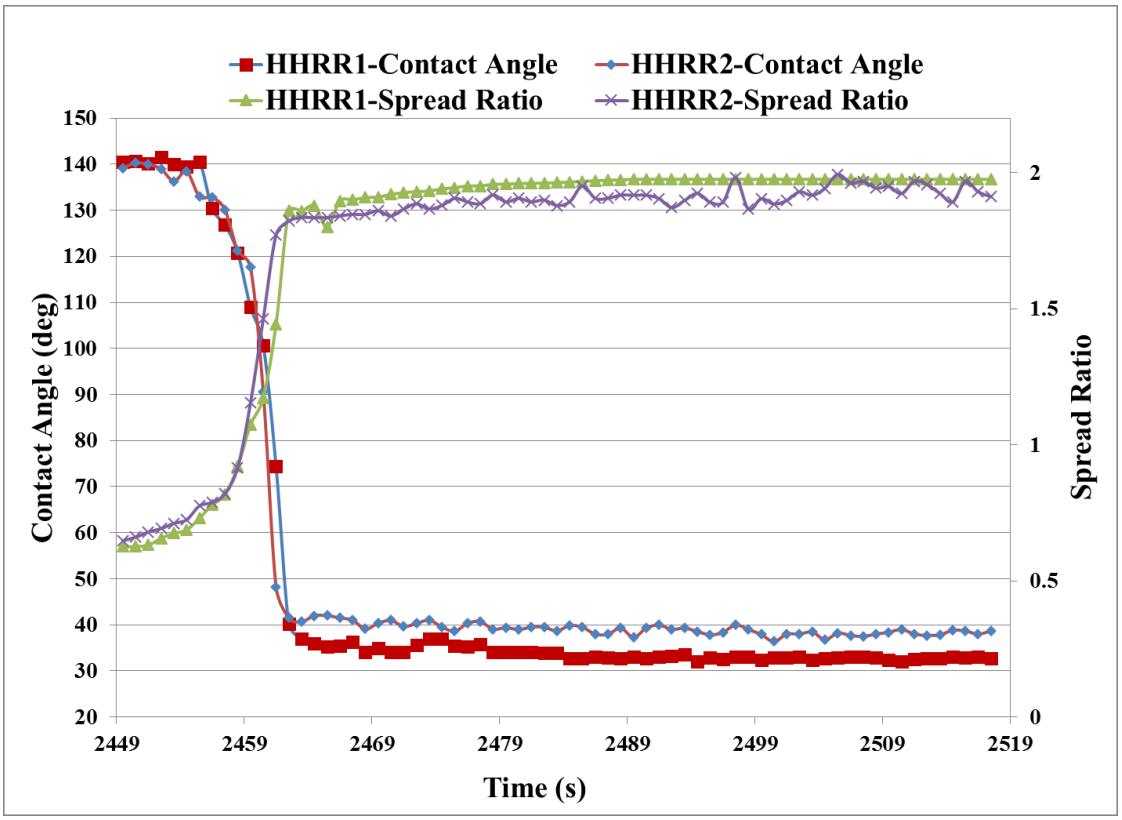

Figure 4-1. Variations of contact angle and spread ratio with time under the condition of 6.8ºC/s heating rate with 120 grit SiC paper ground substrate.

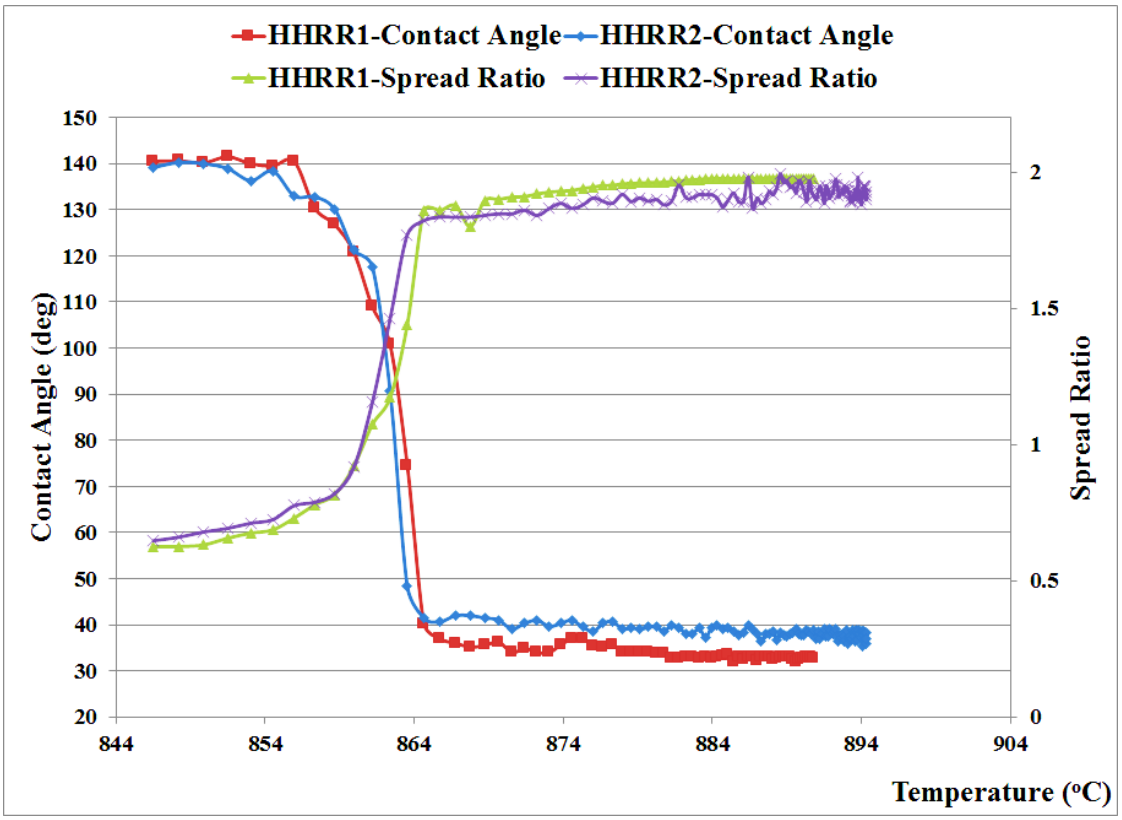

Figure 4-2. Variations of contact angle and spread ratio with temperature under the condition of 6.8°C/s heating rate with 120 grit SiC paper ground substrate.

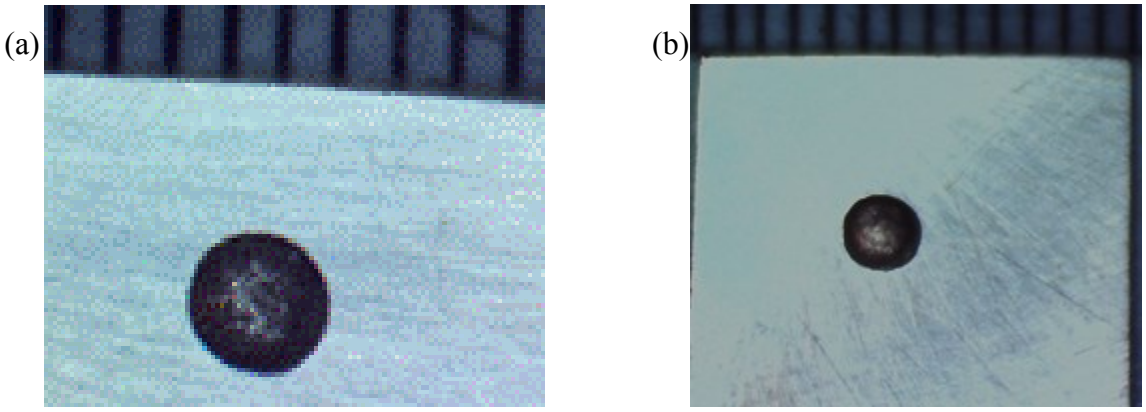

Figure 4-3. Macrograph of sample (a) HHRR1 (b) HHRR2 after the wetting test.

4.1.2 High heating rate (6.8^{o}C/s) with 1200 grit SiC paper ground substrate

Two replicas, HHRS1 and HHRS2, were used for the experiments, under the condition of high heating rate (6.8^{o}C/s) with 1200 grit SiC paper ground substrates. The variations of the contact angle and spread ratio with time and temperature are shown in Figures 4-4 and 4-5, respectively. The results are repeatable. A very fast spreading (primary spreading) could be observed in the spread ratio-time graph (Fig. 4-4) immediately after melting. This primary spreading ended after approximately 11 s. The spread ratio-time graph of sample HHRS1 reaches a plateau after this primary spreading stage. However, for sample HHRS2, a slight increase in the extent of spreading/wetting could be observed in its spread ratio-time graph, after the primary spreading stage, before reaching a plateau. The contact angle equally decreased in a monotonous manner. The average value of the final apparent contact angle was 33 and 34^{o} for samples HHRS1 and HHRS2, respectively. Comparing these results with those obtained for substrates with relatively rough surface, as shown in Figure 4-5, it can be seen that surface roughness does not exert any significant influence on the degree of wetting in this system.

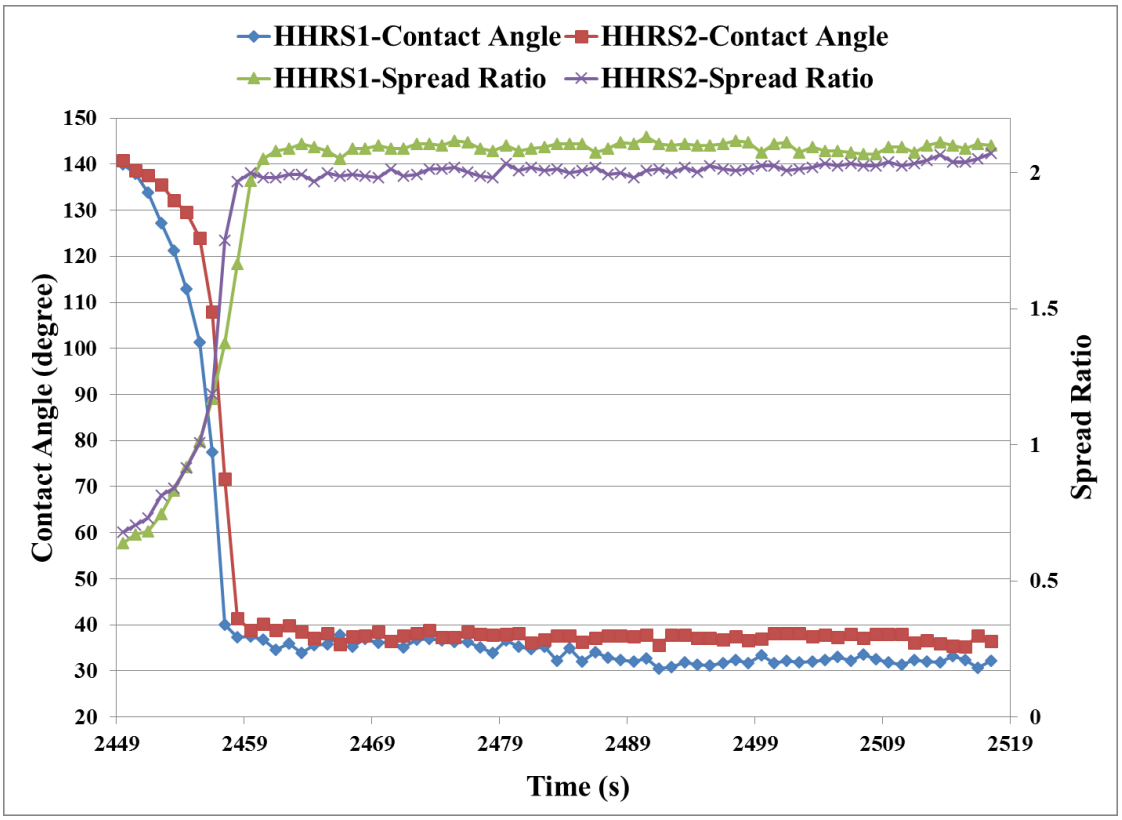

Figure 4-4. Variations of contact angle and spread ratio with time under the condition of 6.8°C/s heating rate with 1200 grit SiC paper ground substrate.

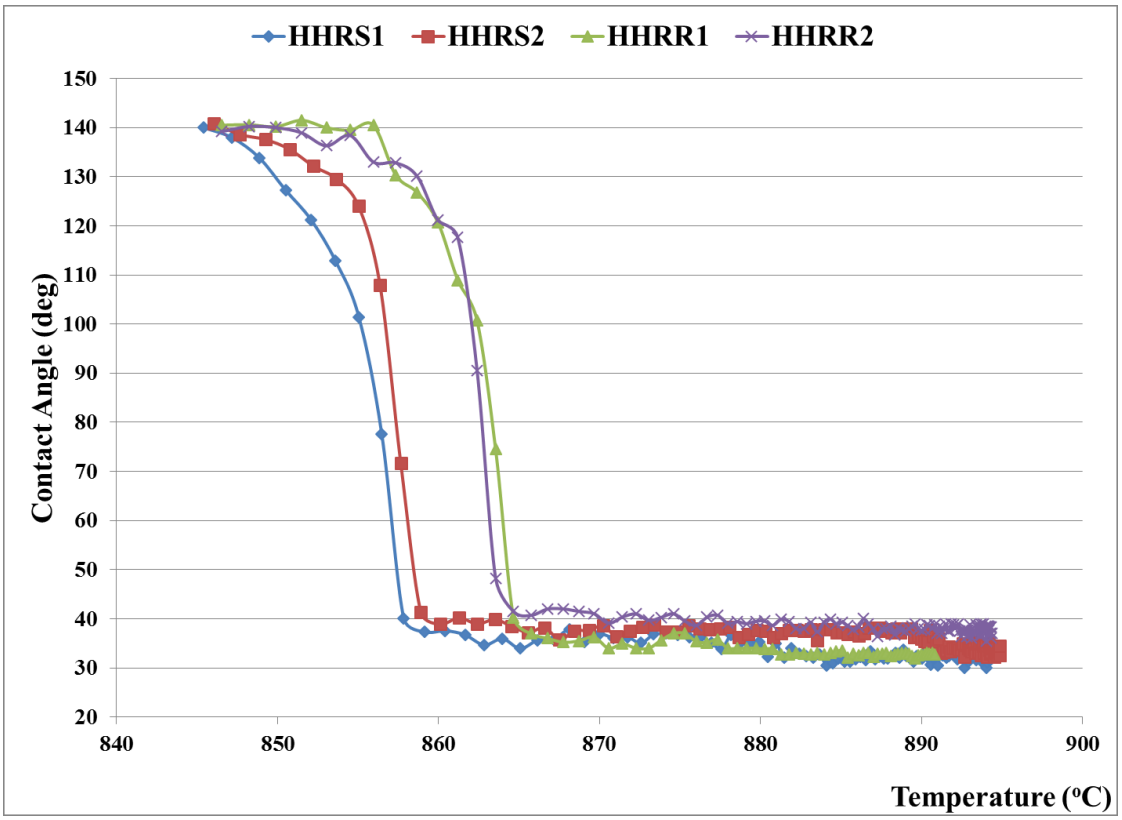

Figure 4-5. Variations of the contact angle with temperature under the condition of 6.8°C/s heating rate with 120 and 1200 grit SiC paper ground substrates.

4.1.3 Microstructural analysis

The micrographs of sample HHRR2, after 15 minutes of wetting test, is shown in Figure 4-6. Figure 4-6a shows a non-planar interface between the brazing filler and the substrate, indicating the dissolution of the substrate into the brazing filler. The interface is fairly uniformly curved, similar to an isoconcentration contour. Also, formation of continuous intermediate layer, with an average thickness of 45 µm, can be seen at the interface between the substrate and the brazing filler. A view of the interfacial layer is seen in Figure 4-6b. This intermediate layer could have been formed before cooling, or after cooling. EDS spot analysis was performed to measure the chemical composition of the formed phases.

Numbers 1 and 2 in Figure 4-6b represent the location of the EDS spot analysis. The result of this analysis is listed in Table 4-1.

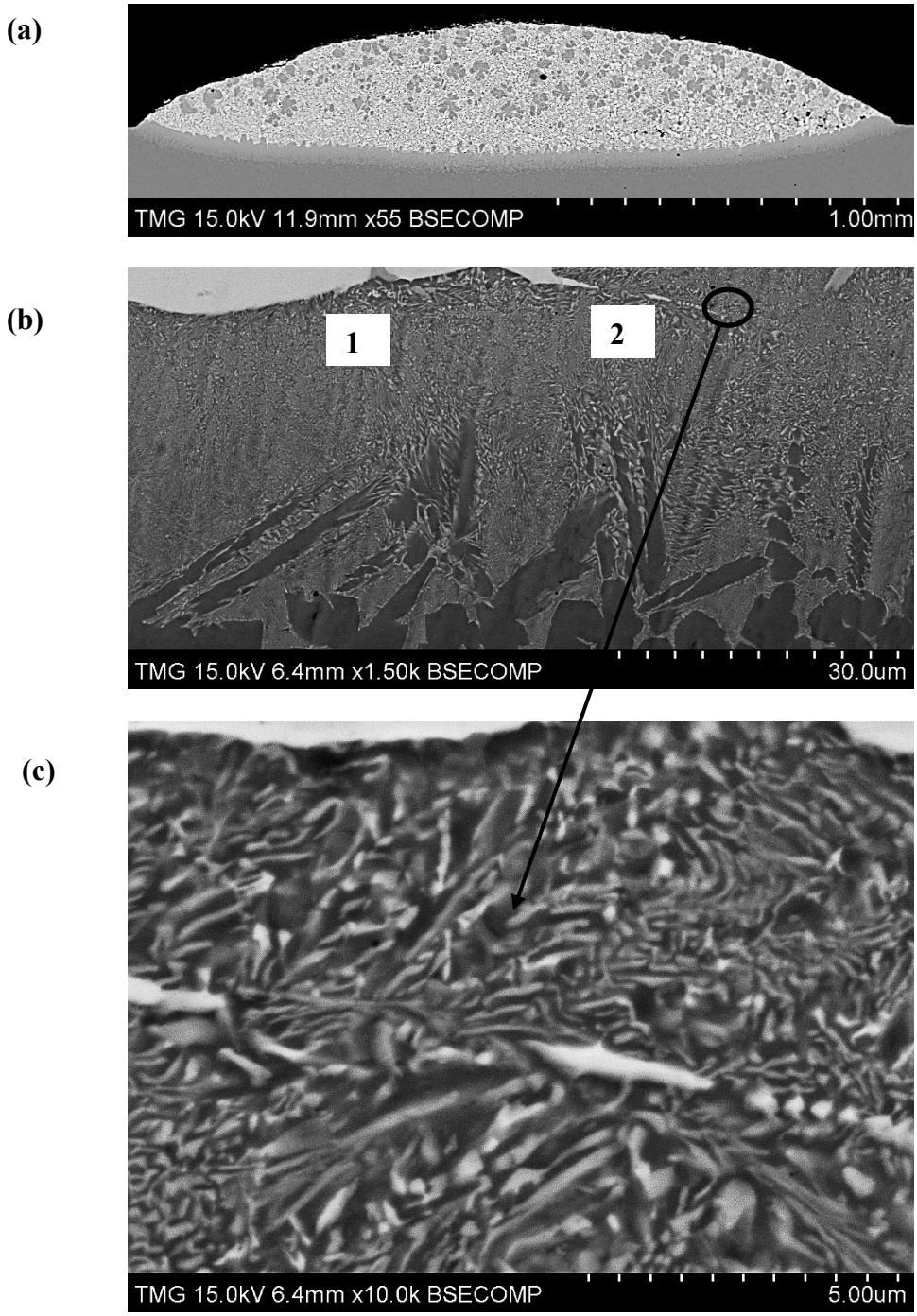

Figure 4-6. SEM back scattered electron image of (a) sample HHRR1 (b) intermediate layer (c) enlarged view of the interfacial layer.

Table 4-1. EDS analysis of the intermediate layer in atomic %.

Point	Al	Ti	V	Ni	Cu	Zr
1	5.13	75.24	2.61	4.93	7.15	4.94
2	5.08	75.48	2.68	4.83	7.06	4.87

Table 4-2. Data from Ti-Cu and Ti-Ni binary phase diagrams [137].

Alloy System	Ti-Cu	Ti-Ni
Solidification Type	Peritectic	Eutectic
Eutectoid Reaction	$\beta = \alpha + Ti_2Cu$	$\beta = \alpha + Ti_2Ni$
Eutectoid Temperature	790°C	765°C
Eutectoid Composition	5.4 at%	4.5 at%
Maximum Solubility in α-Ti	1.6 at%	0.2 at%
Maximum Solubility in β-Ti	13.5 at%	10 at%

Zr and Ti are almost completely soluble in each other in both solid and liquid states [136]. Also, Cu and Ni form isomorphous system and are both β-Ti stabilizers [136]. The maximum solubility of Cu and Ni in β-Ti is 13.5 and 10 at.%, respectively; while it is 1.6 and 0.2 at.%, respectively, in α-Ti [14]. The EDS chemical analysis in Table 4-1 shows that the interfacial layer is rich in Ti. Transformation or decomposition of β-Ti into α-Ti and γ (Ti_2Cu or Ti_2Ni) is possible in both Ti-Cu and Ti-Ni binary systems as shown in Table 4-2 [137]. Since the test temperature used in this work (900°C) is greater than the eutectoid temperatures of Ti-Ni and Ti-Cu systems (Table 4-2), the decomposition of β-Ti is likely to occur upon cooling. Therefore, this intermediate layer is likely to be composed of α-Ti, Ti_2Cu and/or Ti_2Ni. Looking at the enlarged view of the intermediate layer in Figure 4-6c, it is obvious that it is made up of many phases. The composition of the individual phases

in the eutectoid-like structure could not be obtained, because their size is smaller than the EDS detector size.

It is important to note that during the wetting test, the brazing ball is heated up to the point of melting while in contact with the Ti64 substrate. Also, it takes a fraction of a second for the ball to become sufficiently molten to initiate wetting. During this melting period, there will inevitably be dissolution of the substrate by the molten filler. The longer the melting process takes, the more will be the extent of dissolution of the substrate at this early stage of wetting.

In order to understand the mechanism behind the formation of the interfacial layer under the high heating rate scheme, it is important to look deeper into the mode of transportation of the solute in the liquid filler. The dissolved substrate is transported in the liquid filler by both diffusion and convection. However, the downward convective flow of the liquid at the very early stage of the wetting process, due to the initial melting of the wetting ball, is expected to be stronger than the diffusive transport of the solute into the substrate [72]. This will lead to an increase in concentration of Ti, Al and V atoms at the interface, most especially at the contact line region, relative to the bulk of the liquid. This increase in Ti concentration will lead to an increase in the melting point of the liquid at the interfacial area. This could lead to isothermal solidification or precipitation of this interfacial layer. Although this is a multi-component system, a quick glance at the Ti-Cu and Ti-Ni binary phase diagrams also indicates that the Ti-rich phases are stable at 900^{o}C [14]. This concept was also proposed in the brazing of Ti and Ti-6Al-4V using Ti- and Zr-based amorphous fillers [14, 136].

This idea can be further established by considering the micrographs of sample HHRS3 (Figures 4-7a and 4-7b), which was quenched 5 s after melting in the course of the wetting test. While a slight depression can be observed at the middle, the substrate surface remains essentially flat at the adjoining areas. This depression is due to the melting process of the brazing ball. An EDS line scan from the center of the droplet to the interface (Figure 4-7b), represented in Figure 4-8, also reveals an increase in concentration of Ti, Al and V at the interface, relative to the bulk of the droplet. This is an indication of mixing of the alloying elements from both the substrate and the wetting filler at the interface. Letters A and B in Figures 4-7 and 4-8 indicate the direction of the line scan. The interfacial layer can also be observed in the quenched sample, albeit, with a reduced thickness (about 2 μm), compared to that of a fully annealed sample such as HHRS1 in Figure 4-6 (about 45 μm). This further confirms the idea that the formation of the compound layer takes place at the very early stages of the wetting process, it merely increases in thickness with time.

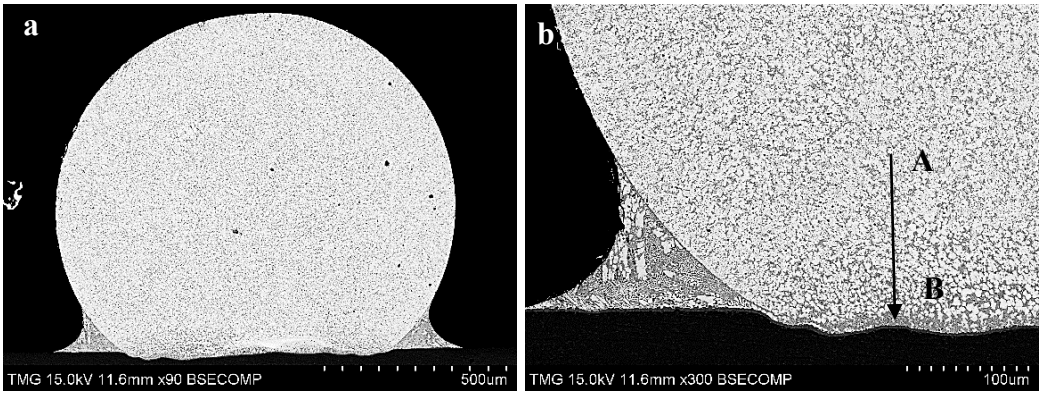

Figure 4-7. SEM back scattered image of (a) sample HHRS3 (b) interface/contact line region, quenched after 5 s. Letters A and B in Figure 4-15b indicate the direction of the line scan, corresponding to that in Figure 4-16.

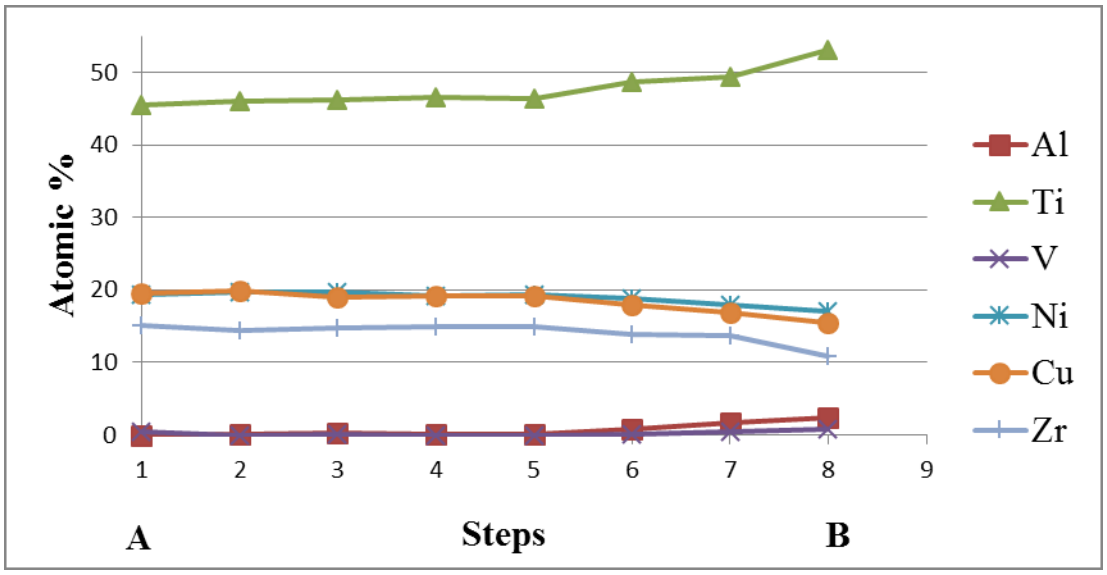

Figure 4-8. Line scan across the quenched sample. Letters A and B in the figure indicate the direction of the line scan, corresponding to that in Figure 4-15b.

In order to further understand the wetting mechanism noticed in this system under the high heating rate (6.8ºC/s) scheme, as seen in Figure 4-1, an attempt was made to correlate the microstructural evolution of the interface of the samples to the observed wetting characteristics. For this purpose, another sample, HHRS4, was quenched 15 s after melting, to ensure that the wetting/spreading is just at the end of the characteristic fast or primary spreading regime, as shown in Figure 4-9. At this stage, noticeable spreading ceases under this heating scheme.

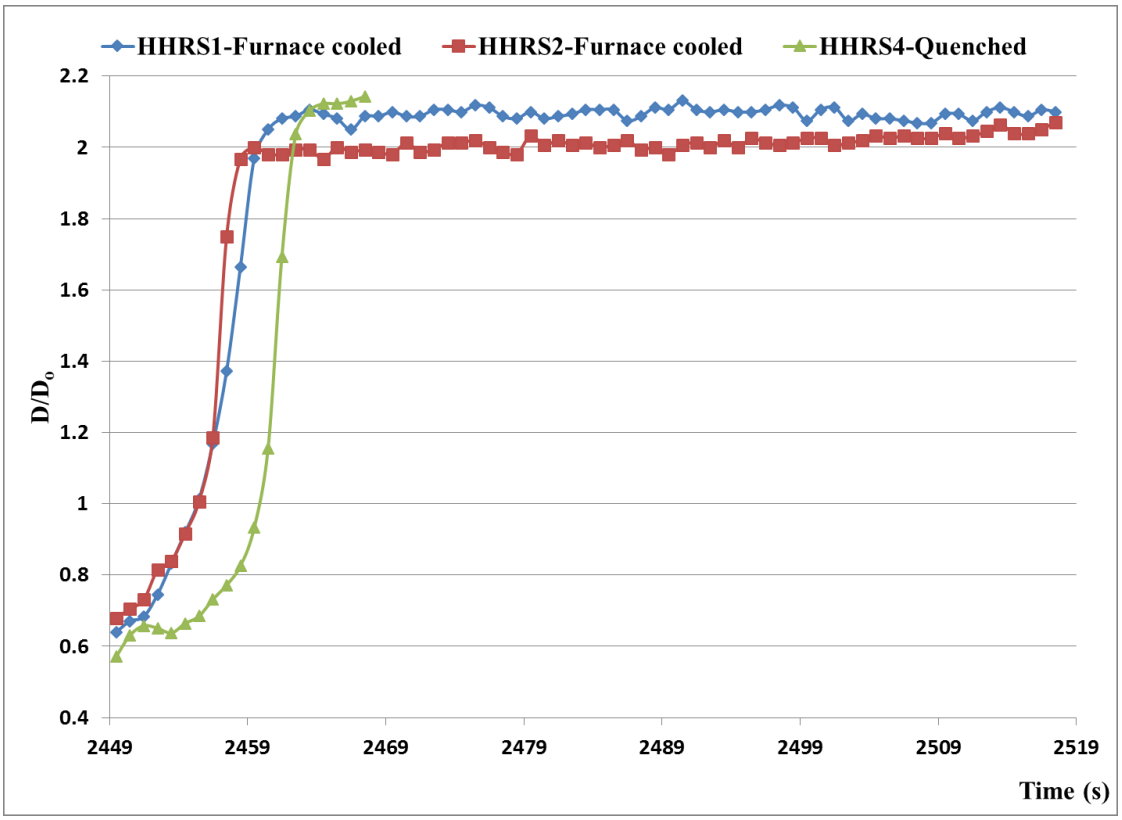

Figure 4-9. Spread ratio-time graph of fully annealed and furnace-cooled (HHRS1 and HHRS2), and quenched (HHRS4) samples.

The back scattered electron images of the quenched sample HHHRS4 are shown in Figure 4-10. The dome or irregular shape of the surface of the droplet is due to the fact that the droplet was quenched before forming a full spherical cap. A critical look at Figure 4-10a indicates that apart from the little depression at the centre of the substrate, due to the melting of the ball at the initial point of contact, the other parts of the interface between the substrate and the filler are fairly flat with minimal dissolution. This is a striking contrast to that obtained for the fully annealed and furnace-cooled sample, HHRS1, after 15 minutes of wetting test (Figure 4-6). This confirms the fact that the spreading at this stage (primary spreading) takes place with very minimal dissolution of the substrate. This observed

minimal dissolution of the substrate could be due to the fact that, at the very early wetting stage, most of the dissolved alloying elements (Ti, V and Al) are "restricted" to the interface, especially at the contact line region, due to the expected dominance of convective flow over diffusive flow. This might lead to a sort of transient saturation in terms of the concentrations of the dissolved alloying elements, thereby drastically limiting further dissolution of the substrate. The interfacial layer could also be observed in Figure 4-10b, with an average thickness of around 2 μm, same as that of sample HHRS3 quenched after 5 s (Figure 4-7). This layer is also expected to further limit the dissolution rate of the substrate. Technically speaking, this spreading regime may not be described as being non-reactive due to the little dissolution of the substrate and the formation of the thin interfacial layer. It is, however, very much non-reactive like. This evidence is sufficient enough to suggest that this primary spreading stage might actually be non-reactive, if another experimental approach, where the melting stage can be completely isolated from spreading, could be used.

Therefore, what takes place in the case when the wetting test is conducted for longer period of time is mere smoothening out of the initial central depression, created in the substrate due to the melting process, by further dissolution of the substrate. At this later stage, diffusion becomes the dominant means of mass transport of atoms. This further dissolution of the substrate is not accompanied by any appreciable or noticeable increase in the extent of spreading of the filler on the substrate. This implies that an increase in Ti, V and Al concentrations in the liquid filler does not alter the surface tension of the liquid, which would have led to an increase or decrease in the extent of spreading.

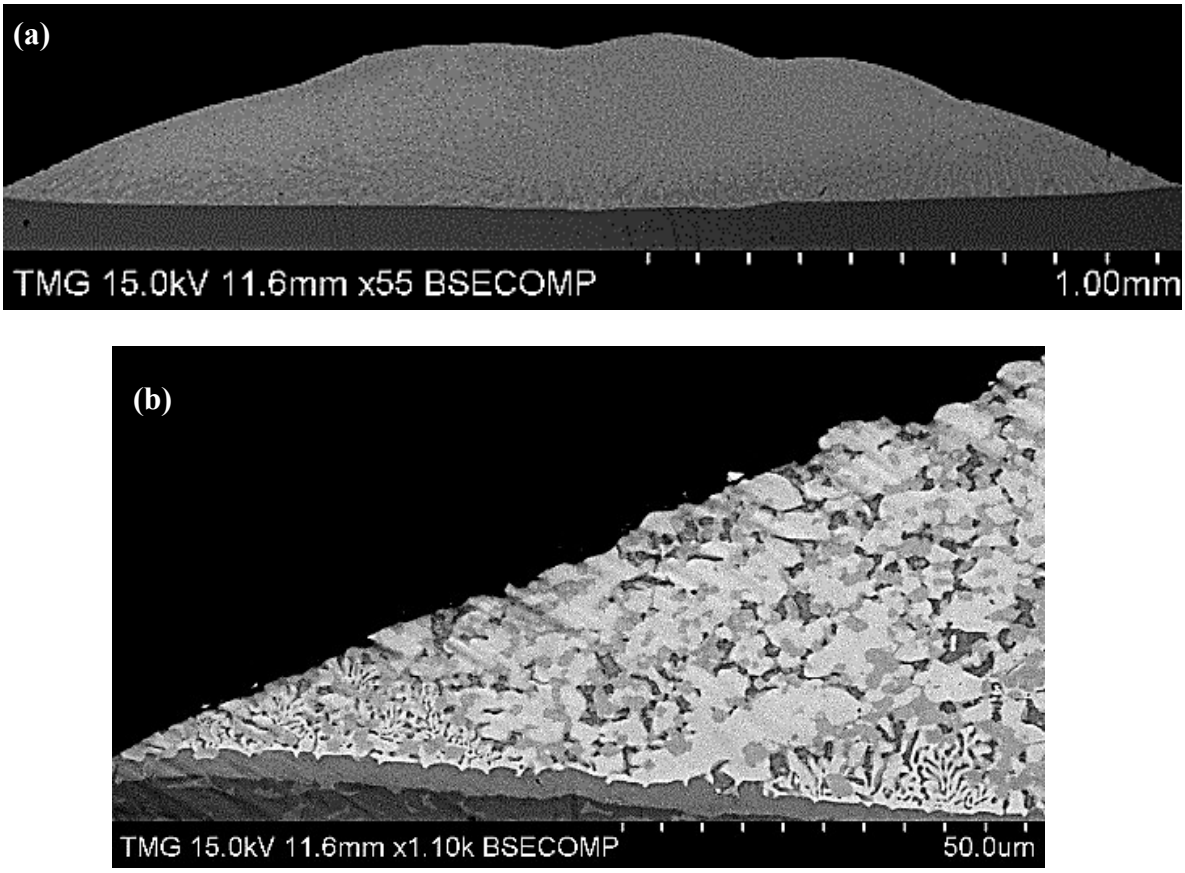

Figure 4-10. SEM back scattered images of (a) sample B10 (b) contact line/interface region, quenched after 15 s.

4.2 Low heating rate (1.7ºC/s)

4.2.1 Low heating rate (1.7ºC/s) with 120 grit SiC paper ground substrate

Two replicas, SHRR1 and SHRR2, were used for this experiments as shown in Figure 4-11. In reactive wetting; the primary spreading stage, synonymous with very high spreading rate, is usually followed by a secondary wetting/spreading stage. In the secondary reactive wetting/spreading stage, reaction exerts a first-order effect in the triple line region, and the time scale at which reaction takes place is comparable with the time scale of advancement of the triple line [69].

For sample SHRR1, the first 17 s of the wetting process is confounded with the melting of the wetting ball, and this is very significant. Between points A and B, a relatively fast wetting/spreading is observed. The time period between these two points is approximately 18 s. Considering the magnitude of time between these 2 points, this wetting stage is unlikely to be purely primary stage. It is most likely to be a combination of both primary and secondary wetting/spreading. Between points B and C, another wetting rate could be observed. This wetting graph, at this stage, is linear and the spreading rate is lower than the previous stage. This behaviour is synonymous to a secondary wetting stage and reaction appears to be exerting a first-order effect on the time scale of the triple line movement. It is significant to note that this period lasted for about 55 s. No appreciable wetting or spreading could be observed between points C and D. The final macrograph of sample SHRR1 is shown in Figure 4-12a. The rough and irregular edge of the droplet is an indication of intense reaction between the brazing filler and the substrate [126]. The dark colouration of the surface of the substrate was due to oxidation, which was successfully prevented under the high heating rate scheme.

The wetting behaviour of sample SHRR2 can be likened to that of SHRR1, although, there is a shift or lag in time with respect to the response or behaviour of these two replicas. This shift or lag could be due to the intense reaction between the brazing filler and the substrate, synonymous to this heating scheme. A relatively fast spreading/wetting could be observed between points E and F. However, this fast spreading did not start until about 40 s after the start of melting. This stage was also followed by another (F-G) with a lower spreading rate. The duration of this stage (25 s) is shorter than the corresponding stage in SHRR1 (55 s). Noticeable spreading ceased between points G and H. The final macrograph of sample

SHRR2 is shown in Figure 4-12b. The substrate was also oxidized. The edge of the droplet was, however, less rough and irregular, compared to that of sample SHRR1. This could be an indication of a reduction in the degree of reactivity between the brazing filler and the substrate. The final apparent contact angles of samples SHRR1 and SHRR2 were 14 and 17^{o}, respectively. The low apparent contact angle recorded under this heating scheme indicates that this scheme might be good for brazing. However, the intense reaction between the brazing filler and substrates implies that the brazed samples might be susceptible to erosion.

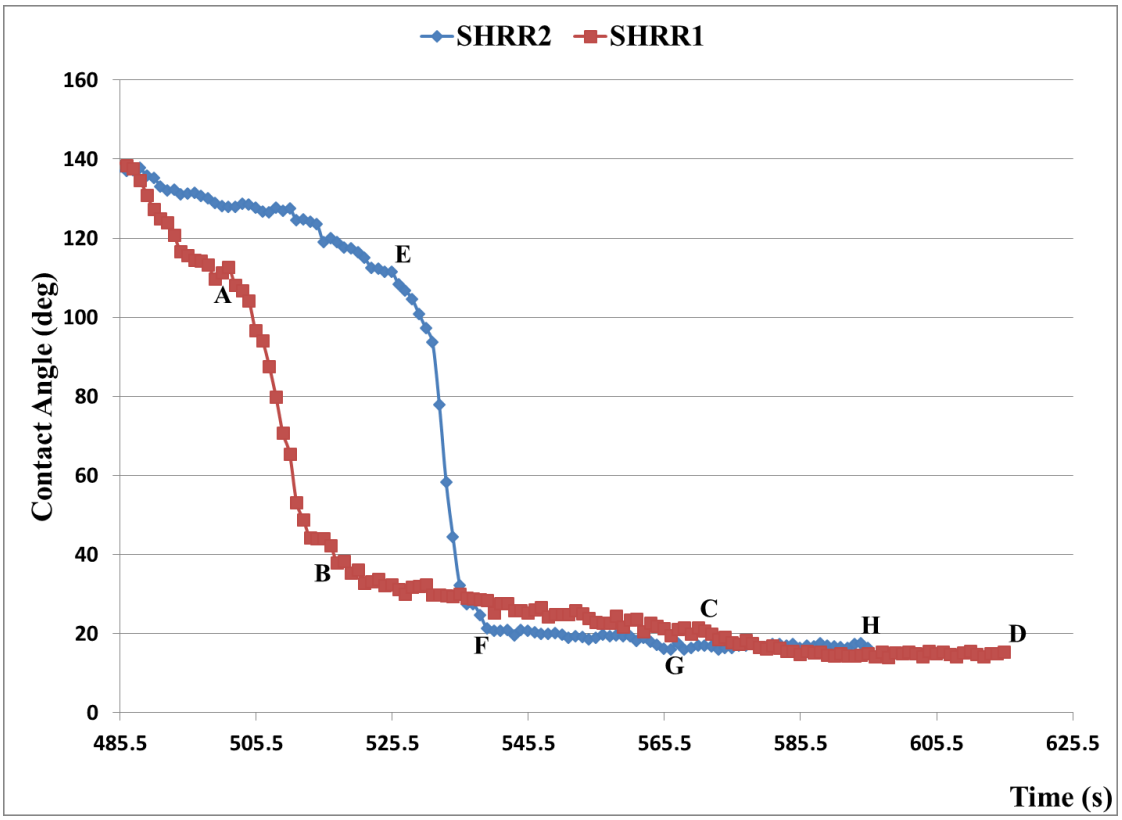

Figure 4-11. Variation of contact angle with time under the condition of 1.7^{o}C/s heating rate with 120 size SiC paper ground substrate.

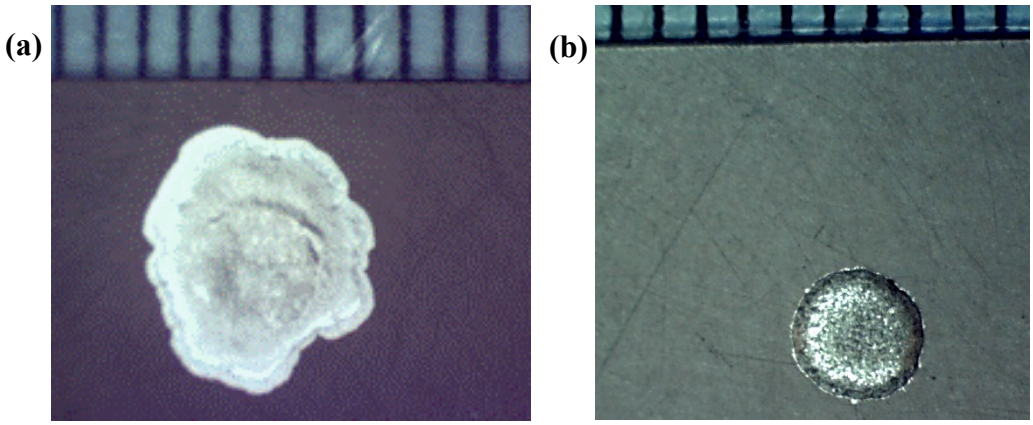

Figure 4-12. Final macrographs of samples (a) SHRR1 and (b) SHRR2.

4.2.2 Low heating rate (1.7°C/s) with 1200 grit SiC paper ground substrate

The two replica samples, SHRS1 and SHRS2, were used for the experiments under this particular experimental combination as shown in Figure 4-13. The trends observed under low heating rate condition, with relatively rough surface substrate (Figure 4-11) are repeated here.

For sample SHRS1, the wetting/spreading between points A and B is a combination of both primary wetting and secondary wetting. Between points B and C, a lower and linear spreading rate could be observed, which is an indication of a secondary stage wetting. There is a slight discontinuity (increased spreading rate) between points C and D which was not observed in Sample SHRR1. No significant spreading could be observed between points D and E.

Sample SHRS2 also show similar trends but at different time scales. The stage F-G represents the initial relatively fast wetting/spreading. This was followed by the stage (G-H) with the lower and linear rate. Noticeable wetting/spreading ceased between points H and I.

Due to the nature of this particular heating scheme, some distinct features could be noticed, in general. Firstly, the spreading rate is low compared to the spreading rate observed with the high heating rate scheme. This could be due to the fact that de-oxidation of the surface of the substrate has to take place first before wetting/spreading can occur. Therefore, the time for complete spreading/wetting is much longer than in the case with high heating rate. Secondly, the reaction between the brazing filler and the substrate is much more intense, compared to what obtained under the high heating rate scheme.

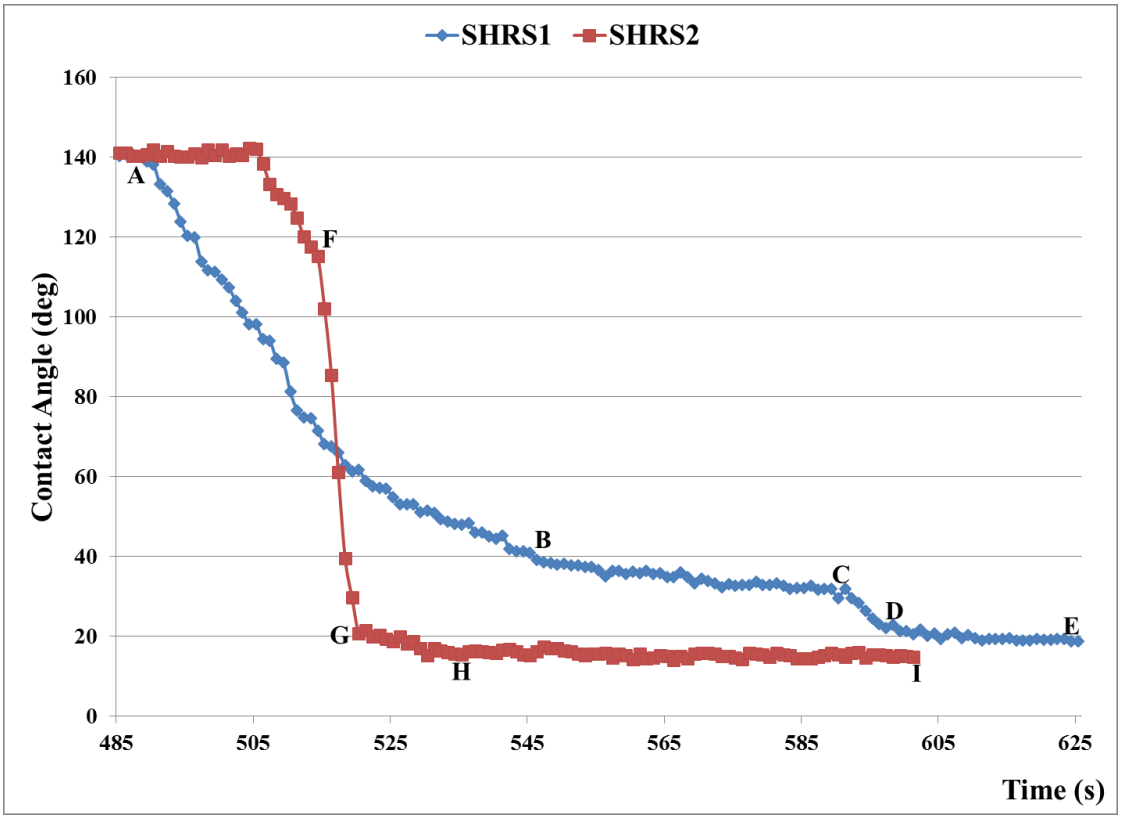

Figure 4-13. Variation of contact angle with time under the condition of 1.7°/s heating rate with 1200 grit SiC paper ground substrate.

4.2.3 Microstructural analysis

In order to further investigate and understand the wetting mechanism under this particular heating scheme, sample SHRR1 was sectioned and subjected to microstructural observation. The SEM back scattered electron images of the sample are shown in Figure 4-14. For this sample, 3 distinct curvatures can be seen at the interface between the brazing filler and the substrate, represented by W, XY and YZ in Figure 4-14b.

Due to the low heating rate, the time it takes for the brazing ball to be sufficiently molten enough to initiate wetting is much longer here than that obtained under high heating rate (6.8^{o}C/s) scheme. The implication of this is that there will be more dissolution of the central part or the initial point of contact between the ball and the substrate during the melting stage, compared to the case with high heating rate. This is the reason behind the relatively deep depression at the center of the substrate (point W) as seen in Figure 4-14b. This was followed by another curvature between points X and Y. There is also a clear sign of dissolution at this stage which is less than that at the central part (W). The dissolution depth decreases from X to Y.

The last distinct curvature is that between points Y and Z. This is a very distinct feature. The surface of the substrate between these 2 points is flat with the formation of the intermediate layer between the substrate and the filler. It is important to recall that in the contact angle-time graph of sample SHRR1 (Figure 4-11), a linear wetting/spreading stage with a low spreading rate (BC) was identified, in which reaction was suggested to be exerting first-order effect on the time-scale of advancement of the triple line. This last curvature, with its distinct characteristics, seems to confirm this suggestion. The wetting time under this heating scheme is quite long compared to that obtained under the high

heating rate scheme. Therefore, at this stage of wetting/spreading, diffusion will be the dominant means of mass transport of atoms in the droplet. However, the interfacial layer must have grown in thickness. As a result, the diffusion of atoms through this layer has to take place through solid-state diffusion, which is expected to be very slow, relative to the solid-liquid diffusion. Also, there seems to be formation of the compound layer at the top of the filler. This is an indication of saturation of alloying elements (Ti, Al, V) in the droplet, not only at the interface but also at the top of the droplet, as shown in Figure 4-14c. This suggests that solidification at the triple point might have actually led to the arrest in wetting/spreading. All these conditions favour the formation of the interfacial layer. At this stage of wetting/spreading, the rate of formation of this interfacial layer is expected to control the wetting rate. This also suggests that the interfacial layer might be more wettable than the bulk Ti64.

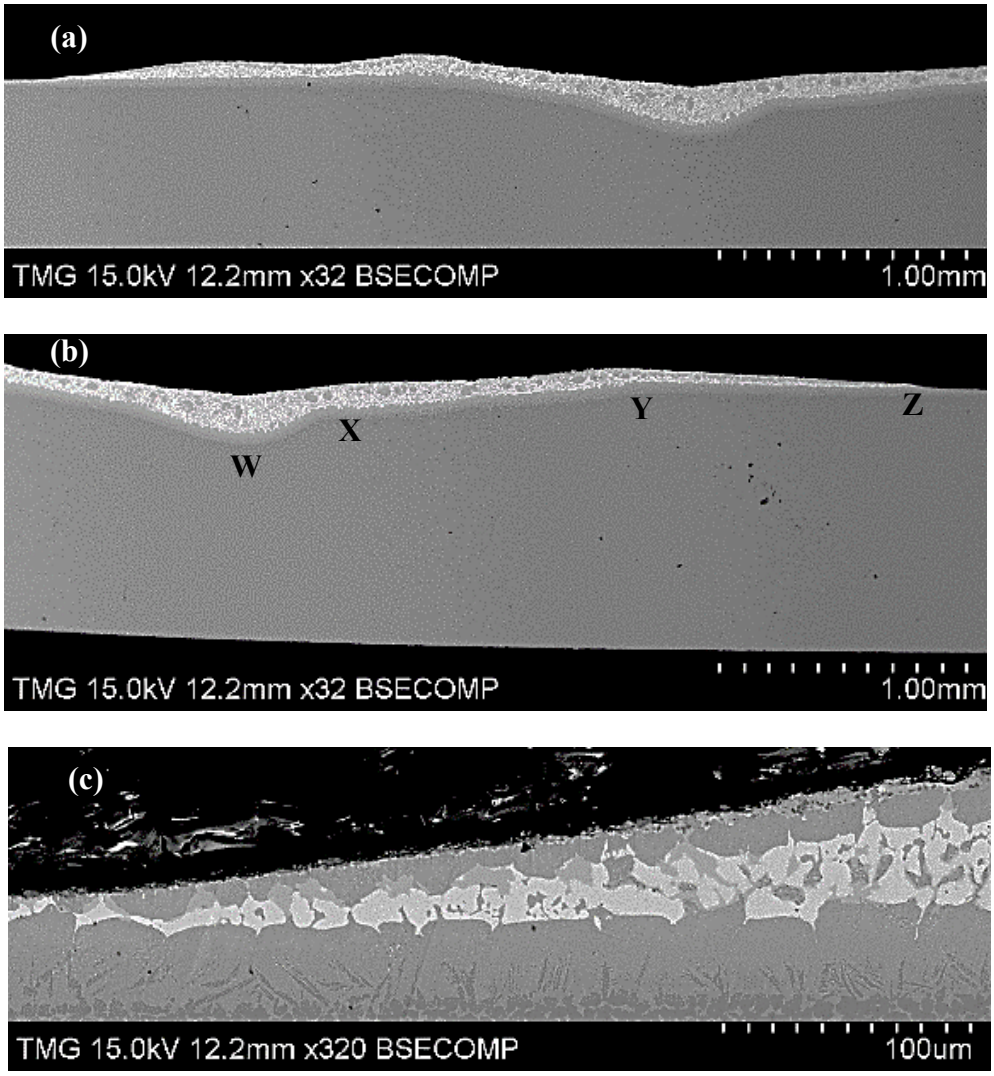

Figure 4-14. SEM back scattered electron images of sample SHRR1 showing (a) left hand side (b) right hand side (c) top surface of the droplet at the contact line region.

There is a sign of the formation of this interfacial layer ahead of the droplet as shown in Figures 4-15a and 4-15b (points A and B). This might be the reason for the shiny appearance of the edge of the droplet as shown in the final macrograph of the sample (Figure 4-12). The result of the EDS spot (1, 2, 3) analysis done at the edge of the droplet is shown in Table 4-3. This result is similar to the result obtained for the spot analysis done

on the intermediate layer in Figure 4-6b (Table 4-1), confirming the formation of this interfacial layer ahead of the spreading droplet.

Table 4-3. EDS analysis of the shiny edge in atomic %.

Point	Al	Ti	V	Ni	Cu	Zr
1	7.57	72.16	4.13	3.71	7.88	4.56
2	8.00	71.41	4.00	4.91	6.92	4.77
3	7.94	75.68	4.85	4.45	4.63	2.44

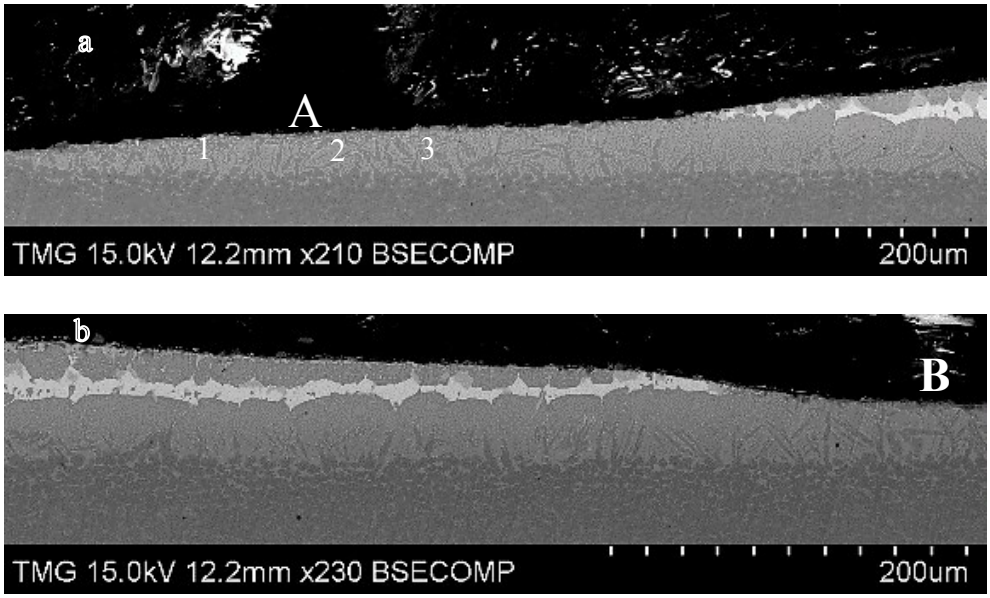

Figure 4-15. SEM back scattered electron images of sample SHRR1 showing the formation of the interfacial layer ahead of the droplet at (a) left hand side (b) right hand side of the triple/contact line region.

4.3 High heating rate with intermediate soaking

This heating scheme was used to evaluate the effect of soaking or preheating, if any, on the wetting of the substrate by the brazing filler. This was done to ensure that both the substrate and the brazing filler (wetting ball) are at the same uniform and equilibrium temperature

before heating up to the test temperature. A soaking temperature of 650^{o}C was used, well below the solidus of the brazing filler. The soaking time was between 5-10 minutes.

4.3.1 High heating rate (5.6^{o}C/s) with soaking at 650^{o}C and 120 grit SiC paper ground substrate

The wetting characteristic of the brazing filler on a relatively rough surface Ti-6Al-4V substrate (HHRSR1) is shown in Figure 4-16. This sample was soaked for duration of 5 minutes. A very rapid and monotonous drop in contact angle in the first 9 s (up to point A, Figure 4-16) could be observed in the spreading behaviour, an indication of primary spreading regime. This was followed by a short period (from point A to point B) of secondary spreading with the characteristic lower spreading rate, compared to the primary regime. After point B, the spreading curve reached a plateau.

With reference to the effect of surface roughness on the final apparent contact angle, it can be seen from Figure 4-16 that both the relatively rough surface substrate (HHRSR1) and the relatively smooth surface (HHRSS1) have essentially the same final apparent contact angle. The final apparent contact angles of all the samples with relatively rough surface done in this work under this heating scheme lie within the range of 17-22^{o}, while those of the relatively smooth surface substrates lie within the range of 16-20^{o}. The low apparent contact angle recorded under this heating scheme makes it a good choice for brazing. Equally, the tendency for reduced reactivity between the brazing filler and the droplet, as indicated by the short duration of the secondary wetting stage (samples HHRSS1 and HHRSS2), implies less erosion of brazed samples, compared to brazing under low heating rate scheme. Also, the incorporation of soaking stage in this heating scheme is very

important in reducing thermal differential in the samples, especially in brazing of large samples.

These results, again, highlight the negligible influence of surface roughness on the degree of wetting/spreading in this system. These results should not, however, be taken to mean that generally surface roughness does not influence wetting/spreading.

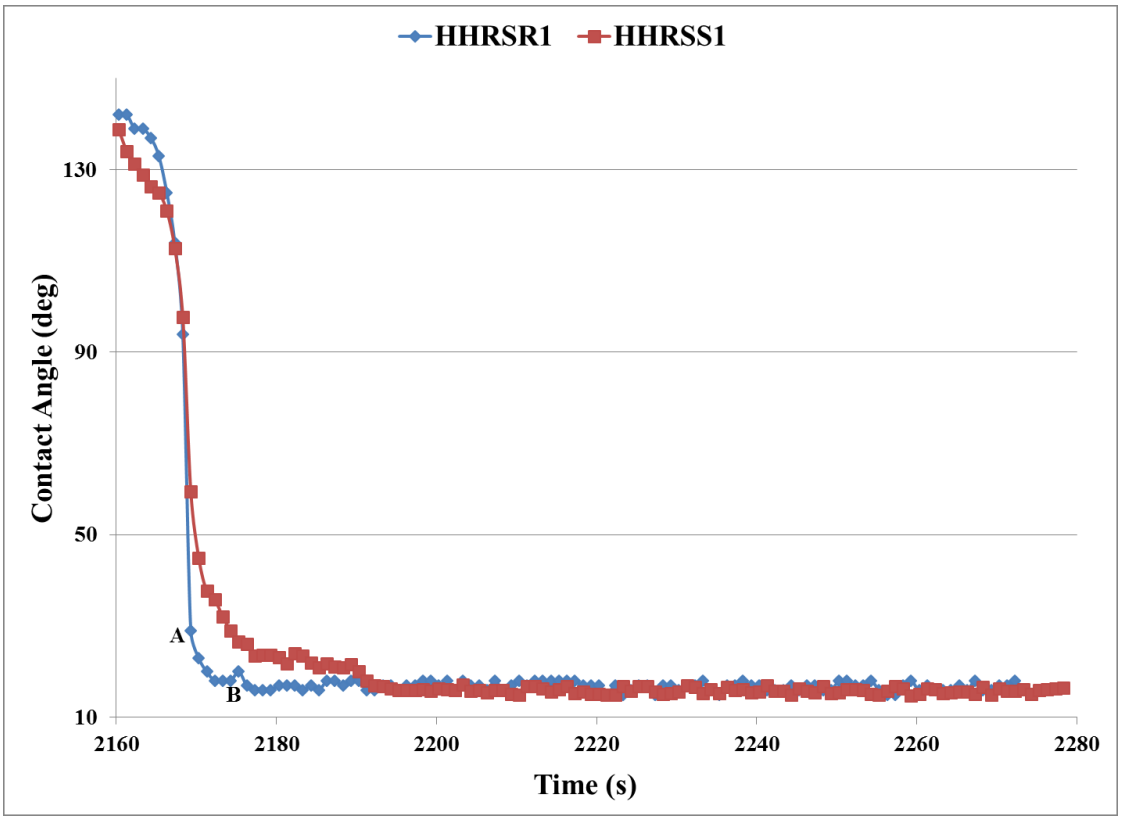

Figure 4-16. Variation of contact angle with time under the condition of 5.6°C/s heating rate with soaking at 650°C.

4.3.2 High heating rate (5.6°C/s) with soaking at 650°C and 1200 grit SiC paper ground substrate

Three samples, HHRSS1, HHRSS2 and HHRSS3 were subjected to a soaking temperature of 650°C for a period of 5, 8 and 10 minutes, respectively. The different soaking periods

were used to evaluate the effect of soaking duration on wetting. The results of these wetting tests are shown in Figure 4-17.

With respect to sample HHRSS1, after the very first few seconds of the wetting/spreading, which represents the melting of the brazing ball, a very high spreading rate was observed. This very fast spreading regime ended at the point marked A on the spread ratio-time curve in Figure 4-17, after about 12 s. This is a typical characteristic of primary spreading. From point A to point B, spreading at a lower rate could be observed, which is synonymous to secondary stage of wetting. Noticeable spreading ceases after passing through point B. Considering sample HHRSS2, which was soaked for a period of 8 minutes, after the very early melting stage, a very high spreading rate could also be observed, up to the point marked C on the spread ratio-time curve in Figure 4-17. This fast spreading ended after about 11 s. However, the extent of this regime with a very high spreading rate is a bit smaller than that noticed in sample HHRSS1, which was soaked for 5 minutes. This fast regime was followed by another regime (point C to point D) with a lower spreading rate (secondary spreading). The extent of this secondary wetting regime is a bit longer than that observed in sample HHRSS1. The curve reaches a plateau after point D.

The spread ratio-time curve of sample HHRSS3 is substantially more unique. Both primary and secondary wetting stages could be observed in the curve, just like in samples HHRSS1 and HHRSS2. However, the extent of the primary spreading regime is considerably smaller (up to point E) than those of samples HHRSS1 and HHRSS2. It lasted for only about 7 s. On the other hand, the secondary spreading stage (point E to point F) of this sample is much longer than those of the 2 other samples.

Considering the fact that secondary wetting/spreading stage is characterized by metallurgical reaction between the brazing filler and substrate, it implies that long soaking period will induce and enhance metallurgical reaction between the substrate and the brazing filler. The longer the soaking period, the more intense the reaction between the substrate and the brazing filler will be. This will lead to a reduction in the extent of the primary spreading stage and an enhanced secondary wetting stage. The final macrograph of one of the samples, HHRSS1, is shown in Figure 4-18. The edge of the droplet is fairly smooth.

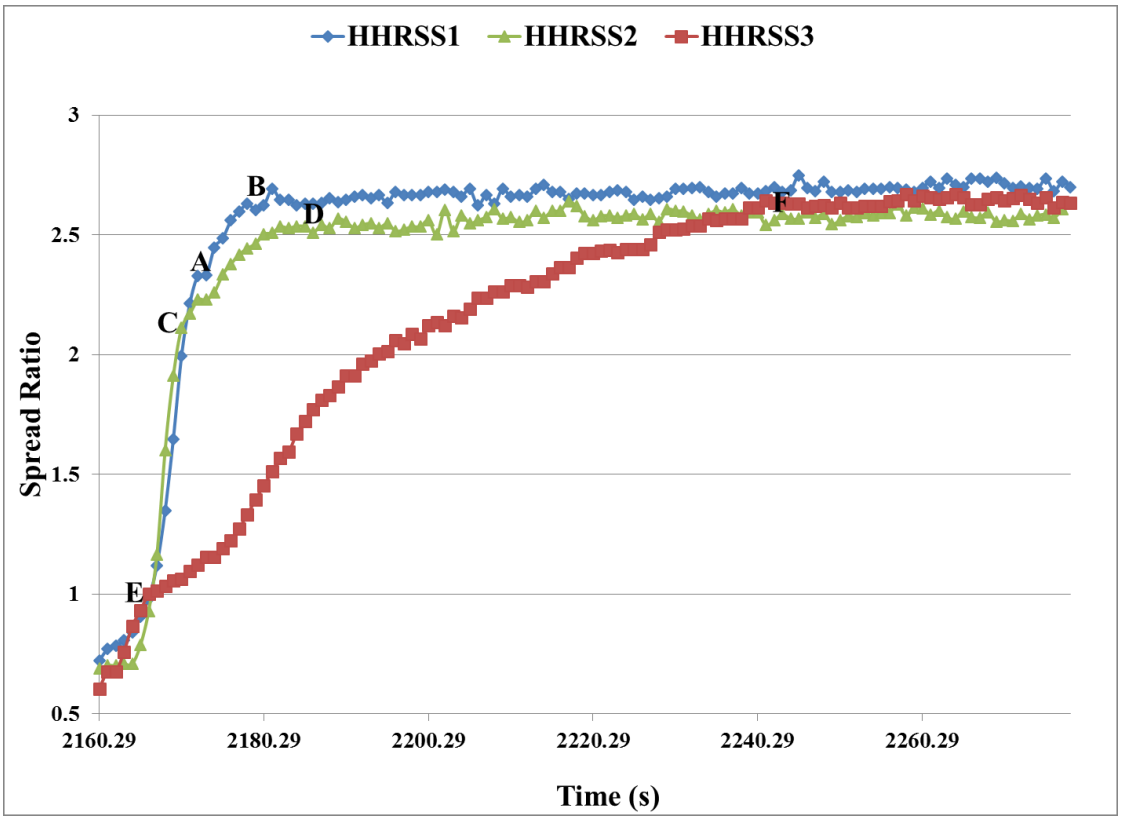

Figure 4-17. Variation of spread ratio with time under the condition of 5.6°C/s heating rate with soaking at 650°C and 1200 grit SiC paper ground substrate.

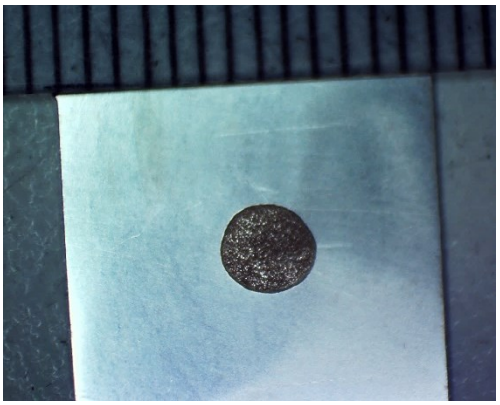

Figure 4-18. The final macrograph of sample HHRSS1 after the wetting test.

4.3.4 Microstructural analysis

The SEM back scattered images of samples HHRSS3 and HHRSS1 are shown in Figure 4-19a and 4-19b, respectively. The interface of sample HHRSS3, which was soaked for 10 minutes, is fairly symmetrical; with the deepest point of dissolution being at the center. This symmetry of interface could be due to the long duration of the secondary regime of spreading in the spread ratio-time graph of the sample in Figure 4-17. Also, based on the curvature of the interface, it is obvious that this secondary spreading regime is dominated by the formation of new phases of the interfacial layer with less dissolution of the substrate. Based on the characteristic of this regime and that of sample SHRR1, it can be inferred that continuous formation of the interfacial layer is essential for wetting/spreading in this system. The interface of sample HHRSS1, on the other hand, is asymmetrical with the deepest point of dissolution being close to the left hand side contact line. This could be due to the short duration of secondary stage of spreading exhibited by the sample (Figure 4-17).

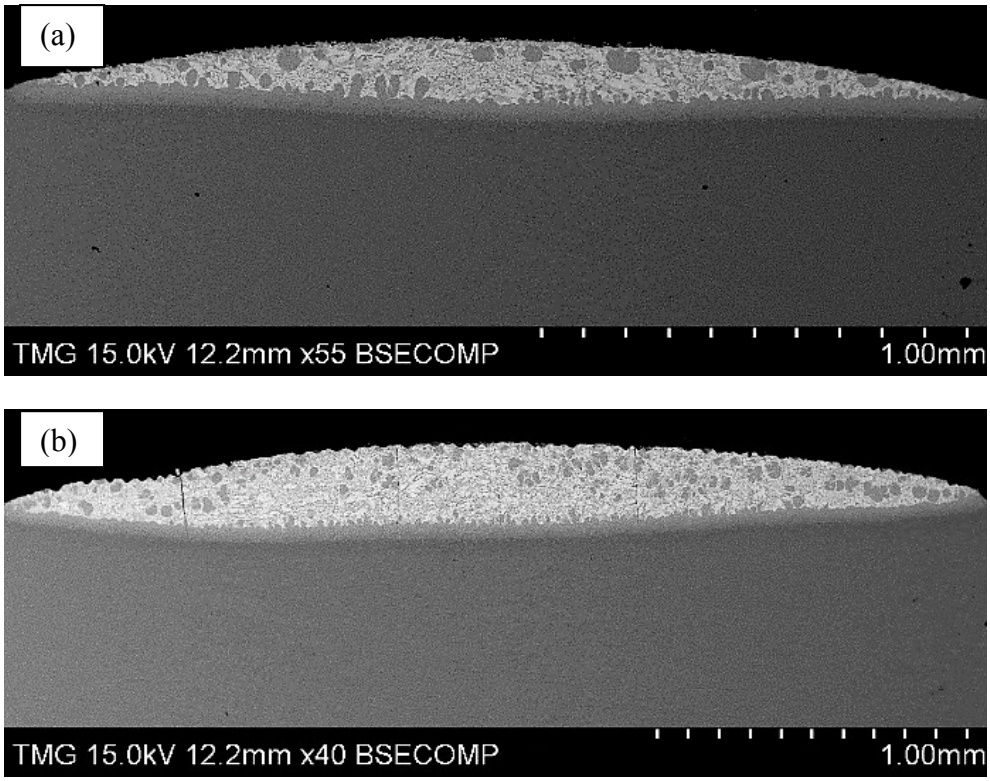

Figure 4-19. SEM back scattered images of samples (a) HHRSS3 (b) HHRSS1.

4.4 Statistical analysis of the results

In order to critically evaluate the influence of surface roughness and heating scheme on the wetting of Ti64 by the brazing filler metal (Ti-20Zr-20Cu-20Ni), it is important to put the results into statistical context. Design of experiments has been used to analyse the results through Minitab program. The plot of the main effects of surface roughness and heating scheme on the apparent contact angle, Figure 4-20, reveals that only the heating scheme has significant effect on the degree of wetting. The effect of surface roughness is well within the limit of error of measurement. Also, interaction plot of the effects, Figure 4-21, reveals that there is no significant interaction between the effects of the surface roughness and heating scheme on wetting. The mean value of the apparent contact angle obtained in this work under the condition of high heating rate was 34^{o}. However, under the conditions

of high heating rate with intermediate soaking, and low heating rate, the mean value were 18 and 16^{o}, respectively.

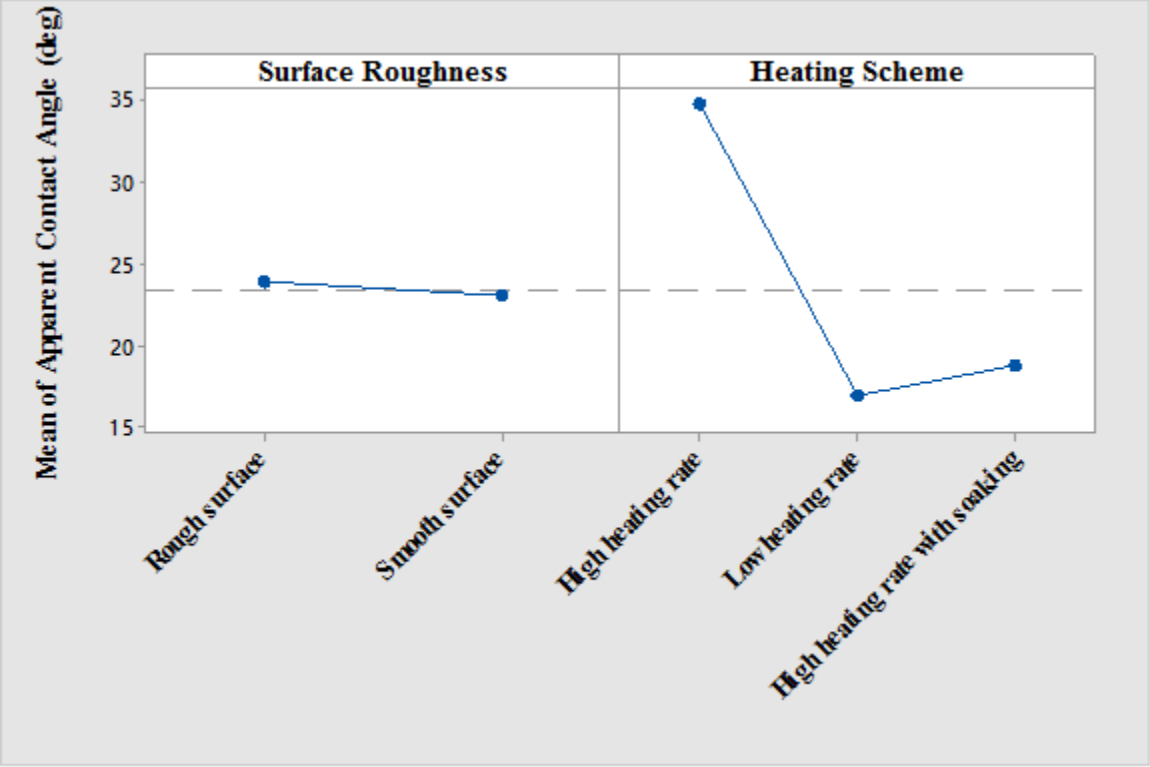

Figure 4-20. Main effects of surface roughness and heating scheme on the apparent contact angle.

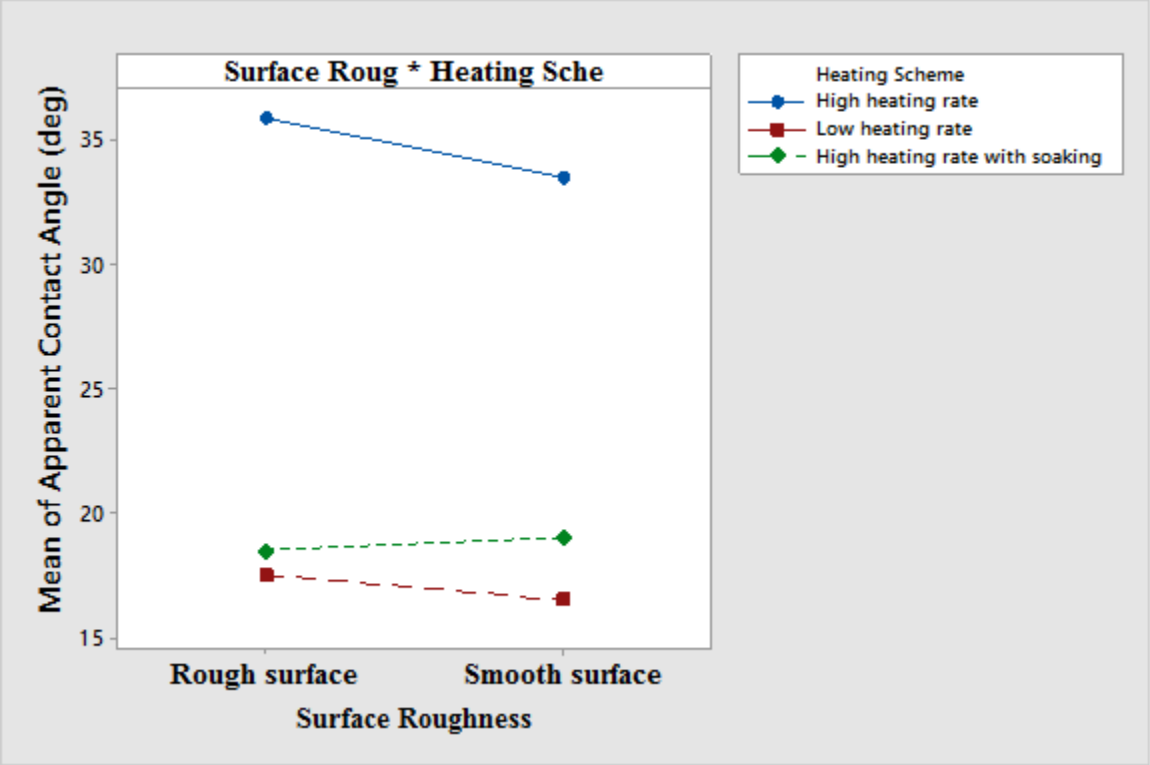

Figure 4-21. Interaction plot of the effects of surface roughness and heating scheme on the apparent contact angle.

Chapter 5 Conclusions, Contributions and Suggestions for the Future Work

5.1 Conclusions

The effects of surface roughness of the substrate and the heating scheme on the wetting of Ti-6Al-4V by Ti-20Zr-20Cu-20Ni brazing filler have been studied in this work. Based on this research work, the following concluding remarks can be drawn.

- The nature of wetting in this system has been found to be reactive, it entails the dissolution of the substrate and the formation of interfacial layer.
- In cases involving a heating scheme with a high heating rate (6.8^{o}C/s), a non-reactive like primary spreading stage has been identified. This stage is characterized with a high wetting/spreading rate with little or no dissolution of the substrate. The stage is followed by a secondary spreading stage, characterized by a relatively low spreading rate (compared to the first stage) and increased interfacial reaction.
- In heating scheme involving soaking at 650^{o}C, the soaking process duration has been found to influence the wetting/spreading mechanism. When the soaking duration is less than 10 minutes, the wetting/spreading is found to be dominated by the primary wetting stage. However, for soaking duration lasting for 10 minutes and above, the wetting/spreading is dominated by the secondary wetting stage.
- The ability of the system to form the interfacial reaction layer has been found to have profound effect on the degree of wetting.
- Surface roughness of the substrate has been found to have little or no effect on the degree of wetting of the substrate by the brazing filler in this system. This could be because of the fact that the wetting in this system is essentially reactive.

- The heating scheme, on the other hand, has been found to have profound influence on the wetting behaviour of the brazing filler on the substrate. When the heating rate was high (6.8^{o}C/s), the average value of the apparent contact angle of the filler on the substrate was 34^{o}. When the high heating rate was supplemented with an intermediate soaking scheme at a temperature of 650^{o}C, the average value of the apparent contact angle was found to be 18^{o}. A very low heating rate (1.7^{o}C/s) led to a measured apparent contact angle with an average value of 16^{o}.
- Under the heating scheme with low heating rate, repeatability of results was found difficult to achieve because of the intense brazing filler-substrate interaction. Therefore, from practical point of view, low heating rate brazing of this system should be avoided to prevent reliability issue in production.
- Based on the results of different heating schemes used in this work, brazing using high heating rate with intermediate soaking is recommended. With this heating scheme, Ti-20Zr-20Cu-20Ni brazing filler can wet Ti-6Al-4V substrate with final apparent contact angle as low as 18^{o}, coupled with reduced dissolution or erosion of the substrate. Also, thermal gradient is eliminated in the sample during temperature ramping.

5.2 Contributions

This work is very important to bridge the glaring and unfortunate research gap that currently exists in the study of the wetting behaviour of brazing filler on titanium alloys, despite the huge industrial importance and wide usage of titanium alloys. Detailed information about the progress in wettability study, especially in reactive systems, has also been provided in this work.

Also, the approach adopted to carry out this research work (sessile drop technique) is very similar to the industrial brazing technique. Therefore, the results of the work can provide necessary guideline and information for industrial brazing.

Equally, light has been shed on the evolution of the wetting process and the associated mechanism in this system, through the combination of sequential quenching process and microstructural analysis.

5.3 Recommendations for future work

- The use of other experimental technique like dispense drop technique is highly recommended. This will make it possible to isolate completely the initial melting stage from wetting and this might be very helpful in proving beyond doubt that the early stage of wetting in this system is purely inert. This will also make the study to be truly isothermal.
- While the present study has been done under a vacuum atmosphere, it might be interesting to see the effect of inert gas atmosphere on wetting in this system.
- The modelling of the experimental results of this system is equally recommended to shed more light on its wetting kinetics.
- Equally, it will be interesting to see if the manufacturing process used to produce the Ti64 foils might, in anyway, influence the behaviour of the brazing filler (Ti-20Zr-20Cu-20Ni) on it. Perhaps, the degree of wetting or the wetting mechanism on a forged Ti64 substrate might be different for a rolled Ti64 substrate.

REFERENCES

[1] P. J. Arrazola, A. Garay, L. M. Iriarte, M. Armendia, S. Marya, and F. Le Maître, "Machinability of titanium alloys (Ti6Al4V and Ti555.3)," *J. Mater. Process. Technol.*, vol. 209, no. 5, pp. 2223–2230, 2009.

[2] R. R. Boyer, "An overview on the use of titanium in the aerospace industry," *Mater. Sci. Eng. A*, vol. 213, no. 1–2, pp. 103–114, 1996.

[3] C. T. Chang, Y. C. Du, R. K. Shiue, and C. S. Chang, "Infrared brazing of high-strength titanium alloys by Ti–15Cu–15Ni and Ti–15Cu–25Ni filler foils," *Mater. Sci. Eng. A*, vol. 420, no. 1–2, pp. 155–164, 2006.

[4] W. Callister and D. Rethwisch, *Materials science and engineering: an introduction*, Eigth Edit. John Wiley & Sons, Inc., 2007, p. 885.

[5] C. T. Chang, Z. Y. Wu, R. K. Shiue, and C. S. Chang, "Infrared brazing Ti–6Al–4V and SP-700 alloys using the Ti–20Zr–20Cu–20Ni braze alloy," *Mater. Lett.*, vol. 61, no. 3, pp. 842–845, 2007.

[6] C. T. Chang and R. K. Shiue, "Infrared brazing Ti–6Al–4V and Mo using the Ti–15Cu–15Ni braze alloy," *Int. J. Refract. Met. Hard Mater.*, vol. 23, no. 3, pp. 161–170, 2005.

[7] H. Y. Chan and R. K. Shiue, "Study of brazing Ti-6Al-4V and TZM alloy using pure silver," *J. Mater. Sci. Lett.*, vol. 22, no. 23, pp. 1659–1663, 2003.

[8] H. Izui and Y. Suezawa, "Study on Ti-6Al-4V alloy brazed with Ag-5Al-0.5 Mn filler metal," *Weld. Int.*, vol. 3, no. 11, pp. 954–959, 1989.

[9] S. Y. Chang, L. C. Tsao, Y. H. Lei, S. M. Mao, and C. H. Huang, "Brazing of 6061 aluminum alloy/Ti–6Al–4V using Al–Si–Cu–Ge filler metals," *J. Mater. Process. Technol.*, vol. 212, no. 1, pp. 8–14, 2012.

[10] "Titanium alloy guide." [Online]. Available: http://www.rtiintl.com/Titanium/RTI-Titanium-Alloy-Guide.pdf. [Accessed: 08-Sep-2014].

[11] P. M. Roberts, *Brazing.* Oxford: Oxford University Press, 1975, pp. 1–21.

[12] G. Humpston and D. M. Jacobson, *Principles of Soldering and Brazing*, Third Edit. Ohio: ASM International, Materials Park, Ohio., 1996, pp. 1–257.

[13] A. E. Shapiro and Y. A. Flom, "Brazing of Titanium at Temperatures below 800°C: Review and Prospective Applications," Ohio, 2007.

[14] E. Ganjeh, H. Sarkhosh, M. E. Bajgholi, H. Khorsand, and M. Ghaffari, "Increasing Ti–6Al–4V brazed joint strength equal to the base metal by Ti and Zr amorphous filler alloys," *Mater. Charact.*, vol. 71, no. 15, pp. 31–40, 2012.

[15] M. M. Schwartz, *Brazing*. Ohio: ASM International, Materials Park, Ohio., 1987, pp. 1–455.

[16] A. Shafiei, P. Abachi, K. Dehghani, and K. Pourazarang, "On the Formation of Intermetallics during the Furnace Brazing of Pure Titanium to 304 Stainless Steel Using Ag (30–50%)–Cu Filler Metals," *Mater. Manuf. Process.*, vol. 25, no. 11, pp. 1333–1340, 2010.

[17] P. G. de Gennes, "Wetting: statics and dynamics," *Rev. Mod. Phys.*, vol. 57, no. 3, pp. 827–863, 1985.

[18] V. H. López and A. R. Kennedy, "Flux-assisted wetting and spreading of Al on TiC.," *J. Colloid Interface Sci.*, vol. 298, no. 1, pp. 356–62, 2006.

[19] D. R. Milner, "A survey of the scientific principles related to wetting and spreading.," *Br. Weld. J.*, vol. 5, pp. 90–105, 1958.

[20] C. A. Leon, V. H. Lopez, E. Bedolla, and R. A. L. Drew, "Wettability of TiC by commercial aluminum alloys," *J. Mater. Sci.*, vol. 37, no. 16, pp. 3509–3514, 2002.

[21] S. Amore, E. Ricci, G. Borzone, and R. Novakovic, "Wetting behaviour of lead-free Sn-based alloys on Cu and Ni substrates," *Mater. Sci. Eng. A*, vol. 495, no. 1–2, pp. 108–112, 2008.

[22] B. Lavi and A. Marmur, "The exponential power law: partial wetting kinetics and dynamic contact angles," *Colloids Surfaces A Physicochem. Eng. Asp.*, vol. 250, no. 1–3, pp. 409–414, 2004.

[23] G. W. Liu, F. Valenza, M. L. Muolo, G. J. Qiao, and a. Passerone, "Wetting and interfacial behavior of Ni–Si alloy on different substrates," *J. Mater. Sci.*, vol. 44, no. 22, pp. 5990–5997, 2009.

[24] T. D. Blake and K. J. Ruschak, "A maximum speed of wetting," *Nature*, vol. 282, no. 5738, pp. 489–491, 1979.

[25] D. Chatain and W. C. Carter, "Spreading of metallic drops," *Nat. Mater.*, vol. 3, no. 12, pp. 843–845, 2004.

[26] E. Saiz, M. Benhassine, J. De Coninck, and A. P. Tomsia, "Early stages of dissolutive spreading," *Scr. Mater.*, vol. 62, no. 12, pp. 934–938, 2010.

[27] E. Saiz, a. Tomsia, N. Rauch, C. Scheu, M. Ruehle, M. Benhassine, D. Seveno, J. de Coninck, and S. Lopez-Esteban, "Nonreactive spreading at high temperature: Molten metals and oxides on molybdenum," *Phys. Rev. E*, vol. 76, no. 4, p. 041602, 2007.

[28] E. Saiz and A. Tomsia, "Atomic dynamics and Marangoni films during liquid-metal spreading," *Nat. Mater.*, vol. 3, no. 12, pp. 903–9, 2004.

[29] T. Ondarcuhu and M. Veyssié, "Relaxation modes of the contact line of a liquid spreading on a surface," *Nature*, vol. 352, no. 6334, pp. 418–420, 1991.

[30] A. Eddi, K. G. Winkels, and J. H. Snoeijer, "Short time dynamics of viscous drop spreading," *Phys. Fluids*, vol. 25, no. 1, p. 013102, 2013.

[31] J.-G. Li, "Wetting of ceramic materials by liquid silicon, aluminium and metallic melts containing titanium and other reactive elements: A review," *Ceram. Int.*, vol. 20, no. 6, pp. 391–412, 1994.

[32] J. C. Ambrose and M. G. Nicholas, "Wetting and spreading of nickel-phosphorus brazes : detailed real time observations of spreading on iron-chromium substrates," *Mater. Sci. Technol.*, vol. 12, no. 1, pp. 72–80, 1996.

[33] F. Gnecco, E. Ricci, S. Amore, D. Giuranno, G. Borzone, G. Zanicchi, and R. Novakovic, "Wetting behaviour and reactivity of lead free Au–In–Sn and Bi–In–Sn alloys on copper substrates," *Int. J. Adhes. Adhes.*, vol. 27, no. 5, pp. 409–416, 2007.

[34] H. Xu, Z. Yuan, H. Matsuura, and F. Tsukihashi, "Hysteresis phenomenon and wetting characteristics of molten Sn–3.0wt.%Ag–0.5wt.%Cu on different tilting substrates," *J. Alloys Compd.*, vol. 487, no. 1–2, pp. 121–125, 2009.

[35] P. R. Chidambaram, G. R. Edwards, and D. L. Olson, "A thermodynamic criterion to predict wettability at metal-alumina interfaces," *Metall. Trans. B*, vol. 23, no. 2, pp. 215–221, 1992.

[36] D. Chatain, "Anisotropy of Wetting," *Annu. Rev. Mater. Res.*, vol. 38, no. 1, pp. 45–70, 2008.

[37] S. J. Hitchcock, N. T. Carroll, and M. G. Nicholas, "Some effects of substrate roughness on wettability," *J. Mater. Sci.*, vol. 16, no. 3, pp. 714–732, 1981.

[38] T. D. Blake and J. De Coninck, "The influence of solid - liquid interactions on dynamic wetting," *Adv. Colloid Interface Sci.*, vol. 96, no. 1–3, pp. 21–36, 2002.

[39] J. Bird, S. Mandre, and H. Stone, "Short-Time Dynamics of Partial Wetting," *Phys. Rev. Lett.*, vol. 100, no. 23, p. 234501, 2008.

[40] D. Bonn, J. Eggers, J. Indekeu, J. Meunier, and E. Rolley, "Wetting and spreading," *Rev. Mod. Phys.*, vol. 81, no. 2, pp. 739–805, 2009.

[41] A. M. Cazabat, S. Gerdes, M. P. Valignat, and S. Villette, "Dynamics of Wetting : From Theory to Experiment," *Interface Sci.*, vol. 5, no. 2–3, pp. 129–139, 1997.

[42] I. A. Aksay, C. E. Hoge, and J. A. Pask, "Wetting under chemical equilibrium and nonequilibrium conditions," *J. Phys. Chem.*, vol. 78, no. 12, pp. 1178–1183, 1974.

[43] L. Leger and J. F. Joanny, "Liquid spreading," *Reports Prog. Phys.*, vol. 55, no. 4, pp. 431–486, 1992.

[44] G. Kumar and K. N. Prabhu, "Review of non-reactive and reactive wetting of liquids on surfaces.," *Adv. Colloid Interface Sci.*, vol. 133, no. 2, pp. 61–89, 2007.

[45] G. T. Barnes and I. R. Gentle, *Interfacial Science: An Introduction. Second Edition.*, Oxford University Press, 2011, p. 352.

[46] A. B. D. Cassie, "Contact angles," *Discuss. Faraday Soc.*, vol. 3, pp. 11–16, 1948.

[47] D. Quéré, "Rough ideas on wetting," *Phys. A Stat. Mech. its Appl.*, vol. 313, pp. 32–46, 2002.

[48] B. He, J. Lee, and N. A. Patankar, "Contact angle hysteresis on rough hydrophobic surfaces," *Colloids Surfaces A Physicochem. Eng. Asp.*, vol. 248, no. 1–3, pp. 101–104, 2004.

[49] L. Yin, B. T. Murray, S. Su, Y. Sun, Y. Efraim, H. Taitelbaum, and T. J. Singler, "Reactive wetting in metal-metal systems.," *J. Phys. Condens. Matter*, vol. 21, no. 46, pp. 1–11, 2009.

[50] P. R. Sharps, A. P. Tomsia, and J. A. Pask, "Wetting and spreading in the Cu-Ag system," *Acta Metall.*, vol. 29, no. 5, pp. 855–865, 1981.

[51] P. Protsenko, J. P. Garandet, R. Voytovych, and N. Eustathopoulos, "Thermodynamics and kinetics of dissolutive wetting of Si by liquid Cu," *Acta Mater.*, vol. 58, no. 20, pp. 6565–6574, 2010.

[52] M. E. R. Shanahan, "A simple analysis of local wetting hysteresis on a Wilhelmy plate," *Surf. Interface Anal.*, vol. 17, no. 7, pp. 489–495, 1991.

[53] A. M. Schwartz, "The dynamics of contact angle phenomena.," *Adv. Colloid Interface Sci.*, vol. 4, no. 4, pp. 349–374, 1975.

[54] H. Tavana and A. W. Neumann, "On the question of rate-dependence of contact angles," *Colloids Surfaces A Physicochem. Eng. Asp.*, vol. 282–283, pp. 256–262, 2006.

[55] W. Li and A. Amirfazli, "A thermodynamic approach for determining the contact angle hysteresis for superhydrophobic surfaces.," *J. Colloid Interface Sci.*, vol. 292, no. 1, pp. 195–201, 2005.

[56] A. Nakajima, "Design of hydrophobic surfaces for liquid droplet control," *NPG Asia Mater.*, vol. 3, no. 5, pp. 49–56, 2011.

[57] X. S. Cui and W. Li, "On the possibility of superhydrophobic behavior for hydrophilic materials.," *J. Colloid Interface Sci.*, vol. 347, no. 1, pp. 156–62, 2010.

[58] S. Vedantam and M. V. Panchagnula, "Constitutive modeling of contact angle hysteresis.," *J. Colloid Interface Sci.*, vol. 321, no. 2, pp. 393–400, 2008.

[59] W. D. Kaplan, D. Chatain, P. Wynblatt, and W. C. Carter, "A review of wetting versus adsorption, complexions, and related phenomena: the rosetta stone of wetting," *J. Mater. Sci.*, vol. 48, no. 17, pp. 5681–5717, 2013.

[60] J. F. Joanny and P. G. de Gennes, "A model for contact angle hysteresis," *J. Chem. Phys.*, vol. 81, no. 1, pp. 552–562, 1984.

[61] M. Iwamatsu, "Contact angle hysteresis of cylindrical drops on chemically heterogeneous striped surfaces.," *J. Colloid Interface Sci.*, vol. 297, no. 2, pp. 772–7, 2006.

[62] B. B. Sauer and W. G. Kampert, "Influence of Viscosity on Forced and Spontaneous Spreading: Wilhelmy Fiber Studies Including Practical Methods for Rapid Viscosity Measurement," *J. Colloid Interface Sci.*, vol. 199, no. 1, pp. 28–37, 1998.

[63] B. He, N. A. Patankar, and J. Lee, "Multiple Equilibrium Droplet Shapes and Design Criterion for Rough Hydrophobic Surfaces," *Langmuir*, vol. 19, no. 12, pp. 4999–5003, 2003.

[64] H. Kamusewitz, W. Possart, and D. Paul, "The relation between Young's equilibrium contact angle and the hysteresis on rough paraffin wax surfaces," *Colloids Surfaces A Physicochem. Eng. Asp.*, vol. 156, no. 1–3, pp. 271–279, 1999.

[65] J. Long, M. N. Hyder, R. Y. M. Huang, and P. Chen, "Thermodynamic modeling of contact angles on rough, heterogeneous surfaces.," *Adv. Colloid Interface Sci.*, vol. 118, no. 1–3, pp. 173–90, 2005.

[66] A. Marmur, "Wetting on Hydrophobic Rough Surfaces: To Be Heterogeneous or Not To Be?," *Langmuir*, vol. 19, no. 20, pp. 8343–8348, 2003.

[67] R. Voitovitch, A. Mortensen, F. Hodaj, and N. Eustathopoulos, “Diffusion-limited reactive wetting: study of spreading kinetics of Cu–Cr alloys on carbon substrates,” *Acta Mater.*, vol. 47, no. 4, pp. 1117–1128, 1999.

[68] L. Yin, S. J. Meschter, and T. J. Singler, “Wetting in the Au–Sn System,” *Acta Mater.*, vol. 52, no. 10, pp. 2873–2888, 2004.

[69] L. Yin, A. Chauhan, and T. J. Singler, “Reactive wetting in metal/metal systems: Dissolutive versus compound-forming systems,” *Mater. Sci. Eng. A*, vol. 495, no. 1–2, pp. 80–89, 2008.

[70] O. Dezellus, F. Hodaj, and N. Eustathopoulos, “Progress in modelling of chemical-reaction limited wetting,” *J. Eur. Ceram. Soc.*, vol. 23, no. 15, pp. 2797–2803, 2003.

[71] O. Kozlova, R. Voytovych, P. Protsenko, and N. Eustathopoulos, “Non-reactive versus dissolutive wetting of Ag–Cu alloys on Cu substrates,” *J. Mater. Sci.*, vol. 45, no. 8, pp. 2099–2105, 2009.

[72] L. Yin, B. T. Murray, and T. J. Singler, “Dissolutive wetting in the Bi–Sn system,” *Acta Mater.*, vol. 54, no. 13, pp. 3561–3574, 2006.

[73] H. Shibata, X. Jiang, M. Valdez, and A. W. Cramb, “The Contact Angle between Liquid Iron and a Single-Crystal Magnesium Oxide Substrate at 1873 K,” *Metall. Mater. Trans. B*, vol. 35, no. 1, pp. 179–181, 2004.

[74] G. L. J. Bailey and H. C. Watkins, “The flow of liquid metals on solid metal surfaces and its relation to soldering, brazing and hot-dip coating.,” *J. Inst. Met.*, vol. 80, pp. 57–76, 1951.

[75] R. Shuttleworth and G. L. J. Bailey, “The spreading of a liquid over a rough solid,” *Discuss. Faraday Soc.*, vol. 3, no. 16, p. 16, 1948.

[76] R. N. Wenzel, “Resistance of solid surfaces to wetting by water,” *Ind. Eng. Chem.*, vol. 28, pp. 988–994, 1936.

[77] S. G. Kandlikar and M. E. Steinke, “Contact angles and interface behavior during rapid evaporation of liquid on a heated surface,” *Int. J. Heat Mass Transf.*, vol. 45, no. 18, pp. 3771–3780, 2002.

[78] J. D. Bernardin, I. Mudawar, C. B. Walsh, and E. I. Fransesi, “Contact angle temperature dependence for water droplets on practical aluminum surfaces,” *Int. J. Heat Mass Transf.*, vol. 40, no. 5, pp. 1017–1033, 1997.

[79] N. Eustathopoulos, M. G. Nicholas, and B. Drevert, *Wettability at High Temperatures.*, First Edit. Pergamon Materials Series. Elsevier Science Ltd, 1999.

[80] R. E. J. Johnson and R. H. Dettre, “Contact angle hysteresis. III. Study of an Idealized Heterogeneous Surface,” *J. Phys. Chem.*, vol. 68, no. 7, pp. 1744–1750, 1964.

[81] N. A. Patankar, “On the Modeling of Hydrophobic Contact Angles on Rough Surfaces,” *Langmuir*, vol. 19, no. 4, pp. 1249–1253, 2003.

[82] P. Costa, A. Passerone, and E. Ricci, “Oxygen fluxes and the measurement of the surface tension of liquid metals.,” *High Temp. Press.*, vol. 20, no. 1, pp. 59–72., 1998.

[83] D. R. Milner and R. L. Apps, *Introduction to Welding and Brazing*, First Edit. London: Pergamon Press, 1968, pp. 1–219.

[84] H. Takao, T. Tsukada, K. Yamada, M. Yamashita, and H. Hasegawa, “Development of Wettability Evaluation Technique Applying Contact Angle Measurement during Soldering,” *Tech. J. R D Rev. Toyota CRDL.*, vol. 39, no. 2, pp. 41–48, 2004.

[85] A. J. Wall and D. R. Milner, “Wetting and Spreading Phenomena in a Vacuum,” *J. Inst. Met.*, vol. 90, pp. 394–402, 1962.

[86] A. Sakamoto, “Wetting in vacuum-inert gas partial pressure atmosphere brazing,” *Weld. J.*, pp. 272–280, 1983.

[87] Y. O. Kabova, V. V. Kuznetsov, and O. A. Kabov, “Temperature dependent viscosity and surface tension effects on deformations of non-isothermal falling liquid film,” *Int. J. Heat Mass Transf.*, vol. 55, no. 4, pp. 1271–1278, 2012.

[88] H. D. Samarasekera and Z. A. Munir, “An investigation of the contact angles between low melting metals and substrates of niobium and zirconium,” *J. Less Common Met.*, vol. 64, no. 2, pp. 255–266, 1979.

[89] W. Feduska, “High-Temperature Brazing Alloy-Base Metal Wetting Reactions,” *Weld. J.*, vol. 38, no. 3, pp. 122–131, 1959.

[90] A. Sangghaleh and M. Halali, “An investigation on the wetting of polycrystalline alumina by aluminium,” *J. Mater. Process. Technol.*, vol. 197, no. 1–3, pp. 156–160, 2008.

[91] X. Yang, P. Xiao, S. Liang, J. Zou, and Z. Fan, “Alloying Effect of Ni And Cr on the Wettability of Copper On W Substrate,” *Acta Metall. Sin.*, vol. 21, no. 5, pp. 369–379, 2008.

[92] E. Candan, “Effect of Alloying Elements to Aluminium on the Wettability of Al / SiC System,” *Turkish J. Eng. Environ. Sci.*, vol. 26, no. 1, pp. 1–5, 2002.

[93] D. Q. Yu, H. P. Xie, and L. Wang, “Investigation of interfacial microstructure and wetting property of newly developed Sn–Zn–Cu solders with Cu substrate,” *J. Alloys Compd.*, vol. 385, no. 1–2, pp. 119–125, 2004.

[94] P. Protsenko, O. Kozlova, R. Voytovych, and N. Eustathopoulos, “Dissolutive wetting of Si by molten Cu,” *J. Mater. Sci.*, vol. 43, no. 16, pp. 5669–5671, 2008.

[95] P. Bhagawath, K. N. Prabhu, and Satyanarayan, “Wetting Behavior of Reactive and Non–Reactive Wetting of Liquids on Metallic Substrates,” *World Acad. Sci. Eng. Technol.*, vol. 73, pp. 978–981, 2013.

[96] O. Dezellus and N. Eustathopoulos, “Fundamental issues of reactive wetting by liquid metals,” *J. Mater. Sci.*, vol. 45, no. 16, pp. 4256–4264, 2010.

[97] A.-L. Biance, C. Clanet, and D. Quéré, “First steps in the spreading of a liquid droplet,” *Phys. Rev. E*, vol. 69, no. 1, p. 016301, 2004.

[98] L. Tanner, “The spreading of silicone oil drops on horizontal surfaces,” *J. Phys. D. Appl. Phys.*, vol. 12, no. 9, pp. 1473–1484, 1979.

[99] S. Rafaï, D. Sarker, V. Bergeron, J. Meunier, and D. Bonn, “Superspreading: aqueous surfactant drops spreading on hydrophobic surfaces,” *Langmuir*, vol. 18, no. 26, pp. 10486–10488, 2002.

[100] L. Chen, G. K. Auernhammer, and E. Bonaccurso, “Short time wetting dynamics on soft surfaces,” *Soft Matter*, vol. 7, no. 19, pp. 9084–9089, 2011.

[101] J. Eggers, J. R. Lister, and H. A. Stone, “Coalescence of liquid drops,” *J. Fluid Mech.*, vol. 401, pp. 293–310, 1999.

[102] L. Duchemin, J. Eggers, and C. Josserand, “Inviscid coalescence of drops,” *J. Fluid Mech.*, vol. 487, pp. 167–178, 2003.

[103] K. Winkels, J. Weijs, A. Eddi, and J. Snoeijer, “Initial spreading of low-viscosity drops on partially wetting surfaces,” *Phys. Rev. E*, pp. 1–5, 2012.

[104] L. Courbin, J. C. Bird, M. Reyssat, and H. A. Stone, “Dynamics of wetting: from inertial spreading to viscous imbibition.,” *J. Phys. Condens. Matter*, vol. 21, no. 46, p. 464127, 2009.

[105] J. D. Paulsen, J. C. Burton, and S. R. Nagel, “Viscous to Inertial Crossover in Liquid Drop Coalescence,” *Phys. Rev. Lett.*, vol. 106, no. 11, p. 114501, 2011.

[106] S. Case and S. Nagel, “Coalescence in Low-Viscosity Liquids,” *Phys. Rev. Lett.*, vol. 100, no. 8, p. 084503, 2008.

[107] M. Wu, T. Cubaud, and C.-M. Ho, "Scaling law in liquid drop coalescence driven by surface tension," *Phys. Fluids*, vol. 16, no. 7, pp. L51–L54, 2004.

[108] A. Carlson, M. Do-Quang, and G. Amberg, "Dissipation in rapid dynamic wetting," *J. Fluid Mech.*, vol. 682, pp. 213–240, 2011.

[109] C. Redon, F. Brochard-Wyart, H. Hervet, and F. Rondelez, "Spreading of ' Heavy ' Droplets," *J. Colloid Interface Sci.*, vol. 149, no. 2, pp. 580–591, 1992.

[110] R. Holdich, V. M. Starov, P. Prokopovich, D. O. Njobuenwu, R. G. Rubio, S. Zhdanov, and M. G. Velarde, "Spreading of liquid drops from a liquid source," *Colloids Surfaces A Physicochem. Eng. Asp.*, vol. 282–283, pp. 247–255, 2006.

[111] K. Landry and N. Eustathopoulos, "Dynamics of Wetting in Reactive Metal/Ceramic Systems : Linear Spreading," *Acta Mater.*, vol. 44, no. 10, pp. 3923–3932, 1996.

[112] N. Eustathopoulos, "Progress in understanding and modeling reactive wetting of metals on ceramics," *Curr. Opin. Solid State Mater. Sci.*, vol. 9, no. 4–5, pp. 152–160, 2005.

[113] A. Mortensen, B. Drevet, and N. Eustathopoulos, "Kinetics of Diffusion-Limited Spreading of Sessile Drops in Reactive Wetting," *Scr. Mater.*, vol. 36, no. 6, pp. 645–651, 1997.

[114] K. Landry, C. Rado, and N. Eustathopoulos, "Influence of interfacial reaction rates on the wetting driving force in metal/ceramic systems," *Metall. Mater. Trans. A*, vol. 27A, no. 10, pp. 3181–3186, 1996.

[115] O. Dezellus and N. Eustathopoulos, "Fundamental issues of reactive wetting by liquid metals," *J. Mater. Sci.*, vol. 45, no. 16, pp. 4256–4264, 2010.

[116] J. C. Ambrose, M. G. Nicholas, and A. M. Stoneham, "Dynamics of braze spreading," *Acta Metall. Mater.*, vol. 40, no. 10, pp. 2483–2488, 1992.

[117] C. D. Bain, G. D. Burnett-Hall, and R. R. Montgomerie, "Rapid motion of liquid drops," *Nature*, vol. 372, no. 6505, pp. 414–415, 1994.

[118] F. Dos Santos and T. Ondarcuhu, "Free-running droplets," *Phys. Rev. Lett.*, vol. 75, no. 16, pp. 2972–2975, 1995.

[119] M. E. R. Shanahan and P.-G. de Gennes, "Start-up of a reactive droplet," *Comptes Rendus l'Académie des Sci. - Ser. IIB - Mech.*, vol. 324, no. 4, pp. 261–268, 1997.

[120] C. D. Bain and G. M. Whitesides, "A study by contact angle of the acid-base behavior of monolayers containing omega-mercaptocarboxylic acids adsorbed on

gold: an example of reactive spreading," *Langmuir*, vol. 5, no. 6, pp. 1370–1378, 1989.

[121] M. K. Chaudhury and G. M. Whitesides, "How to make water run uphill," *Science (80-.).*, vol. 256, no. 5063, pp. 1539–1541, 1992.

[122] F. Brochard, "Motions of droplets on solid surfaces induced by chemical or thermal gradients," *Langmuir*, vol. 5, no. 2, pp. 432–438, 1989.

[123] P. G. de Gennes, "Running droplets in a random medium," *Comptes Rendus l'Académie des Sci. IIB*, vol. 327, no. 1, pp. 147–154, 1999.

[124] E. Raphaël, "Spreading of droplets on a patchy surface," *C. R. Acad. Sci. Paris.*, vol. 306, 1988.

[125] F. Brochard-Wyart and P. G. de Gennes, "Spontaneous motion of a reactive droplet," *Comptes Rendus l'Académie des Sci. - Ser. IIB .*, vol. 321, no. 7, pp. 285–288, 1995.

[126] C. C. Liu, C. L. Ou, and R. K. Shiue, "The microstructural observation and wettability study of brazing Ti-6Al-4V and 304 stainless steel using three braze alloys," *J. Mater. Sci.*, vol. 37, pp. 2225–2235, 2002.

[127] T. Chung, J. Kim, J. Bang, B. Rhee, and D. Nam, "Microstructures of brazing zone between titanium alloy and stainless steel using various filler metals," *Trans. Nonferrous Met. Soc. China*, vol. 22, pp. 639–644, 2012.

[128] H. Y. Chan, D. W. Liaw, and R. K. Shiue, "The microstructural observation of brazing Ti–6Al–4V and TZM using the BAg-8 braze alloy," *Int. J. Refract. Met. Hard Mater.*, vol. 22, no. 1, pp. 27–33, 2004.

[129] I.-T. Hong and C.-H. Koo, "Microstructural evolution and shear strength of brazing C103 and Ti–6Al–4V using Ti–20Cu–20Ni–20Zr (wt.%) filler metal," *Int. J. Refract. Met. Hard Mater.*, vol. 24, no. 3, pp. 247–252, 2006.

[130] R. A. Khoja-mendwi, "Design , Fabrication and Test of an Apparatus to Monitor the Wetting Behaviour of High Service Temperature Brazing Materials," Concordia University, 2009.

[131] "Revised thermocouple reference tables." [Online]. Available: www.omega.ca/teperature/Z/pdf/z204-206.pdf. [Accessed: 10-Sep-2014].

[132] B. Lautrup, *Physics of Continuous Matter: Exotic and Everyday Phenomena in the Macroscopic World*, Second. CRC Press, 2011, p. 696.

[133] J. E. Sprittles and Y. D. Shikhmurzaev, “Dynamics of liquid drops coalescing in the inertial regime,” *Phys. Rev. E*, vol. 89, no. 6, p. 063008, 2014.

[134] L. Liu, “Automated measurement of contact angles for sessile droplets using matlab image and analysis library,” Toronto, Canada.

[135] I.-T. Hong and C.-H. Koo, “Vacuum-furnace brazing of C103 and Ti–6Al–4V with Ti–15Cu–15Ni filler-metal,” *Mater. Sci. Eng. A*, vol. 398, no. 1–2, pp. 113–127, 2005.

[136] J. G. Lee, G. H. Kim, M. K. Lee, and C. K. Rhee, “Intermetallic formation in a Ti–Cu dissimilar joint brazed using a Zr-based amorphous alloy filler,” *Intermetallics*, vol. 18, no. 4, pp. 529–535, 2010.

[137] J. J. Stephens and S. K. Weil, Eds., “Brazing and Soldering. Proceedings of the 3rd International Brazing and Soldering Conference.,” 2006, pp. 1–413.